NANOCOMPOSITES BASED ON NANOCELLULOSE WHISKERS

A Dissertation
Presented to
The Academic Faculty

by

Amit Saxena

In Partial Fulfillment
of the Requirements for the Degree
Doctor of Philosophy in the
School of Chemistry and Biochemistry
Georgia Institute of Technology

May, 2013

NANOCOMPOSITES BASED ON NANOCELLULOSE WHISKERS

Approved by:

Dr. Arthur J. Ragauskas, Advisor
School of Chemistry and Biochemistry
Georgia Institute of Technology

Dr. Lawrence A. Bottomley
School of Chemistry and Biochemistry
Georgia Institute of Technology

Dr. Yulin Deng
School of Chemical and Biomolecular Engineering
Georgia Institute of Technology

Dr. Preet Singh
School of Materials Science and Engineering
Georgia Institute of Technology

Dr. John Zhang
School of Chemistry and Biochemistry
Georgia Institute of Technology

Date Approved: January 3rd, 2013

DEDICATION

This dissertation is dedicated to my lovely wife Shilpi with love and admiration and my parents for their love, support, care and encouragement throughout the course of my doctoral research.

ACKNOWLEDGEMENTS

I wish to thank Dr. Art Ragauskas for his support, advice and mentorship during my doctoral studies. I would also like to thank my thesis committee, Dr. Yulin Deng, Dr. Preet Singh, Dr. John Zhang and Dr. Lawrence Bottomley, for their insightful comments and support from the initial to the final level of this project.

I am grateful to my co-workers at Georgia Tech, especially Dr. Marcus Foston, Dr. Mohamad Kassaee, for their support in many aspects during the completion of this project.

I am grateful to all the friends I made along the way, for making my stay in Atlanta so memorable. Finally, thanks to my wife and my parents for their undying support and all my strength from their unconditional love. I derived inspiration from their sacrifice, encouragement from their faith, found happiness in their pride.

I also would like to acknowledge the financial support from the Paper Science and Engineering Fellowship program at the Institute of Paper Science and Technology.

TABLE OF CONTENTS

LIST OF TABLES

LIST OF FIGURES

CHAPTER 1

INTRODUCTION

The majority of engineered plastic materials used today are made from synthetic polymers. Petrochemically based polymers have been increasingly used as packaging materials due, in part, to their availability, low cost and favorable mechanical properties [1]. The use of conventional petroleum-based polymer products creates potential problems due to their non-renewable nature and ultimate disposal. More than 40 % of all plastic materials are used in packaging, and their disposal contributes to growing landfills and enhanced greenhouse effects when burned [1]. Environmental concerns arising from the use of nondegradable plastics have resulted in search for suitable substitutes [2-5]. In the recent years concern is growing in finding new ways to utilize biopolymers such as polysaccharides, proteins and lipids to create biodegradable films due to their ready availability, sustainability and contribution to the reduction of environmental pollution and simplified end-of-life disposal issues [2-5]. High barrier packaging materials require low oxygen permeability with good mechanical strength. Replacing existing oxygen barriers such as aluminum and synthetic polymers with biopolymers is a research topic of increased interest. Early studies examined the use of chitosan, starch and cellulose derivatives to address these challenges and were shown to have good film forming behavior [6]. Xylan which is the most abundant of the hemicelluloses found in the cell wall of the land plants has been used to enhance the strength properties of cellulosic fiber networks [7]. In addition, glucuronoxylan isolated from aspen has been used to produce films [8, 9] which show improved strength properties when plasticized with xylitol or

sorbitol. Such films have exhibited good oxygen barrier properties with respect to control glucuronoxylan films. Höije et al. [10] have shown that arabinoxylan film can be prepared from the extracts of barley husks without the need for plasticizers. The resulting films were stiff and rather brittle with high water content. Dammström et al. [11] prepared composite films of glucuronoxylan reinforced with bacterial cellulose and showed that they formed transparent strong films. The use of xylan for the production of biodegradable composite films in combination with wheat gluten has been investigated [12]. The presence of xylan did not adversely affect the film forming quality or the water vapor transmission rate, though the mechanical and solubility properties depended on the xylan type, compositions and process conditions. Acetylated galactoglucomannan (AcGGM) hemicellulose was found to be an excellent candidate for making new renewable barrier materials [13]. The oxygen barrier permeability of the AcGGM films were found to be similar to, or lower than, the values reported on oxygen barrier films made from glucuronoxylan [8] and other polysaccharides, such as starch [14], chitosan [15] and mixtures of various polysaccharides [16]. The rate of water vapor transmission rate is considered to be an important property for many film packaging applications because it may influence both shelf life and product stability. Tock et al. [17] has reviewed the permeability and water vapor transmission rate properties of commercial polymeric films and provided an early overview of how structural changes, such as crystallinity, and the presence of plasticizers and lamination could influence the barrier properties of polymer films.

In view of the importance of polymeric barriers, many authors have explored ways in which biopolymers including cellulose can be utilized in packaging. Cellulose is

the most abundant biomaterial, and a lot of attention is now given to find new ways of utilizing this biopolymer to create environmentally benign biobased materials [3, 18, 19-21]. Cellulose and its derivatives are known to display a variety of structural motifs such as nanosized cellulose whiskers and spheres, microsized cellulose fines, cholesteric superstructures containing long range order, and hierarchical morphologies like raw wood whose elements cover many length scales [22]. It is well known that native cellulose, when subjected to strong acid hydrolysis, can be readily hydrolyzed to micro or nanocrystalline cellulose (NCC) [7, 23-24]. The length of the nanocellulose crystals is dependent on the sample origin but typically they are 100 – 300 nm in length and 5 – 20 nm in width [25-28]. Nanocrystalline cellulose has high aspect ratio (length/diameter) between 30-150 depending on the source from which it is obtained and also the condition under which it is isolated [29-30]. NCC has higher strength than steel and higher stiffness than aluminum, with its elastic modulus and bending strength being reported as 138-167 and 10 GPa respectively [31-33]. The properties of nanocomposite materials and their property enhancements depend not only on their individual constituents but also on the interaction between the matrix and the reinforcing phases and their morphology [34, 35]. NCC can provide excellent properties when they are incorporated within a polymer matrix and act as reinforcing filler.

Indeed, it is already known that cellulose whiskers can be used as the reinforcement in polymer matrices, and to prepare high strength composite materials including composites from polyvinylchloride [36-38], polypropylene [39], polyoxyethylene [40-42] and cellulose acrylic latex films [43]. By employing 6% cellulose whiskers derived from tunicate cellulose in latex polymerized from styrene and

butyl acrylate, it has been possible to produce composite films exhibiting a twofold increase in the shear modulus over control films containing no whiskers. Aqueous and solvent solution casting is the most common method of preparing cellulose nanocomposites [5, 30, 43-46]. However, Oksman and co-workers have utilized a twin screw melt-extrusion of cellulose nanocomposites with polylactic acid and cellulose acetate butyrate. Lagaron et al. [47] discussed the role of crystalline structure of polymers and emphasized that high crystallinity improves barrier properties. Nanocrystalline cellulose is greater than 60% crystalline [48-49] and this property together with the resulting rigid hydrogen-bonded network of nanocrystalline cellulose can cause an increase in tortuosity and reduction of pore size for nanocomposites which may be utilized to create high barrier materials. In a recent study, spruce galactoglucomannans (GGM) and konjac glucomannan (KGM) were mixed with nanocrystalline cellulose (NCC) to study the mechanical and barrier properties of the films [50-51].The system we have considered here is xylan-nanocellulose composite system wherein cellulose particles are used as reinforcement for improving mechanical and barrier properties of xylan.

The hypothesis of this thesis is that incorporation of nanocellulose whiskers in the traditional “green polymers” can be utilized to develop novel xylan nanocomposite films with enhanced structural and physical properties. To verify hypothesis, the work presented in the following chapters of this thesis required synthesizing different types of composites, described below, for understanding the reinforcement mechanism in xylan-cellulose composites and factors influencing composite properties. Chapter 4 presents our understanding of the influence of nanocellulose whiskers on the mechanical properties of plasticized xylan and and the effect of the addition of nanocellulose particles on

composite properties. For this, a composite system of xylan and nanocellulose particles - was synthesized using solution processing techniques and containing 0-10 % by weight of nanocellulose whiskers. Chapter 5 presents the understanding of the influence of nanocellulose whiskers on water transmission properties of neat xylan and xylan nanocellulose composites and the effect of nanocellulose particle addition on composite properties. For this a composite system containing xylan and nanocellulose particles - was synthesized using solution processing techniques and containing 0-50 % by weight of nanocellulose whiskers. Chapter 6 presents the study of the influence of types of reinforcing agents such as acacia fibers, softwood fibers and cellulose whiskers on composite properties. The particle morphology may be changed via hydrochloric or sulfuric acid hydrolysis. This also affects the charge on surface. Xylan films reinforced with hydrochloric acid and sulfuric acid prepared nanocrystalline cellulose whiskers were then compared against acacia and softwood bleached kraft fibers. The bleached acacia kraft fiber has been selected because it is one of the shortest commercially available pulp fibers with a weighted length of 0.62 mm and width of ~0.02 mm and yet is approximately 4000 orders of magnitude larger than the cellulosic whiskers. This leads to xylan and sulfonated nanocellulose whiskers, xylan and hydrochloric acid made nanocrystalline cellulose, xylan and softwood fibers and xylan and acacia fibers composite samples. Chapter 7 presents the influence of nanocellulose whiskers on oxygen transmission properties of neat xylan and xylan nanocellulose composites and the effect of nanocellulose particle addition on composite properties. For this a composite system of xylan reinforced with nanocellulose particles has been synthesized using solution processing techniques and containing 0-50 % by weight of nanocellulose

whiskers**.** Chapter 8 presents results on fundamental studies on the structure-property relationship of high strength and barrier nanocomposite films. It also includes results on the mechanical properties, transverse relaxation of nanocomposites and the interaction of nanofillers with the xylan matrix. Finally, Chapter 9 summarizes the findings in each chapter.

CHAPTER 2

LITERATURE REVIEW

2.1 Cellulose

Cellulose is a biopolymer which is renewable, biodegradable and is considered to be the most abundant renewable polymer on Earth [52]. It can be obtained from various sources such as trees, algae, fungi, tunicates and bacteria. Cellulose is a polydispersed linear polymer consisting of β-D-glucopyranose units linked by a glucoside bond between their C-1 and C-4 hydroxyl groups. Figure 1 shows the structure of cellulose in its chair configuration.

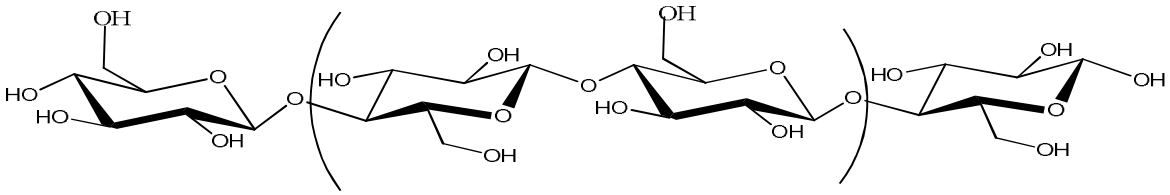

Figure 1. Molecular structure of cellulose

Cellulose can be considered as a syndiotactic polyacetal of glucose. The C-1 hydroxyl at one end of the molecule is an aldehyde hydrate group with enhanced activity. In contrast to this, the C-4 hydroxyl on the other end of the chain is non-reducing [53]. The chemical character of the cellulose molecule is determined by the β-glucosidic linkage between the glucose repeating units, to hydrolytic attack, and by the presence of three reactive hydroxyl groups, one primary and two secondary, in each of the base units.

These reactive hydroxyl groups are able to undergo etherification and esterification reactions. The main cause for the relative stiffness and rigidity of the cellulose molecule is the intra- and inter-intermolecular hydrogen bonding, which is reflected in its high viscosity in solution, its high tendency to crystallize and the ability to form fibrillar strands [54]. The chain length of cellulose expressed in the number of constituent AGUs (degree of polymerization, DP) varies with the origin and treatment of the raw material. Acid-chlorite delignification of lignocellulosic material followed by alkali treatment technique for cellulose isolation has been used by several studies prior to the measurement of cellulose DP [55, 56-60]. Cellulose has to be purified or isolated from its native source in order to adequately determine it's DP [61, 62]. The two most commonly used techniques to measure the DP of cellulose are the viscometry and the gel permeation chromatography (GPC) methods. Cellulose tricarbanilate (CTC) is the most utilized derivative for GPC studies. DP values of several native woody and non-woody cellulose samples are listed in Table 1 [63]. It appears from the data in Table 1 and also as stated by Kumar et al. that viscometry is more popular in determining DP of cellulose in lignocellulosic biomass [55]. The viscometry technique involves dissolving cellulose in 0.5 M cupriethylenediamine solution. According to the TAPPI T 230 om-08 method, dry cellulose is added to distilled water and followed by cupriethylenediamine solution, with continuous nitrogen flushing. Shaking and heating might be required to solubilize cellulose. The intrinsic viscosity is then measured for the resulting homogeneous solution. A Cannon-Fenske capillary viscometer is used in the measurements. A reasonable good approximation to degree of polymerization is obtained by multiplying intrinsic viscosity by 190 [64, 65]. The degree of polymerization D.P. = $260[\eta]_{Cu\ Am}$ =

260/1.365 $[\eta]_{C.E.D.}$ = 190.5 $[\eta]_{C.E.D.}$. The subscripts CuAm and C.E.D. stand for cuprammonium and cupriethylenediamine, respectively. The cellulose DP lies in the range of 1500 – 4500 which includes sources from agricultural residues, such as bagasse and wheat straw, have lower cellulose DP (~1000) than hardwoods and soft woods, which possess higher DP cellulose in the range of 4000–5500. Hardwoods, such as poplar and aspen, have cellulose DP values of 3500 and 4500, respectively. Sweet et al. [59] and recently Hallac and Ragauskas et al. [63] reported a DP of 1450 for α-cellulose of southern pine, which is significantly less than the DP values reported for hardwoods. The molecular weight distribution of α-cellulose of southern pine was measured by gel permeation chromatography. The DP for α-cellulose of southern pine was determined by dividing the measured molecular weight of the cellulose tricarbanilate by the molecular mass of a single cellulose tricarbanilate unit.

Table 1. DP of native and non-woody celluloses [55, 66-69].

Species	Measurement Technique	DP
Native Southern Pine	CTC and GPC	1450 [59, 63]
DDGS	Cuen and Viscometry	2243
Corn kernels	Cuen and Viscometry	1693
Dhaincha	Cuen and Viscometry	2520
Cotton stalk (cellulose isolated using steam explosion technology)	Cuen and Viscometry	1820
Jute fiber	Cuen and Viscometry	3875
Wheat straw	Cuen and Viscometry	2660
Rice straw	Cuen and Viscometry	1820
Corn stover	Cuen and Viscometry	2520
Poplar	Cuen and Viscometry	3500
Aspen	Cuen and Viscometry	4581
Nalita (12 months)	Cuen and Viscometry	3181
Nalita (18 months)	Cuen and Viscometry	3383
Nalita (24 months)	Cuen and Viscometry	3518
Nalita (30 months)	Cuen and Viscometry	3611

In agricultural residues DP varies over a range of 1800-4000. The isolation of cellulose from cotton stalk was done using steam explosion technology at 220 °C for 5 min and this biomass was found to have a DP of 1820. Cellulose in jute fiber has a large DP value when compared to corn kernels, cotton stalks, wheat straw, and rice straw. It is therefore important to keep in mind that the length of polymer chains varies according to the source of cellulose or even with respect to the part of the fiber where analysis is performed [70].

2.2.1 Crystalline Structure of Cellulose

Cellulose is known to exist in several crystalline forms. Cellulose I, the dominant form in nature [71], consists of a microfibrillar crystalline array of linear β-1, 4-glucan chains, all of which are oriented parallel to one another with the same polarity [72]. The cellulose I allomorph is the thermodynamically metastable form of cellulose [73]. There are two known suballomorphs of cellulose I first discovered by Atalla & VanderHart in 1984 [74] using NMR and later confirmed by Wada et al. [75] using electron diffraction (cellulose I_α and cellulose I_β). The ^{13}C CP-MAS spectra of cellulose I_α has singlets at C-1 and C-6 and a closely spaced doublet at C-4. The cellulose I_β has doublets at C-1, C4 and C-6. Of these two forms, cellulose I_β is thermodynamically more stable. The two forms of celluloses in which I_α is dominant in celluloses from lower plants on the other hand I_β is dominant in celluloses from higher plants where the major component is secondary wall [74]. Table 2 summarizes the I_α fractions in specimens of various origins [76]. Nishiyama et al. [50] reported that tunicin, the cellulose from tunicate—a sea animal—consists of nearly pure (around 90%) I_β phase. On the contrary, freshwater alga Glaucocystis sp. consists of nearly pure (around 90%) I_α cellulose.

Table 2. I_α fractions in specimens of various origins [76].

Sample	Iα fraction
Cladophora	0.76
Valonia ventricoa	0.64
Boergisenia foebesii	0.55
Annelaed cladophora	0.24
Glaucocystis sp	0.90
Tunicin	0.10
Western yellow pine	0.62
Yellow cedar	0.62
Eucalyptus	0.68
Tanbark-oak	0.56

Cellulose I_α has a triclinic one-chain unit cell where parallel cellulose chains stack, via van der Waals interactions, with progressive shear parallel to the chain axis. Cellulose I_β has a monoclinic two-chain unit cell, which means parallel cellulose chains are stacked with alternating shear [77]. Furthermore, it has been shown that cellulose I_α transforms into cellulose I_β without losing its crystallinity, by hydrothermal treatment [78-80] or by treatments with various solvents. In these two lattices, *i.e.*, I_α and I_β, the conformation of the polysaccharide chains is similar although the hydrogen-bonding pattern is different [48]. Both phases show hydrogen bonding only between polymer chains inside a layer of chains. Figure 2a and 2b shows atomic arrangement and hydrogen bonding network in cellulose I_α and cellulose I_β [50].

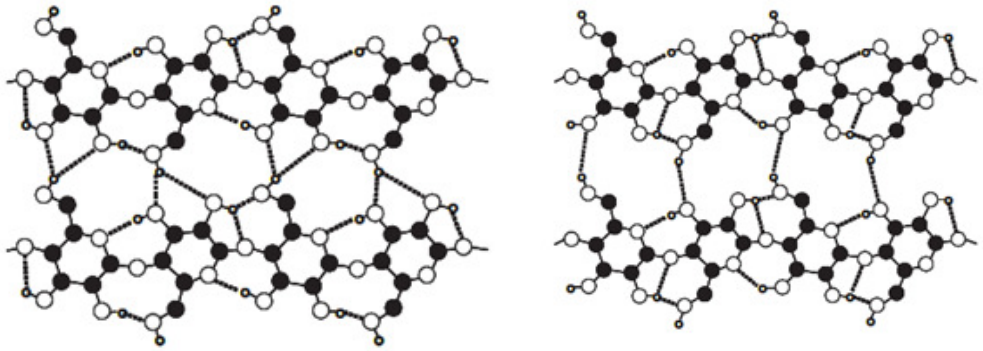

(a) (b)

Figure 2. (a) Atomic arrangement and hydrogen bonding network in cellulose I_α. Hydrogen bonding is indicated by dotted lines (b) hydrogen bonding network in cellulose I_β [50]

Cellulose I is responsible for mechanical properties of reinforced composites due to its high modulus of elasticity and crystallinity. Table 3 summarizes the degree of crystallinity and the lateral dimension of elementary fibrils from several cellulose samples measured by X-ray diffraction (XRD).

Table 3. Degree of crystallinity (W_C) and lateral dimension (D) of elementary fibrils from
several cellulose samples [81- 84, 45].

Sample	W_C, %	D, nm
Natural softwood/hardwood cellulose	60-62	3-4
Isolated sulfite cellulose	62-63	5-6
Isolated Kraft cellulose	64-65	6-7
Natural cotton cellulose	68-69	5-6
Isolated cotton cellulose	70-72	7-8
Natural flax or ramie cellulose	65-66	4-5
Isolated flax or ramie cellulose	67-68	6-7
Bacterial cellulose	75-80	7-8
Algae cellulose	75-80	10-15

2.2.2 Amorphous Regions

Besides the crystalline region, cellulose also has bundles of amorphous regions [85]. Amorphous cellulose is also located between cellulose microfibrils [86]. In the amorphous regions the cellulose chains are randomly oriented in a spaghetti-like arrangement leading to a lower density in these domains [87]. This makes the amorphous regions susceptible to attack by acids. Wide-angle X-ray scattering has been used to study possible structures for amorphous cellulose. Diffraction studies show light and dark areas along a cellulose microfibril, which have been attributed to crystalline and amorphous cellulose, respectively [85]. Cellulose from cotton has a high amount of crystalline cellulose and a small amount of amorphous cellulose. On the other hand, regenerated cellulose has relatively higher amount of amorphous cellulose. The high amorphous fraction in cellulose means high accessibility of chemicals to cellulose structure. A schematic of amorphous cellulose and crystalline cellulose is shown in Figure 3. Disordered domain (DD) represents amorphous cellulose and ordered region is crystalline cellulose [86]. In the amorphous or less ordered regions the cellulose chains are not so tightly packed and thus they are more available for hydrogen bonding to other molecules such as water.

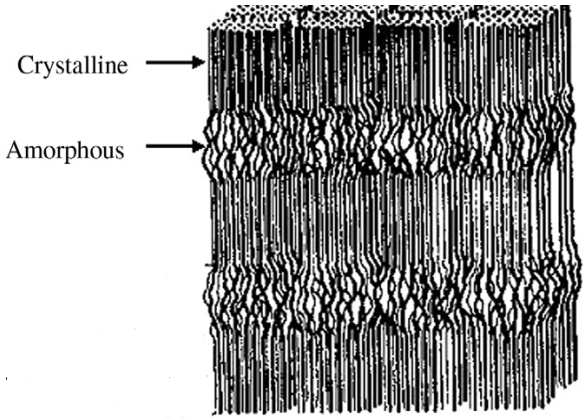

Figure 3. Schematic of amorphous cellulose and crystalline cellulose [86]

In nature, cellulose chains forms microfibrils due to hydrogen bonding between hydroxyl groups of adjacent molecules, within which highly ordered crystalline regions alternate with less ordered amorphous regions [33]. The molecular arrangement of these fibrillar bundles is called microfibrils, within which highly ordered crystalline regions alternate with less ordered amorphous regions [33]. The microfibrils are about 10-30 nm wide and containing cellulose molecules of a degree of polymerization from 2×10^3 to 6×10^3 [33]. The range of microfibrils diameter of various cellulose samples are listed in Table 4. Figure 4 shows the schematic of hierarchical structure of wood [88].

Table 4. Range of diameters of microfibril of various cellulose samples [89].

Sample	Microfibril diameter (nm)
Bacterial cellulose	4-7
Cotton linters	7-9
Ramie	10-15
Dissolving pulp	10-30
Valonia cellulose	10-35

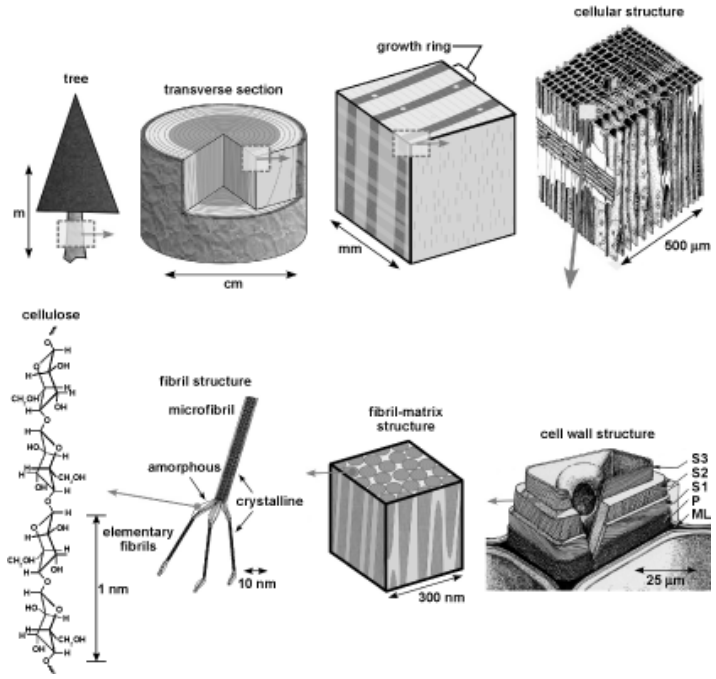

Figure 4. The schematic of hierarchical structure of a wood from wood to nanoscale [88]

Since the cell walls differ in their composition and in the orientation of the microfibrils, the mechanical properties of cellulose fibers depend on the cellulose content and the spiral angle of the fibril. The modulus of elasticity of the perfect crystal of cellulose has been calculated by several authors and it has been estimated to lie between 130 to 250 GPa, while the tensile strength is assessed to be approximately 0.8 to 10 GPa [90].

The wood pulp fibers have multiscale characteristics; roughly typical lengths of fibers are 1 to 2 mm for hardwood, 3 to 7 mm for softwood and typical widths are 10 to 50 µm [91]. The dimensions of fibers derived from different sources are shown in Table 5. High resolution electron micrographs of negatively stained specimens of cellulose show that the microfibrils are comprised of regular subfibrils, termed “elementary” fibrils, which have a width of 35 Å. The microfibrils of *Valonia* (algal) cellulose have cross-sectional dimensions of ~200 X100 Å and cotton microfibrils vary in width from

~100 to ~500 Å. The major differences between celluloses from different sources occur in the packing of the elementary fibrils within the microfibril; this packing is expected to be dictated by the biosynthesis conditions. Crystallite widths which lie between the elementary and microfibril widths occur for most celluloses. It has been suggested that when the elementary fibrils are assembled to form the microfibril, some lateral fasciations occurs giving rise to the larger crystallites. It is clear that many of the physical and mechanical properties of cellulose materials will depend on the nature of this array.

Table 5. Length and width of selected natural fibers [92].

Species	Fiber length, mm	Fiber width, μm
Acacia	0.62-0.75	0.02
Aspen	0.7-1.6	20-30
Kenaf (Core)	0.4-1.1	18-37
Kenaf (Bast)	1.4-5.0	14-23
Southern Yellow Pine softwood kraft fibers	2.7-4.6	32-43
Douglas- fir	2.7-4.6	32-43
Birch	1.1-1.5	16-22

The fiber wall thickness is roughly between 1 and 5 μm (Figure 5). The fiber wall is composed of defined layers (Figure 5b), including the primary wall (P) and several secondary wall layers (S1, S2 and S3). Each of these layers is characterized by a specific arrangement of fibrils. Chemical pulp fibers have a surface, which is characterized by a particular pattern created by wrinkles and microfibrils in the outer layers of the fiber wall structure (Figure 5a). The S2 layer is characterized by a structure of microfibrils organized in a helical manner [93]. Using transmission electron microscopy researchers

have attempted to disintegrate cellulose fibers into single microfibrils/elementary fibrils for ultra structural studies.

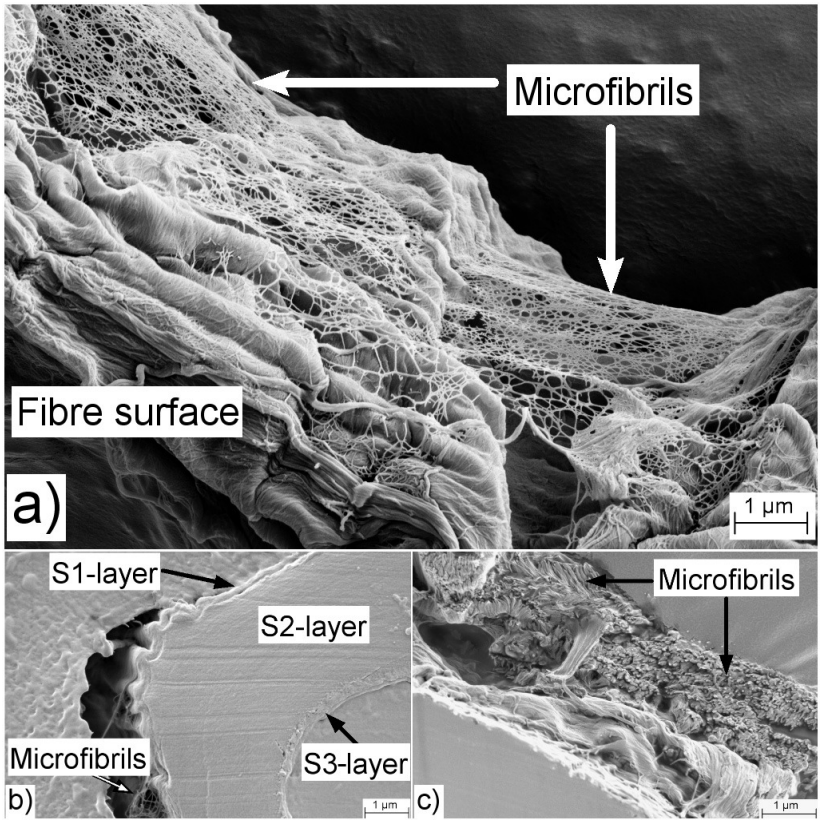

Figure 5. Structure of wood pulp fibers. (a) The network of microfibrils covering the outer wall layer. (b) Microtomed cross section showing the S1, S2 and S3 layers. (c) Cross-sectional fracture area, showing the microfibrils in the S2 layer. Reproduced with modification from Chinga-Carrasco [91]

2.3 Cellulose Whiskers

In the 1950s, Ranby reported for the first time that colloidal suspensions of cellulose nanocrystals can be obtained by controlled sulfuric acid-catalyzed degradation of cellulose fibers [94, 95-97]. Crystal dimension and degree of crystallinity of elementary fibrils from several cellulose samples are dependent on the origin of cellulose. Algal and tunicate cellulose microfibrils yield nanocrystals that are several micrometers in length whereas wood microfibrils yield much shorter nanocrystals of only a couple of hundred

nanometers [20]. Cellulose whiskers from wood are 3-15 nm in width and 100-200 nm in length, while those for Valonia, a sea plant, are reported to be 20 nm in width and 1000-2000 nm in length. Likewise, the average dimensions of crystallites produced from cotton are about 4-10 nm in diameter and 100-300 nm in length [29] and tunicate, a sea animal, gives particles of ca. 10-20 nm in width and 500-2000 nm in length [98]. The length and width of cellulose whiskers obtained from various sources are listed in Table 6. Morphologies of cellulose nanowhiskers have been studied by several authors. A few representative images drawn from published literature are shown in Figure 6. The hydrolysis of cellulose with strong hydrochloric or sulfuric acid induced a rapid decrease of its degree of polymerization (DP) toward a lower value – the so called level-off DP (LODP) – that remained constant for quite a while, even during prolonged hydrolysis. The value of LODP has been shown to depend on the cellulose origin: typical values of 250 being recorded for hydrolyzed cotton, 140 –200 for bleached wood pulp and up to 6000 for the highly crystalline Valonia cellulose. These individual crystallites (nanofibrils) have been calculated to have tensile strength of 10 GPa and modulus of 150 GPa [99]. The bending strength that is nearly one-sixth of the corresponding value (63 GPa) for carbon nanotubes whose tensile strength is predicted to be as high 300 GPa at modulus of 1 TPa [100-101]. The moduli and the specific moduli (modulus/density) of a number of commonly used engineering materials are reported in Table 7, which show that the specific modulus of crystalline cellulose exceeds engineering materials such as steel, concrete, glass and aluminium.

Table 6. Examples of the Length (L) and Diameter (D) of CNs from various sources obtained by different techniques.

Source	L (nm)	D (nm)	Reaction Conditions	Ref
Bacterial	100-1000	10-50	65% sulfuric acid;75°C	[102]
	100-1000	5-10 × 30-50		[103], [104]
Cotton	100-150	5-10	65% sulfuric acid, 60 min, 45°C	[105]
	70-170	~ 7	64% sulfuric acid, 120 min, 60°C	[106]
	200-300	8	64% sulfuric acid, 120 min, 45°C	[107]
	255	15		[108]
	150-210	5-11		[109]
Cotton linter	100-200	10-20		[110]
	25-320	6-70		[25]
	300-500	15-30		[111]
Microcrystalline Cellulose	35-265	3-48	63.5% sulfuric acid,2 hour	[25]
	250-270	23		[112]
	~500	10		[113]
Ramie	150-250	6-8		[114]
	50-150	5-10		[115]
Sisal	100-500	3-5	65% sulfuric acid, 15 min, 60°C	[116,117]
	100-several microns	10-20	55% sulfuric acid, 20 min, 60°C	[116,117]
Tunicate	500- 1-2 microns	10	55% sulfuric acid, 20 min, 60°C	[119]
	500-1-2 microns	15	60%, 30 min, 65°C	[118]
	1- several microns	10-20 nm	55%, 20 min, 60°C	[119]
	1-2 microns	8-15 nm	65%, overnight, room temp	[120]

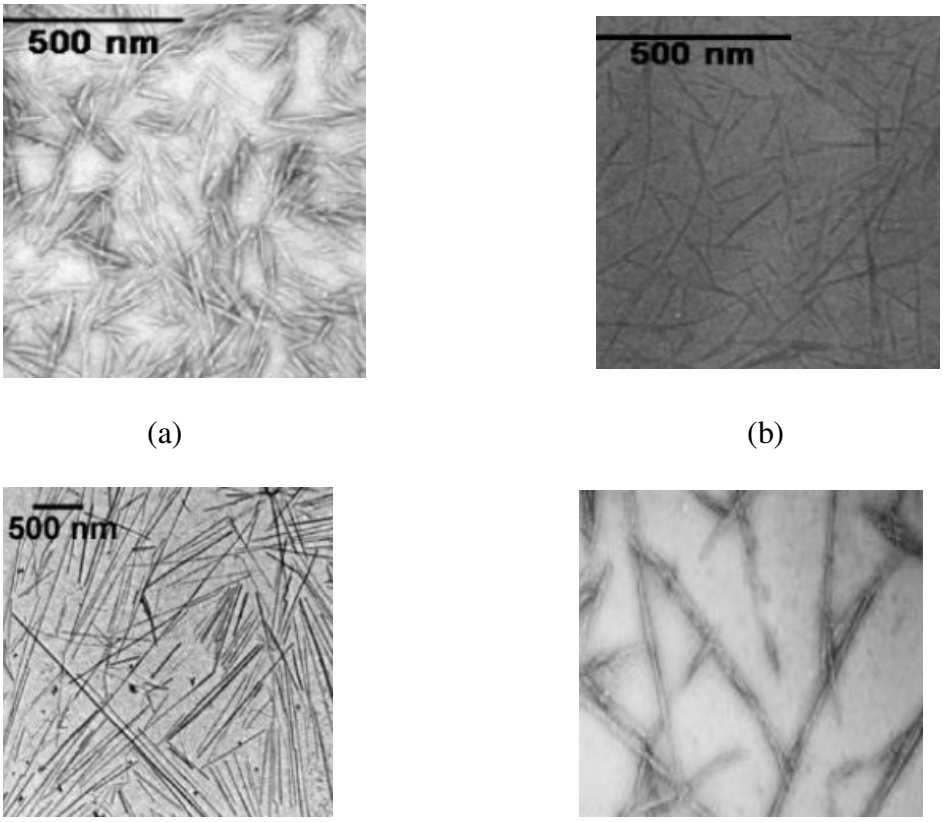

Figure 6. Transmission electron microscopic images of cellulose whiskers from a dilute suspension of hydrolyzed (a) cotton [3], (b) sugar-beet pulp [3] (c) tunicin [3] and (d) bacterial cellulose [45]

Table 7. Moduli of engineering materials compared to cellulose.

Material	Modulus (GPa)	Density (mg/m^3)	Specific Modulus ($GPa\ mg^{-1}\ m^3$)	Reference
Aluminum	69	2.7	26	[121]
Steel	200	7.8	26	[121]
Glass	69	2.5	28	[121]
Cellulose whiskers	138	1.5	92	[122]

2.4 Cellulose Whiskers Preparation

Araki et al. [123] compared the effects of using sulfuric acid or hydrochloric acid to produce stable suspensions of cellulosic nanocrystals. Sulfuric acid provides more stable aqueous suspensions of nanocrystals than hydrochloric acid [123]. The use of sulfuric acid results in esterification of the surface hydroxyl groups of cellulose nanocrystals to give charged sulfate groups [14, 20, 95]. It has been suggested that the introduction of negative charge on the surface of sulfuric acid-prepared nanocrystals gives more stable dispersion [52] than hydrochloric acid prepared cellulose nanocrystals which have a lower surface charge. HCl-whiskers of SW kraft pulp were reported to be approximately 180 nm in length and 3.5 nm in width, while cotton yielded HCl-whiskers were around 100 nm in length and 5-10 nm in width [123, 124, 125]. The acid hydrolysis of cellulose fibers is a heterogeneous acid diffusion process wherein the hydronium ions are able to penetrate the less ordered amorphous domains of cellulose chains and promote the hydrolytic cleavage of the glycosidic bonds. The reaction proceeds until all the accessible glycosidic bonds are hydrolyzed [126]. Dong et al. have shown that a temperature of 45 °C and time of 60 min provide optimum conditions to achieve complete hydrolysis of the amorphous regions of cellulose to produce particle lengths in the order of 200 nm [73]. Recently, cellulose nanowhiskers were also prepared by sulfuric acid hydrolysis of cotton fiber [127], microcrystalline cellulose (MCC) [128-129] and sisal fiber [130] by following the same general procedure described above.

A comprehensive compilation of preparative conditions employing sulfuric acid hydrolysis and the average dimensions of cellulose nanowhiskers derived from different sources is shown in Table 8.

Table 8. Dimensions of cellulose nanowhiskers prepared under different sulfuric acid hydrolysis conditions [20, 28, 29, 123, 131, 132, 106, 116, 124, 127-129, 133-136].

Cellulose source	H_2SO_4 conc., % (w/w)	Time, min	T,°C	Acid/cellulose, mL/g	Dimension, length (nm)×width (nm)
Bleached	64	10	70	8.78	~200×5
softwood	60	20	<70 °C	8.75	~200×5
kraft pulp	65	10	70	10	185± 75×3.5
	65	60	45	8.75	185± 75×3.5
	64	45	45	17.5	100-250×5.15
Bleached	64	25	45	8.75	147± 7×3.5
hardwood	64	25	45	8.75	141± 6×3.0± 0.3
kraft	64	45	45	17.3	120± 5×4.9± 0.3
pulp	64	45	45	8.75	105± 4×4.5± 0.3
Cotton	64	120	45	8.75	~200×5
	64	60	45	8.75	115±10×~7
	64	45	45	17.5	176± 21× 13± 3
	64	120	60	8.33	70-130×10-20
	65	60	45	8.75	100-150×5-10
Sisal	65	15	60	16.2	~250×4
Flax	64	240	45	8.33	327± 108×21± 7
Wheat straw	65	60	25	34.3	150-300× ~5
MCC	63.5	130.3	44	10	200-400×<10
	64	300	45	8.75	41-320×<100
	64	180	45	17.5	60-120×8-10
	64		45	8.75	100-225×10-15

The penetration of H_3O^+ ions into the crystallites and the actual cleavage of the glycosidic bond depend on the hydrolysis conditions, including the type of the acid used, duration and temperature of hydrolysis as well as acid concentration [137]. The probable mechanism of acid hydrolysis is depicted in Figure 7. Hydrolysis of cellulose with sulfuric acid involves protonation of glucosidic oxygen (path 1) or cyclic oxygen (path 2), followed by dissociation of glucosidic bonds induced by the addition of water (Figure 7) [126]. This hydrolysis process yields two fragments with shorter chains while preserving the basic nature of the chain polymer. Beside chain scission, cellulose hydrolysis with sulfuric acid also involves esterification of the hydroxyl groups. The presence of sulfate groups on the cellulose nanocrystal surfaces results in negatively charged surfaces above acidic pH. A colloidal gel was observed at the beginning of dialysis when the cellulose nanocrystals suspension was still acidic, then disappeared as the pH became neutral with the removal of the residual acid.

In suspension, cellulose nanocrystals have a strong propensity to align along a vector director because of their rigid rod-like shape. This alignment produces a macroscopic birefringence that can be directly observed through crossed polarizers. The first observation of the birefringent nature of cellulose nanocrystals was made by Marchessault et al. [138]. When the cellulose nanocrystals suspension reaches a critical concentration a chiral nematic ordered phase displaying optical characteristics can be formed [106,139]. A colloidal gel is observed at the beginning of dialysis when the cellulose nanocrystals suspension is still acidic, then it disappears as the pH becomes neutral with the removal of the residual acid. In order to avoid the possible desulfation of the sulfate groups on the surface of the cellulose nanocrystals, ultrasonic treatment was

carried out in an ice bath [126]. The degree of sulfonation relies highly on the acid to cellulose ratio and the reaction time as shown in Table 9

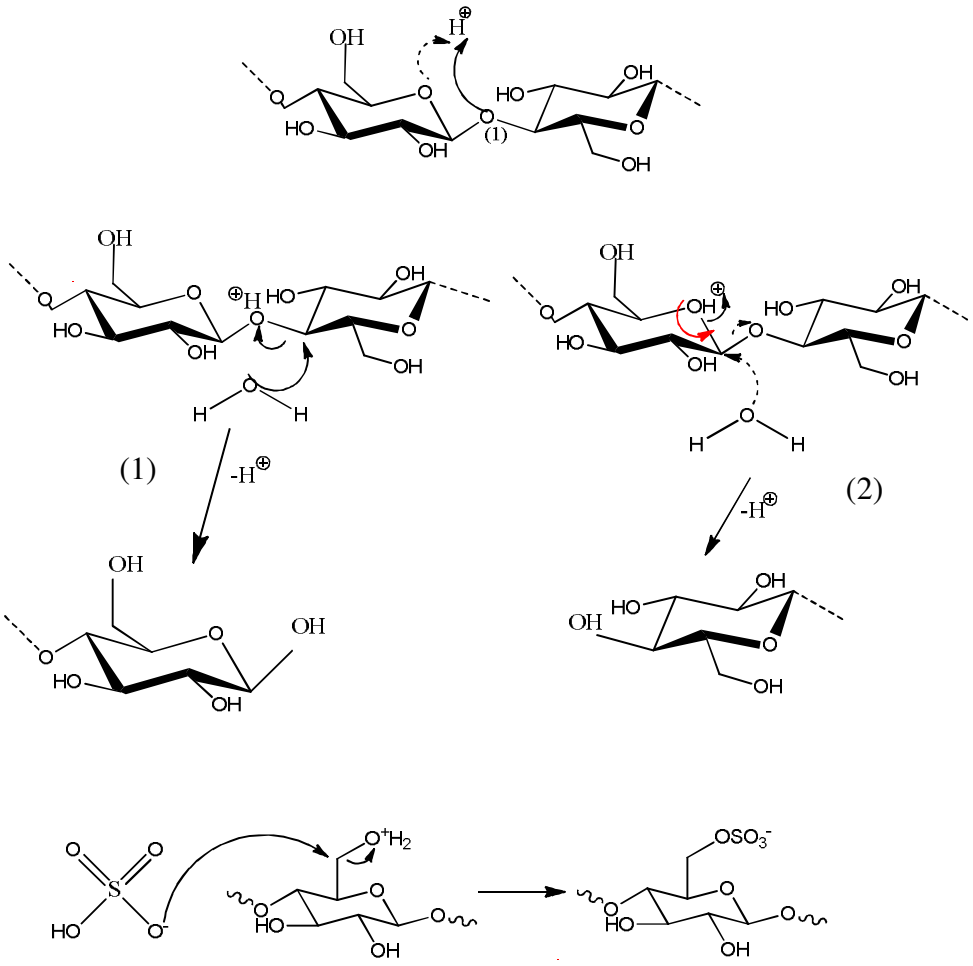

Figure 7. Mechanism of acid-catalyzed hydrolysis of cellulose

Table 9. Effect of sulfuric acid (72%, w/w) hydrolysis condition on the degree of sulfonation of linen pulp [140].

Pulp: Sulfuric acid	Reaction time, min	Sulfur content[a],%	Degree of substitution[b]
1:4	16	49.54	1.67
	17	59.29	2.00
	45	56.67	1.91
1:6	15	59.11	1.99
	19	59.84	2.02
	18	46.26	1.56
1:8	15	62.26	2.10
	20	59.44	2.01
	45	53.70	1.79
1:10	15	60.70	2.05
	23	63.10	2.13
	22	61.50	2.08

[a]Sulfur content is the percentage of sulfur groups based on the total number of hydroxyl and sulfur groups; [b]degree of substitution (DS) is calculated as the average number of hydroxyl groups in the anhydroglucose that are substituted in the particular product

The effect of hydrolysis condition on the appearance of cellulose nanowhiskers suspension is illustrated in Table 10 [131].

Table 10. Effect of hydrolysis condition on the appearance of cellulose nanowhiskers suspension [131].

Sample	T, ºC	Appearance of the suspension	Yield, % (w/w)
1	25	White with pulp particles	89.8
2	25	Ivory white, viscous	34.4
3	45	Ivory white, viscous	43.5
4	65	Yellow, very viscous	48.1
5	65	Black	N/A

Depending on reaction conditions, the appearance of the whiskers suspension could be white with some starting pulp particles (low yield), ivory white viscous suspension (optimal), yellowish or even black viscous suspension (over hydrolyzed) [131]. A temperature of 45 °C yielding an ivory-white suspension in one hour was considered to be optimal for the production of cellulose nanowhiskers via sulfuric acid hydrolysis. The effect of temperature and time of hydrolysis and the duration of the subsequent ultrasonication on the properties of cellulose nanowhiskers were investigated [131] according to an experimental setup illustrated in Table 11.

Table 11. Effect of sulfuric acid hydrolysis time at 45 °C on the sulfur content and length of cellulose nanowhiskers [131].

Sample	Hydrolysis time, min	Sulfur content	Whisker length, nm
1	10	0.53	390
2	20	0.50	332
3	30	0.58	276
4	45	0.62	226
5	60	0.69	197
6	120	0.74	179
7	240	0.75	177

It was also found that the total sulfur content and surface charge of nanowhiskers gradually increased upon increasing the hydrolysis reaction time from 10 to 240 min at 45°C. The average whisker size decreased in the early stage of the hydrolysis and a relatively stable dimension was achieved after 1 hour as summarized in Table 12. Compared to the hydrochloric acid procedure, sulfuric acid hydrolysis needs lower temperature and acid to cellulose ratio, and less time to produce whiskers of similar

dimensions. Moreover, it was proposed that the static electrical repulsion between negatively charged sulfate anions resulted in a more stable suspension instead of easily aggregated whiskers and it was the same reason given for the time independence of suspension viscosity [141].

Table 12. Effect of ultrasonic treatment on the length and surface charge of cellulose nano whiskers [131].

Treatment time, min	Whisker length, nm	Sulfur content
1	214	0.484
2	205	0.487
3	182	0.482
10	183	0.489
20	176	0.507
40	182	0.503

Also, although the particle size decreased during the first 5 min of ultrasonic treatment, no further change was observed upon extended treatment [131]. Formation of well separated grass cellulose nanowhiskers was reported by Korean scientists [142]. While 15 min ultrasonication gave nanowhiskers, 5 min ultrasonication resulted in only 40-50 nm thick agglomerates. Subsequently, Beck-Candanedo et al. [20] also investigated the effect of hydrolysis time on the properties and behaviors of cellulose nanowhiskers. In these studies, bleached black spruce sulfite pulp and bleached eucalyptus kraft pulp were treated with 64% (w/w) sulfuric acid at 45 °C at two acid-to-pulp ratios for two reaction (see table 13 for details). It was shown that longer hydrolysis time produced shorter, less polydispersed whiskers while increased acid to cellulose ratios reduced whiskers dimensions. Chiral nematic pitch decreases with increasing cellulose concentration and decreasing nanocrystal length. Above a critical concentration,

the suspensions spontaneously form an anisotropic chiral nematic liquid crystal phase [20]. The effect of reaction conditions on suspension properties is shown in table 14.

Table 13. Experimental conditions: Reaction time and acid-to-pulp ratios [131].

Sample	Pulp source	Reaction time, min	acid-to-pulp ratios mL/g
E	eucalyptus	25	8.75
S1	black spruce	25	8.75
S2	black spruce	45	8.75
S3	black spruce	45	17.5

Table 14. Effect of reaction conditions on suspension properties.

	E	S1	S2	S3
nanocrystal length, L	147±7 nm	141±6 nm	120±5 nm	105±4 nm
standard deviation in L	65 nm	60 nm	45 nm	36 nm
nanocrystal diameter, D	4.8±0.4 nm	5.0±0.3 nm	4.9±0.3 nm	4.5±0.3 nm
axial ratio, L/D	30.6	28.2	24.5	23.3
sulfur content	0.80±0.03 S%	0.89±0.06 S%	1.06±0.02 S%	0.86±0.02 S%
surface charge density	0.29±0.01 e/nm^2	0.33±0.02 e/nm2	0.38±0.01 e/nm2	
critical concentration, c	4.6 wt %	4.8 wt %	5.3 wt %	6.9 wt %
chiral nematic pitch, P	21μm	18μm	10μm	7μm

To optimize the isolation of cellulose nanowhiskers, Bondeson et al. performed a series of acid hydrolysis experiments with MCC prepared from Norway spruce sulfite pulp using a response surface methodology [128]. Factors included in the study were hydrolysis time, temperature, acid concentration, acid to cellulose ratio, and ultrasonic treatment duration. The dimension and yield of whiskers served as an experimental

response factors. A summary of this is shown in Table 15. Briefly, the optimal condition was determined to be sulfuric acid concentration of 63.5% (w/w), acid to cellulose ratio of 10 mL/g, and 130 min hydrolysis at 44 °C followed by approximately 30 min ultrasonic treatment, which produced whiskers of 200 to 400 nm in length and less than 10 nm in width and a yield of 30% of the initial weight.

Table 15. Optimization of cellulose nanowhiskers isolation.

Sample	(MCC) conc., g/100mL	H_2SO_4 conc., % (w/w)	Hydrolysis time, min	T, °C	Ultrasonic treatment time, min	Whiskers length µm	Yield %
1	5	44.1	10	40	30	19.34	93
2	5	44.1	10	80	10	9.12	88
3	5	64.8	10	40	10	38.68	91
4	5	64.8	10	80	30	10.82	47
5	5	44.1	120	40	10	14.30	94
6	5	44.1	120	80	30	7.01	92
7	5	64.8	120	40	30	0.11	34
8	51	64.8	120	80	10	-	0
9	15	44.1	10	40	10	22.36	95
10	15	44.1	10	80	30	8.53	90
11	15	64.8	10	40	30	14.91	73
12	15	64.8	10	80	10	12.69	23
13	15	44.1	120	40	30	13.80	95
14	15	44.1	120	80	10	6.88	86
15	15	64.8	120	40	10	0.18	18
16	15	64.8	120	80	30	-	0
17	10	55.1	65	60	20	7.93	82
18	10	55.1	65	60	20	8.15	178
19	10	55.1	65	60	20	7.84	78

2.5 Hemicellulose

Hemicellulose is defined as the alkali-soluble material after the removal of pectic substances from plant cell walls [137]. Hemicelluloses usually account for 20 to 30% w/w of the dry weight of wood. The composition and structure of the hemicelluloses in softwood differ in a characteristic way from those in hardwoods [143]. The main function of the hemicelluloses is to crosslink the cellulose fibrils with the lignin matrix. In contrast to cellulose, the hemicelluloses are heteropolysacharides, with their monomeric components consisting of anhydrohexoses (D-glucose, D-mannose and D-galactose), anhydropentoses (D-xylose and L-arabinose) and anhydrouronic acids (D-glucuronic acid, D-galacturonic acid). Most hemicelluloses have a DP of only 50-300. Four main groups of hemicelluloses may be defined according to their primary structure: xyloglycans (xylans), mannoglycans (mannans), β-glucans, and xyloglucans [144]. In most cases xylans consist of a β (1-4)-D-xylopyranose backbone with side groups on the 2- or 3- position. Nonbranched homoxylans with (1-3, 1-4) or (1-3) glycosidic linkages occur in certain seaweeds. Heteroxylans include glucuronoxylans and arabinoxylans as well as structures with more complex substitution patterns often referred to simply as heteroxylans. Glucuronoxylans have a side chain on the 2-position of either α-D-glucuronic acid or its 4-*O*-methyl derivative, while arabinoxylans are substituted on position 2 and/or 3 with R-L-arabinofuranosyl residues. In softwood, the principal hemicelluloses are galactoglucomannans (about 20%). Their backbone consists of a linear chain built up by (1-4) linked D-glucopyranose and (1-4) linked D-mannopyranose units. The α-D-galactopyranose units are linked as a single unit side chain to the

framework by (1-6) bonds. The main constituents of hemicelluloses are shown in Figure 8.

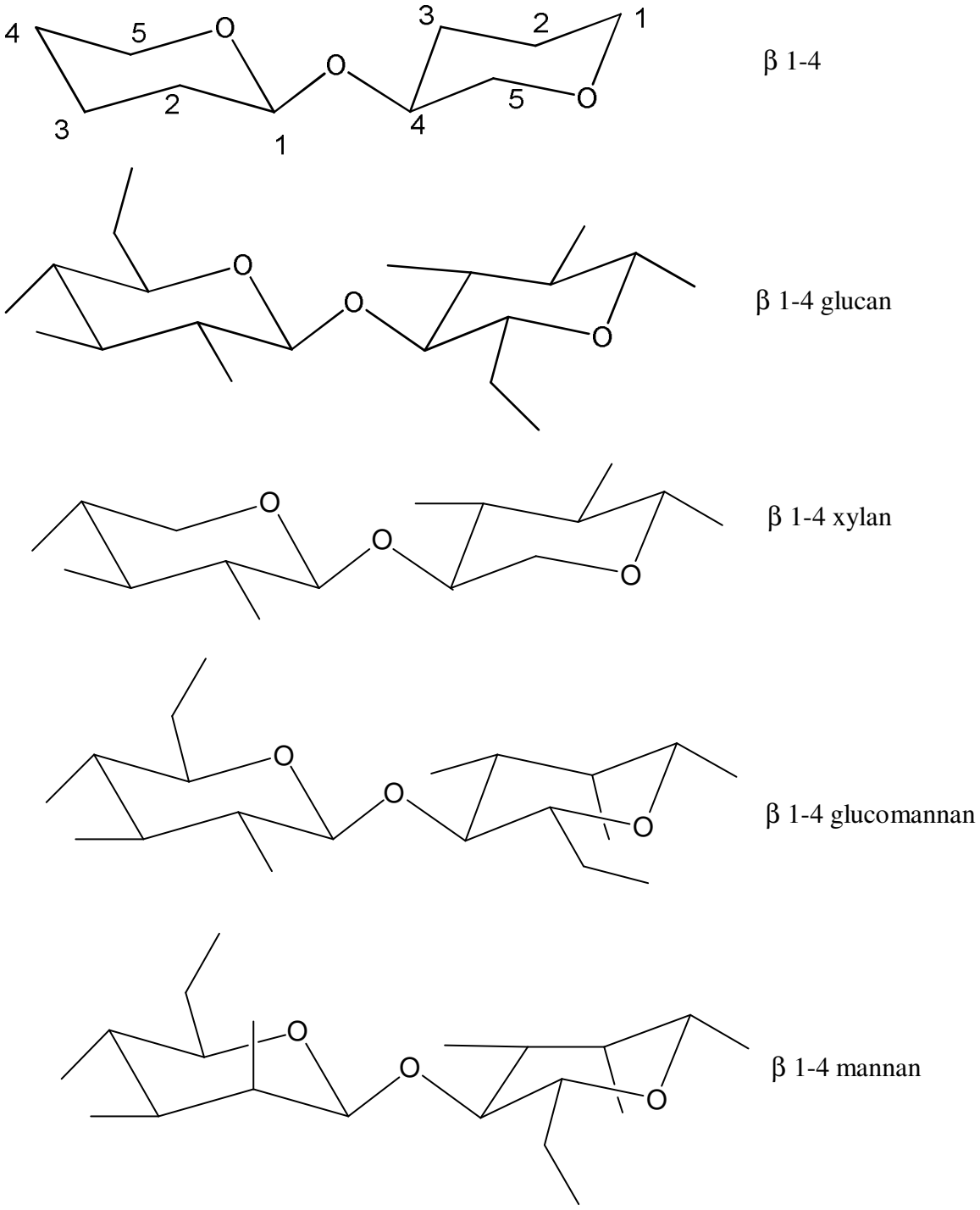

Figure 8. Main constituents of hemicellulose

Representative data providing analyses of carbohydrates are summarized in Table 16. The chemical composition of acacia is summarized in table 17. The hemicellulose content, the main heteropolysaccharides and their degree of polymerization (DP) are summarized in Table 18 in case of hardwoods (HW) and softwoods (SW) [145-146]. Xylan is a predominant hemicellulose component found in plants and in some algae. Xylan represents about 10–15% in softwoods, about 10–35% in hardwoods and about 35–40% of the total mass in the residues of annual plants, such as oat spelts [147].

Table 16. Relative distribution of hemicellulose sugars in select wood resources.

Wood* Species	Ara	Xyl	Gal	Glc	Man	Rha	GlcA	GalA	4-O-MeGlcA	Total **%
Softwood										
Picea abies										
sapwood	0.14	0.61	0.17	0.37	1.00	0.02	0.03	0.16	0.10	24.6
heartwood	0.17	0.69	0.28	0.35	1.00	0.03	0.04	0.20	0.12	24.9
Pinus banksiana										
sapwood	0.18	0.57	0.18	0.40	1.00	0.02	0.05	0.13	0.10	27.2
Hardwood										
Betula pendula										
stemwood	0.02	1.00	0.06	0.08	0.04	0.02	0.01	0.10	0.16	33.6
Populus tremuloide										
sapwood	0.03	1.00	0.04	0.11	0.05	0.03	0.01	0.12	0.13	29.1
heartwood	0.03	1.00	0.04	0.12	0.09	0.03	0.01	0.12	0.13	28.8

*Salmen and Olsson 1998; Ebringerova et al. 2005.
** mass sugar units/mass dry wood

Table 17. Chemical composition of Acacia.

	Relative abundance, % dry wood[a]
Ashes	0.22
Extractives	
Ethanol/Toluene	4.46
Dichloromethane	1.32
Methanol/water	4.05
Lignin	
Klason lignin	27.1
Acid soluble lignin	0.54
Holocellulose	70.9
Cellulose (Kurschner-Hoffer)	46.5[b]
Pentosans	13.3
Neutral monosaccharides[c]	
Rhamnose	0.3
Arabinose	0.2
Xylose	10.9
Mannose	1.0
Galactose	0.6
Glucose	48.0
Uronic acids	7.6

[a]Extractive-free wood, except for extractive content, [b]Corrected for pentosans content, [c]Determined as anhydrous monosaccharide

Table 18. Relative amount (%) and degree of polymerization of major hemicelluloses in case of different softwood and hardwood species.

Material	**Hemicellulose content**	**Degree of polymerization**
Softwood		
Loblolly pine	15.3	…..
Black Spruce	17.4	……
Galactogucomannan	~20	40-100
Gluconoxylan	5-10	50-185
Hardwood		
Birch	33	……
Gluconoxylan	15-30	~200
Gluconomannan	2-5	~70

Oat spelts are residues of oat flakes production. They contain high amounts of xylan and have relatively low lignin content. Hence this material is an interesting source for the isolation of xylan. Some aspects about the structure of xylan from oat spelts were discussed by Saake et al. [148]. These authors reported that molar masses for xylan from oat spelts lie around 22,000 g/mol [148]. The natural polymers cellulose, lignin and hemicellulose could be detected in the untreated oat spelts by micro Raman spectroscopy, a rapid method determining the constituents of the spelts [147]. Hettrich et al. [147] reported that for an isolated oat spelts xylan the average molecular mass was 79,200 g/mol. The author also reported a low crystallinity of oat spelts xylan as measured by x-ray method. The diffractograms did not show any discrete Bragg reflexes indicating that the sample was amorphous [147].

2.6 Polymer Nanocomposites

The field of polymer nanocomposites is a rapidly expanding area of research generating new materials with novel properties [149]. Several new materials have been developed within the last decade incorporating nanosized filler materials in polymer matrices. Use of nanomaterials has proven to confer various advantages like improved mechanical, thermal and barrier properties compared to nonfilled polymers. These effects are largely due to their high interfacial area, their aspect ratio, their extent of dispersion and percolation, which occur when the filler particles are present in quantities above the threshold where they start interacting [132]. Nanomaterials like glass fibers, carbon nanotubes, exfoliated clay, and cellulose nanocrystals have been successfully employed as fillers in polymer matrices and some systems are being commercialized [122, 150]. One application area for these materials is barrier films, where the nano-sized fillers

impart enhanced mechanical and barrier properties. Research in this area is evolving rapidly to enhance the barrier properties and to overcome certain limitations like durability, weight, robustness, flexibility and packing volume. The most extensively used filler nanomaterial is highly exfoliated clay, whose high surface area provides beneficial barrier and mechanical properties [25, 26]. Films with good thermal resistance and stiffness were obtained with the introduction of <5% clay in polymer matrices such as polyester, polyimide, polypropylene, poly (ethylene terephthalate) and poly (vinyl chloride) [25, 27, 28, 29, 30].

2.6.1 Cellulose Whiskers Nanocomposite

Bionanocomposites are bio-based nanocomposites and can be defined in two ways (i) it could designate nanocomposites as materials made from renewable nanoparticles (e.g., cellulose whiskers and microfibrillated cellulose) and petroleum-derived polymers like PP, PE, and epoxies. However, nanocomposites derived from biopolymers (e.g., polylactic acid and polyhydroxyalkanoate) and synthetic or inorganic nanofillers (e.g., carbon nanotubes and nanoclay) also come under bionanocomposites [5, 121].

The use of cellulose nanoparticles (e.g., whiskers and microfibrillated cellulose) as reinforcement in nanocomposites is a relatively new area of interest. Besides the low cost of the raw material, the use of cellulosic particles as a reinforcing phase in nanocomposites has numerous well-known advantages e.g., low density; renewable nature; wide variety of fillers available throughout the world; low energy consumption; high specific properties; modest abrasivity during processing; biodegradability; relatively reactive surface which can be used for grafting specific groups and almost unlimited availability [3, 102-106].

During recent years, efforts have been made to use nanocrystals obtained from polysaccharides as reinforcing agents in polymer matrices. Studies by Pu et al. [43] have shown improvements in strength properties of acrylic films using cellulose whiskers. Comparable results have been reported employing styrene and butyl acrylate, poly (vinylchloride) [36-38], polypropylene [39], and polyoxyethylene [40-42] which were have been beneficially reinforced with cellulose whiskers. Table 19 shows examples of strength property improvement of different polymer matrices incorporated by cellulose whiskers [133,151-155].

Table 19. Strength property improvement of different polymer matrices incorporated by cellulose whiskers [133,151-155].

Matrix	% of whiskers	Tensile strength improvement % as compared to control
Soy Protein	20	+41.30[1]
SoyProtein	20	+86.4[2]
Polyurethane	6	+102
Polyurethane	10	+120
Xylan from oat spelts	7	+141
Poly(vinyl alcohol)	5	+28

[1]RH: 43%, [2]RH:86.4%

Nanocomposites obtained by casting a mixture of latex and an aqueous suspension of cellulose whiskers have also been studied [29]**.** Their mechanical properties (e.g. shear modulus) are found to increase by more than three orders of magnitude in the rubbery state of the polymer matrix, when the whisker content is 6 wt%. This large and unusual effect is discussed on the basis of different types of mechanical models. A phenomenological mechanical model based on percolation concepts was introduced,

which assumed that the behavior of the composite is driven mainly by the mechanical properties of the cellulose network [29,156-158]. Recent studies of ethylene oxide-epichlorohydrin copolymer/ microcrystalline cellulose (EO-EPI)/MCC nanocomposites, which achieve the maximum mechanical reinforcement predicted by the percolation model. The materials reported display significantly improved mechanical properties, which are of interest in their own right [159].The reinforcement observed in the cotton nanowhisker nanocomposites is demonstrated before[159] related to the formation of a percolating nanofiber network in which stress transfer is facilitated by hydrogen-bonding between the nanowhiskers. Under these circumstances, the mechanical properties can be predicted by calculations obtained using a percolation model [29]. Within the framework of the model, shear storage moduli (G_c') can be expressed as [160-161]

$$G_c^{'} = [(1-2\psi + \Psi X_r)\, G_s^{'} G_r^{'} + (1- X_r)\, \Psi\, G_r^{'2}]/ [(1-X_r)\, G_r^{'} + (x_r - \Psi)\, G_s^{'}]$$

with

$$\Psi= X_r\, [(X_r-X_c)/ (1-X_c)]^{0.4}$$

where ψ is the volume fraction of nanowhiskers that participate in the load transfer, X_r is the volume fraction of the randomly orientated filler, G'_s is the experimentally determined shear storage modulus of the neat EO-EPI (1.6 MPa), and X_c is the critical whisker percolation volume fraction calculated by $0.7/A$. A is the aspect ratio of the filler (10.5 for cotton nanowhiskers and 11 for MCC nanowhiskers).

2.7 Model Studies

In the past, different models have been used like Rule of Mixture (ROM) series model, Halpin Tsai model, Paul model and percolation model based on fish net network to explain the improvement in strength properties of the composite materials [162-165]. Instron and DMA modulus data were fitted to three existing models [162]. The equations for volume fraction, ROM, Halpin-Tsai and Paul model are given below.

The volume fraction of filler was calculated using equation 1

$$V_f = (W_f/\rho_f)/[(W_f/\rho_f) + (W_m/\rho_m)] \qquad (1)$$

where, W_f, W_m – weight of fiber and matrix, P_f,– density of fiber (1.4 g/cm^3) [166], ρ_m – density of matrix (1.25g/cm^3) [167]

Ratio of mixing series model

Modulus of composite with ROM series model was calculated using equation 2. It gives the modulus as the combination of the modulus of the fiber and the matrix by taking volume weighed average of the individual phase properties. This model assumes that the reinforcement has uniform size and the applied load produces equal strains in both matrix and the reinforcement. The latter assumption is similar to considering two phases in parallel. The rule of mixtures model best simulates an orthotropic material loaded uniaxially in the direction of reinforcement [168].

$$E = E_f V_f + E_m V_m \qquad (2)$$

where, V_f and V_m – volume fractions of fiber and matrix respectively and E_f and E_m – fiber and matrix modulus respectively.

Halpin-Tsai model

The Halpin-Tsai model has been proven to work well with different reinforcement geometries such as fibers, ribbons and flakes. The model was developed for predicting the modulus of unidirectional composite material as a function of aspect ratio of the reinforcement.

$$E/E_m = [1 + \xi\eta\Phi_f] / [1 - \eta\Phi_f] \qquad (3)$$

where E is modulus of composite, E_m is modulus of matrix, E_f is modulus of filler, ξ is shape factor and Φ is volume fraction and ε is given by,

$$\eta = [E_f / E_m - 1] / [E_f / E_m + \xi] \qquad (4)$$

For continuous fiber composites, $\xi \rightarrow$ infinity the Halpin-Tsai equation reduces to the same form as the rule of mixtures. Shape factor ξ (= 2 (*l/d*)) is defined as the geometry of filler materials giving a measure of particle reinforcement geometry and this particular form of ξ is used for calculating the longitudinal modulus. Various geometries of fillers and their shape factors are summarized at Table 20.

Table 20. Various geometries and their shape factors.

Geometry of fillers	Disk	Sphere	Tube	
			longitudinal	transverse
Shape factor	$2\frac{diameter\,(D)}{thickness\,(T)}$	2	$2\frac{length\,(L)}{diameter\,(D)}$	2

The modulus of cellulose nanowhiskers reinforced nanocomposites can be expressed using tube geometry shape factor. When cellulose nanowhiskers are aligned

parallel to tensile test direction, longitudinal shape factor can be applied to the model. On the other hand, transverse shape factor can be used if cellulose nanowhiskers are aligned vertical to the tensile test direction. If the alignment of cellulose nanowhiskers in matrix is isotropic, the modulus of nanocomposites is expressed as the fractional summation of E_L and E_T in equation 5.

$$E = 3/8\ (E_L) + 5/8(\ E_T) \qquad (5)$$

where E_L is the longitudinal modulus and E_T is the transverse modulus. The modulus with Paul model was fitted using equation 6. This model is best suited for irregular shaped reinforcement, e.g. microcrystalline cellulose particles or hydrolyzed microcrystalline cellulose particles

$$E/E_m = [E_m + (E_d - E_m)V_d^{2/3}\ ]/\ [E_m + (E_d - E_m)V^{2/3}\ (1 - V_d^{1/3}\ )] \qquad (6)$$

where, E, E_m, E_d = modulus of composite, matrix and reinforcement respectively and V_d = volume fraction of particulate reinforcement. The following assumptions were made when fitting data with any given model,

1. The cellulose particles are uniformly dispersed in the matrix
2. Particles have uniform shape and size
3. Good interfacial interactions exists between matrix and cellulose particles
4. Matrix is free of voids
5. Initially there are no residual stresses in the matrix
6. Both matrix and the cellulose reinforcement behave as linearly elastic materials

Percolation model

When the loading ratio of fillers increases, the interaction between fillers should be considered in mechanical properties of nanocomposites. Cellulose nanowhiskers show relatively large interactions between particles because of the high aspect ratio of the particles and strong hydrogen bonds. To understand better a mechanical percolation effect is tried to model the mechanical behavior of the composite studied by two-dimensional finite element approach. The 2-D handmade meshes similar to fish net network is created from a random distribution of whiskers as shown in Figure 9.

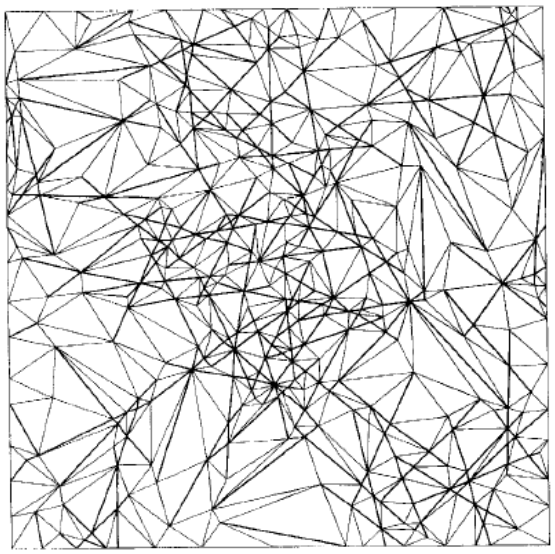

Figure 9. Piece of finite element mesh corresponding to an area fraction of whiskers equal to 7.3%; thick lines correspond to whiskers and thin lines correspond to triangular elements representing the matrix [169]

Percolation theory considers various parameters such as particle-particle interactions, orientation of particles and aspect ratio. In the percolation approach, the elastic modulus E_C of the composites is given by equation 7

$$E_C = [(1-2\Phi + \Phi V_R)\, E_s\, E_R + (1-V_R)\, \Phi E_R^2] / (1-V_R)E_R + (V_R-\Phi)E_S \qquad (7)$$

where subscripts S and R refer to the soft phase (polymeric matrix) and rigid phase (cellulose nanowhiskers), respectively. V and E are the volume ratio and elastic modulus of given phases. φ and V_{RC} defined as

$$\Phi = 0 \quad \text{for } V_R < V_{RC}$$

$$\Phi = v_R \left[(V_R - V_{RC})/(1 - V_{RC})\right]^b \text{ for } V_R > V_{RC}$$

$$V_{RC} = 0.7/ (L/D)$$

where b = 0.4 for a 3D network.V_{RC} is the percolation threshold which means the lowest volume ratio of cellulose nanowhiskers that can be considered as a percolating phase. It was found that percolation theory agrees well with experimental data above $T_g + 50°C$ [170-171]. Figure 10 is the logarithmic plot of the relative tensile modulus of various cellulose nanowhiskers nanocomposites measured at $T_g + 50°C$. Black and white circles are experimental data. A dotted line is the percolation model value and a solid line is Halpin-Tsai model prediction [3].

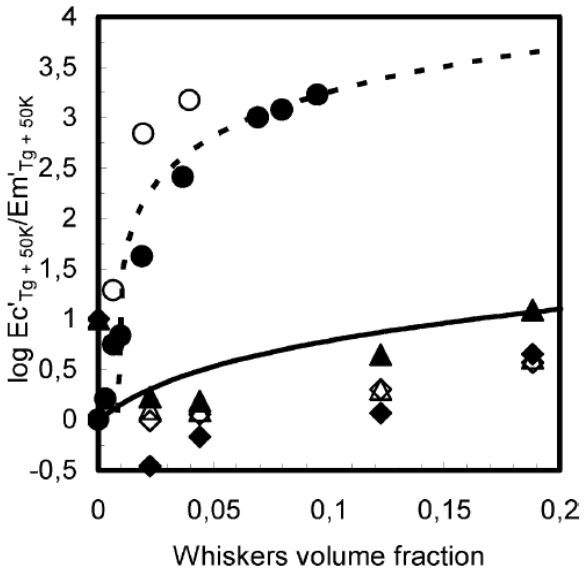

Figure 10. The logarithm plot of the relative tensile modulus of various cellulose nanowhiskers nanocomposites measured at $T_g + 50°C$ [3, 40-41].

The moduli calculated by the Halpin-Kardos mean field approach (solid line) do not fit at all with the experimental data, whereas moduli, estimated by a percolation approach (dotted line) is in good agreement with the mechanical measurements. For values of X_r lower than X_c whiskers get connected in small and isolated aggregates and the model is reduced to a Series model. As soon as $X_r > X_c$ an "infinite" cluster begins to merge resulting in a jump of the theoretical shear modulus

2.8. Biodegradable barrier films

Biobased films have generated increasing interest to replace petrochemical based films in light of their ready availability, sustainability, limited environmental impact and simplified end-of-life disposal issues [2, 3, 5, 18]. High barrier packaging materials require low oxygen permeability with good mechanical strength. Replacing existing oxygen barriers such as aluminum and synthetic polymers with biopolymers is an interesting research topic. In recent years, increasing societal concerns have accelerated efforts to develop new ways to utilize biopolymers such as polysaccharides, proteins and lipids to create biodegradable films due to their ready availability, sustainability and reduced end-of-life environmental concerns [5, 18]. As a general rule, fats are used to reduce water transmission; polysaccharides are used to control oxygen and other gas transmission, while protein films provide mechanical stability [172]. These materials can be utilized individually or as mixed composite blends to form films. Early studies examined the use of chitosan, starch and cellulose derivatives to address these challenges and were shown to have good film forming properties [8]. Many naturally occurring polysaccharides and their derivatives such as starch, cellulose, chitosan, alginates,

carrageenan, pectinate, and various naturally occurring gums have been proposed for use in coating and film formulations. Typically, polysaccharide films possess poor mechanical and barrier properties [173-174], and plasticizers are normally added to improve the strength of the films and aid in stabilizing the film network [175-176]. Table 21 shows the barrier and mechanical properties of polysaccharide films.

Table 21. Barrier and mechanical properties of polysaccharide films [177].

Polysaccharide/ plasticizer (wt/wt)	Water vapor permeability ($g.mm/m^2dkPa$)	Oxygen permeability ($cm^3\mu m/m^2dkPa$)	Tensile strength (MPa)	%Elongation
Methylcellulose: Glycerol 1.52:1-5.88:1	9.07-10.80	101.03	20.83-37.5	50-100
Hydroxypropyl cellulose: Glycerol 1.52:1-5.88:1	7.00	201.46	8.33-12.5	100-125
Methylcellulose: Polyethylene glycol 400 1.52:1-5.88:1	7.78	242	16.67-41.67	78-100
Methylcellulose: Propylene glycol 1.52:1-5.88:1	8.64-30.24	242-1512.5	40-50	25-50
High amylase cornstarch: Glycerol 1:1-5:1	1011-1270		2-32	6-22
High amylose cornstarch: Sorbitol 1:1-5:1	1011-1270		7-47	6-38

Xylan, which is one the most common hemicelluloses and the most abundant polysaccharide in nature after cellulose, is an attractive resource for film production [178-180]. Höije et al. have shown that arabinoxylan film can be prepared from the extracts of barley husks without the need for plasticizers [10]. Films were prepared by mixing 1 g of the isolated

fractions with 35 mL of deionized water during magnetic stirring at 95.8 °C for 15 min. The solutions were poured onto polystyrene petri dishes, and films were allowed to form upon drying at a temperature of 23.8 °C and a relative humidity (RH) of 50%. The films were stored in these conditions until analysis. The resulting films were stiff and rather brittle with high water content. Dammström et al. [11] prepared composite films of glucuronoxylan reinforced with bacterial cellulose. The glucuronoxylan was dissolved in water and heated under stirring at 95.8 °C for 15 min. The glucuronoxylan was then added to the microfibril suspension and the blend was left under stirring for 30 min at room temperature. The resulting gel was distributed among three polystyrene petridishes, and dried at 23.8 °C, 50% relative humidity. The film containing only glucuronoxylan was prepared from a pure glucuronoxylan solution heated at 95.8 °C for 15 min, poured into a polystyrene petri-dish and dried at the same conditions as the composite films. The resulting composite films showed a transparent stronger film as compared to control glucuronoxylan films. Peng et al. [182] recently explored the mechanical properties of xylan-rich hemicelluloses and cellulose nanofibers composite films. The tensile testing results of the films produced are shown in table 22.

Table 22. Mechanical properties of xylan-rich hemicelluloses isolated from holocellulose of bamboo and cellulose nanofibers composite films [182].

Sample	CNF (wt %)	Tensile strength (MPa)	Young's modulus (MPa)
1	0	11.9± 0.9	735± 87
2	5	15.5± 1.2	1322± 98
3	10	20.2± 2.3	1578± 128
4	15	28.9± 1.9	2355± 121
5	20	39.5± 2.2	3404± 138
6	100	150.4± 5.7	17212± 298

The use of xylan for the production of biodegradable composite films in combination with wheat gluten has been investigated [12]. The presence of xylan did not adversely affect the film forming quality or the water vapor transmission rate, though the mechanical and solubility properties depended on the quantity of xylan in the wheat gluten. Table 23 shows the addition of xylan only slightly affected water transfer rate of the films.

Table 23. WVTR of composite films [12].

Film treatment Wheat gluten: Xylan	pH	Xylan source	Drying conditions	
			Room conditions RH	80 °C and 35%
10:0	11	Birchwood	6.4±0.4	6.5±0.5
9:1	11		6.0±0.0	6.0±0.3
8:2	11		6.8±0.0	6.5±0.5
7:3	11		7.0±0.1	6.6±0.5
8:2	11	Corncob	7.1±1.7	
8:2	11	Grass	7.2±0.0	

Recently, acetylated galactoglucomannan (AcGGM) hemicellulose was found to be an alternative material for making new renewable barrier materials [183]. The oxygen barrier permeability of the AcGGM films was found to be similar to, or lower than, the values reported for oxygen barrier films made from glucuronoxylan [184] and other polysaccharides, such as starch [185], chitosan [186] and mixtures of various polysaccharides [187]. Table 24 shows the oxygen permeability of biopolymer films. Glucuronoxylan, isolated from aspen wood, when plasticized with xylitol or sorbitol has been used to produce films that exhibit improved strength and oxygen barrier properties with respect to control glucuronoxylan films [188-190]. Hartman et al. reported oxygen permeability values of 2.0 cm^3 μm m^{-2} day^{-1} kPa^{-1} for GGM-sorbitol film [190]. The oxygen barrier properties of films obtained from a mixture of *O*-acetyl-galactoglucomannan and either alginate or carboxymethylcellulose were also studied. The reported values of oxygen permeability of GGM/alginate/glycerol blend were 4.6

(cm^3 μm)/ (m^2 d kPa) [17]. The oxygen permeability of the GGM films was lower than that of glycerol-plasticized amylose and amylopectin films [191], but not as low as that of sorbitol-plasticized aspen glucuronoxylan films [188, 189]. The oxygen permeability of oat spelt arabinoxylan films plasticized with 40% sorbitol was 4.7 (cm^3 μm)/ (m^2 d kPa), which is slightly lower than that of GGM films [191]. Biobased free-standing films and coatings with low oxygen permeability of 1 (cm^3 μm)/ (m^2 d kPa) have been also prepared from a wood hydrolysate [192].

Table 24. Oxygen Permeability Data on Plasticized Glucuronoxylan Film and Comparable Values for Plasticized Starch Polymers, Ethylene Vinyl Alcohol, and Low Density Polyethylene.

Sample	Oxygen Permeability (cm^3 μm)/ (m^2 d kPa)	
GGM-sorbitol	2.0	[190]
GGM/alginate/glycerol blend	4.6	[190]
Oat spelt arabinoxylan films plasticized with 40% sorbitol	4.7	[191]
Biobased free-standing films and coatings from a wood hydrolysate	1.0	[192]
Amylose with 40 wt% of glycerol	7.0	[10]
Amylopectin with 40 wt% of glycerol	14.0	[10]
Poly (vinyl alcohol) (PVA)	0.21	[10]
Low-density polyethylene (LDPE)	1870	[10]

Miranda et al. studied water vapor transmission values of chitosan film plasticized with sorbitol, glycerol or polyethylene glycol reporting values from 1.3-1.5×10^{-3} [g/(m^2. h. Pa)] [193]. The goal was to decrease the water vapor permeability and

to improve the mechanical properties of chitosan films. Miranda et al. also discussed that in hydrophilic films, water molecules interact with polar groups in the film structure, causing plasticization or swelling, which, in turn results in varying permeability [194]. Aydinli and Tutas [195] determined WVP of 6.3–11.6×10^{-8} [g/ (m. h. Pa)] for polyethylene glycol-plasticized locust bean gum as compared to 6.2-11.6 ×10^{-5}[g .mm/ (m^2. h. Pa)] reported by Mikkonen et al. [196]. The WVP of sorbitol-plasticized oat spelt arabinoxylan films studied by Mikkonen et al. [197] using a fan-equipped desiccator was 4.5×10^{-5} [g. mm/ (m^2. h. Pa)], while Péroval et al. [198] reported a value of 63.7×10^{-8} [g/ (m. h. Pa)] for corn arabinoxylan films. The water vapor transmission values of biopolymer films are listed in Table 25.

Table 25. Water vapor transmission values for biopolymer films.

Sample	Water vapor transmission values	
Chitosan film plasticized with sorbitol/glycerol/polyethylene glycol	1.3-1.5×10^{-3} [g/ (m^2. h. Pa)]	[193]
Polyethylene glycol-plasticized locust bean gum	6.3–11.6×10^{-8} [g/ (m.h.Pa)]	[195]
Sorbitol-plasticized oat spelt arabinoxylan films	4.5×10^{-5} [g. mm/ (m^2. h. Pa)]	[197]
Corn arabinoxylan films	63.7×10^{-8} [g/ (m. h. Pa)]	[198]

The mechanical performance of the films prepared from xylan alone is low because the films are rather brittle and too fragile to handle, which is a well-known issue for obtaining films from pure hemicelluloses. The poor film-forming ability is attributed to the insufficient chain length of the polymer, high glass transition temperature. The glass

transition temperature of xylan has been estimated to be around 180 °C which might explain the poor film formation at room temperature. To suppress the glass transition temperature and to form cohesive films, plasticizers are added like xylitol and sorbitol. Plasticizers work by embedding themselves between the chains of polymers, spacing them apart and thus significantly lowering the glass transition temperature for the plastic and making it softer. However, even with the plasticizers, the mechanical properties of these films have been considered to be poor. Nanocellulose whiskers (NCW) have been studied as reinforcements of various synthetic and natural polymer matrices [199-201] to improve the strength properties of the nanocomposites. They have a high bending strength of 10 GPa, an elastic modulus of 143 GPa [202, 203] and form a rigid hydrogen-bonded network. The properties of nanocomposite materials and the enhancement of these properties, depend not only on their individual components but also on the interaction between the matrix and the reinforcing phases and their morphology [204]. Lagaron et al. [47] discussed the role of crystalline structure of polymers and emphasized that high crystallinity improves barrier properties. Nanocrystalline cellulose is greater than 60% crystalline [48-49] and this property together with the resulting rigid hydrogen-bonded network of nanocrystalline cellulose can cause an increase in tortuosity [205]. Recent studies by Saxena et al. have shown that xylan films reinforced with NCWs can reduce water and oxygen permeability by greater than +70% while increasing physical strength properties by +50% with respect to control xylan/sorbitol film by the addition of 5-10% of NCWs [181,206-207].

2.9 Migration Process

Several important parameters need to be defined to describe diffusion processes in relation to films. Migration between two adjacent volumes separated by a layer or membrane occurs in three basic steps. In the first step, the diffusing molecule comes in contact with surface of the layer or membrane, and is adsorbed onto it. In the second step, the molecule then diffuses through the thickness of the layer or membrane. Lastly, once the diffusing molecule reaches the other side of the layer or membrane, it will desorb. Rate of adsorption and desorption is dependent on the affinity between the diffusing molecule and membrane (film) components, especially for water migration. Despite surface effects noted previously, the most dominant factor in molecular migration is bulk effect – rate of diffusion of molecules while in the membrane or film. In an ideal case, amount of given material (Q) passing through a film can be determined by Fick's law of diffusion in equation 8:

$$Q = PA\Delta pt / d \qquad (8)$$

where Q increases in direct proportion to film surface area (A), and decreases with its increasing thickness (d). Increasing partial pressure difference (Δp) of migrating molecules between two sides of the membrane and time (t) also linearly affects total amount of permeate. Permeability coefficient (P = DS), with D = diffusion coefficient (D) and S = solubility coefficient. In an ideal case, P is a constant determined by characteristics and structure of the film.

2.10 Tortuosity

Tortuosity is the ratio of actual distance traveled between two points to the minimum distance between two points

$$\xi = tortuosity = \frac{\text{actual distance traveled}}{\text{shortest distance}} = \frac{\ell_e}{\ell} \tag{9}$$

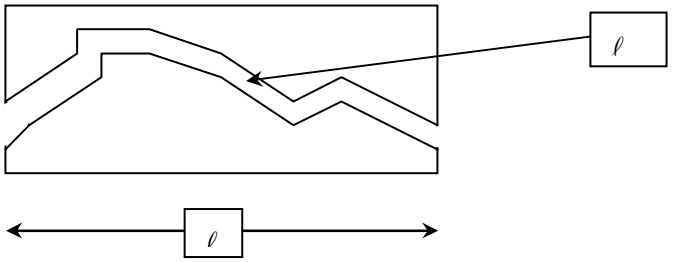

2.11 Tortuosity calculation

Required parameters (units specified as mass, volume, length, and area)

ρ = density (mass/volume) – from pycnometry
V_{tot} = total pore volume (volume/mass)
K = permeability (area)

The tortuosity can be calculated from the following equation 10 [208]:

$$\xi = \sqrt{\frac{\rho}{24K\left(1+\rho V_{tot}\right)\int_{\eta=r_{c,\min}}^{\eta=r_{c,\max}} \eta^2 f_v(\eta) d\eta}} \tag{10}$$

where

$$-f_v(r_c) = \frac{dV(r_c)}{dr_c}, \; from\, MIP \tag{11}$$

with MIP = Mercury Intrusion Porosimetry.

Carniglia et al. [209] has derived a simple expression for calculating the tortuosity factor of porous media. While this expression was derived using Fick's first law of diffusion and is convenient to calculate, the use of this correlation is severely limited by the data required to calculate the tortuosity factor. For nonintersecting cylindrical pores the following simple correlation in equation 12 may be used:

$$\tau = 2.23 - 1.13 V_{tot} \rho_b \qquad 0.05 \le V_{tot} \rho_b \le 0.95 \tag{12}$$

This correlation is limited to values of τ ranging from 1 to 2.2. A generalized correlation has also been developed, however the generalized method requires diffusivity data for the system and conditions of interest (temperature and pressure). It is worth noting that if this diffusivity data is available, tortuosity factor can be calculated directly from equation 12. Tortuosity factor is calculated in equation 13.

$$\tau = \frac{D_{eff}}{D\theta_c} \tag{13}$$

$$\tau = \frac{\xi}{\sigma}$$

$$\tau = \left(2.23 - 1.13 V_{tot} \rho_b\right)\left(0.92\left(\frac{4}{S}\sum \frac{\Delta V_i}{d_i}\right)^{1+\varepsilon}\right) \tag{14}$$

ε = pore shape exponent, Carniglia has assigned a value of 1 for cylinders.
V_{tot} = total pore volume
ρ_b = bulk density
S = total BET surface area
ΔV_i = change in pore volume within a pore size interval
d_i = average diameter within a pore size interval

2.12 Summary

The aim of this thesis is to produce bionanocomposites, where both the reinforcement and the matrix are bio based. Cellulose whiskers combined with hemicelluloses xylan will lead to the development of a new class of biodegradable and environmental friendly nanocomposites. The new family of nanocomposites shows remarkable improvement in mechanical and barrier properties when compared to control xylan films. This new class of renewable nanocomposites can capture new market in packaging application. The structure and properties of the films were characterized by means of tensile testing, optical microscopy, scanning electron microscopy, wide angle x-ray diffraction, nuclear magnetic resonance (NMR), fourier transform infrared spectroscopy. In order to test the barrier properties, further barrier evaluation was applied using oxygen and water vapor transmission rate.

CHAPTER 3

MATERIALS AND METHODOLOGIES

In this chapter the detailed procedures and description is given for the materials used, processing techniques employed and instruments used for preparation and characterization of samples the results of which are reported in the subsequent chapters. The procedures used for cellulose whiskers synthesis, xylan-cellulose whiskers nanocomposite are also given in this chapter

3.1 Materials

Oat spelt xylan and sorbitol were obtained from Aldrich and used as received. Oat spelt xylan was determined to contain 81.0 % xylose, 9.8 % arabinose and 7.6 % glucose. Molecular weight of xylan used was Mn of 2.45×10^3 and Mw of 1.42×10^5. A commercial elemental chlorine-free (ECF) softwood (SW) kraft pulp, manufactured in the southeastern USA, was employed for all studies and fully bleached acacia kraft pulp were also used as received. The arithmetic mean length and curl of acacia kraft fibers and softwood fibers were 0.653 ±0.028 mm, 0.088 ±0.005 and 2.276 ±0.052 mm, 0.089 ±0.006 mm respectively as determined using a Fiber quality analyzer (FQA). Dialysis tubes were purchased from Spectrum Labs. All other reagents and solvents were purchased from Aldrich and used as received

3.2 Processing

3.2.1 Solution processing of xylan-sulfonated nanocellulose whiskers nanocomposite film

Xylan composite films were formed by adding an aqueous suspension of sulfonated whisker suspension to xylan (0.25 g). The solid whisker content in the whisker suspension used was 0, 2.5, 5, 7, 10, 15, 25, 50 wt% of the total mixture of xylan, whisker and sorbitol. The deionized (DI) water used was 35mL. The plasticizer, sorbitol (0.25 g, 1.37 mmol) was added to the mixture with stirring and then heated to 95 ºC for 15 min. The solution was then poured into teflon petri dishes and allowed to dry at room temperature for three days. The film had a thickness of 0.080 ±0.007mm. The resulting thickness of xylan films reinforced with sulfuric cellulose whiskers was 0.091 mm ±0.002 mm thick.

3.2.2 Solution processing of xylan- hydrochloride nanocellulose nanocomposite film

Xylan composite films were formed by adding an aqueous suspension of hydrochloride generated whiskers to xylan (0.25 g) dissolved in water (35.00 ml). The solid whisker contents in the whisker suspension used was 0, 2.5, 5, 7, 10 wt% of the total mixture of xylan, whisker and sorbitol. The plasticizer (0.25 g, 1.37 mmol) was added to the mixture with stirring and then heated to 95 ºC for 15 min. The solution was poured into teflon petri dishes and was allowed to dry at room temperature for three days. The film with xylan-10% hydrochloride nanocrystalline cellulose had a thickness of 0.096 mm and the standard deviation of 0.005 mm.

3.2.3 Solution processing of xylan- kraft softwood fiber and acacia reinforced films

Xylan composite films containing ECF bleached kraft softwood and acacia fibers were prepared with the same procedure used to form xylan- nanocrystalline cellulose composite films except that the cellulose whiskers were replaced with bleached softwood kraft fibers or acacia fibers. The thickness of resulting composite films for xylan-5%, 10% softwood fiber film was 0.154mm, 0.244 mm with standard deviation of 0.005 mm and the xylan-10% acacia fiber was 0.0886 mm with standard deviation of 0.065 mm, respectively.

3.3 Preparation of sulfonated cellulose whiskers

Nanocrystalline cellulose was prepared following the procedure outlined by Pu [30]. In brief, softwood kraft pulp was ground in a Wiley mill to pass through a 20-mesh screen. The acid hydrolysis of the milled pulp was accomplished with 64 wt % sulfuric acid at 45°C for 45 min with stirring. The reaction was halted by adding a 10-fold excess of deionized (DI) water. After standing overnight, the water was decanted and the settled cellulosics were collected with a minimal amount of water. Excess acid was removed with a water wash (200 ml), and centrifuged for 20 min at 11,000 rpm. The aqueous phase was discarded and the wash cycle was repeated an additional two times. The solids suspension was then dialyzed against DI water for 3 days using regenerated cellulose dialysis tubing with a 12000-14000 molecular weight cut off until the pH of the solution reached 7. Sonication was performed on the neutral nanocrystalline cellulose solution for 35 min with an Ultrasonic Processor GEX- 500 sonicator with standard titanium alloy probe (tip diameter 1.27 cm) at 28 Watts power input while immersed in an ice bath. The average yield of nanocrystalline cellulosic was 35%.

3.4 Conductometric titration method: Charge determination

Conductometric titration was used to measure the bulk charge on nanocrystalline cellulose following the method described by Katz (1984) [31]. A known amount of nanocrystalline cellulose (0.31% of suspension containing 0.50 g of whisker) was taken and mixed with 5.00 ml of 0.01 M NaCl before measurement. The solution was titrated with 0.05 M NaOH.

The change in conductivity was recorded with a conductometer. The bulk charge for the nanocrystalline cellulose was found to be 9.73 mmol acid groups/100 g. The bulk carboxylic acid group content of the fibers was measured by conductometric titration methodology. Air-dried fibers equivalent to 1.50 g of oven-dried fibers were added to 300.00 mL of 0.10 M HCl and stirred for 1 h. The pulp was filtered using a vacuum flask and then washed with at least 400 mL of deionized water. The washed pulp was treated with 0.001 M NaCl and 1.50 mL of 0.10 M HCl, stirring and bubbling nitrogen through the solution. The treated pulp was finally titrated with 0.05 M NaOH in 0.25 ml aliquots. The change in conductivity was recorded with conductometer. The bulk charge for the starting cellulose fibers was found to be 3.82 mmol carboxylate groups/100 g.

3.5 Preparation of hydrochloride nanocrystalline cellulose

An aqueous suspension of hydrochloric nanocrystalline cellulose was prepared following the procedure outlined by Araki et al. [18-19]. Fully bleached softwood kraft pulp with 7% wet-basis moisture content was Wiley milled to pass through a 0.5 mm mesh screen. A sample of this ground pulp (36.00 g, oven-dried weight) was treated with an aqueous 4.0 N HCl solution (2600 mL) at 80˚C for 8 h. The reaction was terminated by diluting the mixture with deionized water (8 L). After standing overnight, the clear supernatant

was decanted and the settled cellulosics were diluted with deionized water (8 L) and then allowed to settle. This procedure was repeated until the pH of the supernatant was approximately 3. The cellulosics were then transferred to a series of dialysis tubes (Spectra/Por membrane, MWCO 50K) and dialyzed with against deionized water for several days until the solution pH was > 4 and the supernatant became turbid. The cellulosics were next sonicated with an Ultrasonic Processor GEX-500 for 2 min followed by centrifugation at 3,000 rpm for 5 min. The turbid supernatant was decanted, the sediment was dispersed in deionized water, sonicated for 2 min and re-centrifuged. This procedure was repeated until the supernatant become clear. The cellulosic suspensions were concentrated by centrifugation at 11,000 rpm for 25 min and the clear supernatant was discarded, resulting in a final consistency of 1.57% for the whiskers. The concentrated whisker suspension was used directly to form nanocomposites. The gravimetric yield of HCl generated whiskers was 7~10%. The HCl generated whiskers had an absence of strong acid groups but weak acid groups of 1.4 mmol/100 g.

3.6 Characterization Techniques

3.6.1 Mechanical Properties

Film samples were cut into dimensions of 3.81 cm x 1.27 cm and conditioned at 50% relative humidity at 23.0 °C for 1 day. The conditioned samples were tested on an Instron 4400 R Universal Testing Machine (Model 1122, Instron Corp., USA) with a cross-head speed of 4.23×10^{-4}m/s at 23 °C temperature. The applied load *(f)* was recorded as a function of sample elongation $(l-l_o)$. The tensile strength σ and strain ε of the material was calculated as $\sigma = f/a$, and strain $\varepsilon = (l-l_o)/l_o$, respectively where a was the sample cross-sectional area, l_o the sample initial length and l the length at breaking. The averages of

tensile energy absorption (TEA), tensile strength and strain at failure were obtained. The percentage of error as determined by Percentage error = (Standard Deviation / Mean) × 100 was less than 10 %.

3.6.2 Water vapor transmission rate (WVTR)

The technique used to measure water vapor transmission rate (WVTR) was a modification of the wet cup method described by ASTM E 96-95. The procedure involves using a Petri dish filled with distilled water and covered with a film. The mass of water lost from the dish was monitored as a function of time. Thickness measurements of the films were obtained with a digital gauge at a minimum of five positions on a test specimen. The glass petri dish was filled with distilled water (10.00 mL) and then the film was sealed to the petri dish with a 5-minute epoxy adhesive. After allowing the epoxy to cure for 30 min, the sample dish was weighed and placed in a convection oven at a setting of 37.0 ºC in the oven. The sample dish was periodically removed and weighed. The weight loss over a period of 24 h was determined. The water vapor transmission rate was calculated using: WVTR=mass of water lost/time×area = flux/area with units of g h^{-1} m^{-2}. The percentage of error as determined by Percentage error = (Standard Deviation / Mean) × 100.

3.6.3 Oxygen permeability analysis

The oxygen transmission of the films was measured using a Mocon Ox-Tran 2/21 l apparatus (Modern Controls Inc., Minneapolis, USA) with a coulometric sensor in accordance with ASTM method D 3985-95 [32].

3.6.4 Mercury intrusion porosimetry analysis

Micromeritics' AutoPore IV 9500 Series was used to measure the porosity, bulk density, and average pore diameter and tortuosity factor of the control and nanocomposite films.

3.6.5 Conductometric titration

The bulk charge on the sulfonated and hydrochloride whiskers was determined using the method described by Katz. The change in conductivity was recorded with a VWR Portable Conductivity Meter (Model 2052).

3.6.6 Atomic force microscopy (AFM) analysis

The composite films were analyzed using a Dimension 3100 scanning probe microscope and Nanoscope IIIa controller. The images were acquired in tapping mode in air using a 1-10 ohm-cm phosphorus (n) doped silicon tip with frequency of 150 kHz.

3.6.7 Optical microscopy analysis

The composite films were mounted on microscope slides and examined with Leica DMLM optical microscope. Bright-field images were collected with a transmitted light detector.

3.6.8 Scanning electron microscopy (SEM)

The cross-section and surface morphology of the composite films were analyzed by Hitachi S800, thermally assisted field emission (TFE) scanning electron microscope (SEM). The samples were sputter-coated with gold prior to examination.

3.6.9 Transmission electron microscopy (TEM)

Drops of 0.005 wt % cellulose microcrystal suspensions were deposited on carbon coated TEM grids. The specimens were then negatively stained with 2% uranyl acetate and observed with a JEOL 100CX transmission electron microscope using an acceleration voltage of 100 kV.

3.6.10 Nuclear Magnetic Resonance (NMR) Analysis

NMR samples were prepared with films conditioned overnight at 100% relative humidity and then packed into 4-mm cylindrical ceramic MAS rotors. Solid-state NMR measurements were carried out on a Bruker Avance-400 MHz spectrometer operating at frequencies of 100.55 MHz for ^{13}C NMR experiments using a 4-mm Bruker double-resonance MAS probehead at spinning speeds of 10 kHz. CP/MAS experiments utilized a 5 μs (90°) proton pulse, 2.0 ms contact pulse, 4 s recycle delay and 4-8 K scans. A 10 Hz exponential line-broadening apodization was applied. Line-fitting analyses of the spectra were performed using NUTS NMR Data Processing software (Acorn NMR, Inc). In some cases, averages and standard deviations in parentheses were reported for two replicate films.

3.6.11 XRD (X-ray Diffraction)

Wide Angle X-ray Diffraction (WAXD) patterns were obtained on a Philips X'pert diffractometer equipped with X'celerator using Cu Kα radiation. The patterns were recorded on the prepared films at 45 kV and 40 mA. The pattern was taken over a range of 2θ from 5 to 40° with a step size of 0.02°. The films were prepared as discussed previously and were put on low background holder for XRD measurement.

3.6.12 Fourier Transform Infrared Spectroscopy (FT-IR)

FT-IR analysis was performed in an absorbance range of 4000-500 cm^{-1}, to compare the control xylan films with the nanocomposite films using Bruker Vector 22 FT-IR.

CHAPTER 4

XYLAN-NANOCELLULOSE COMPOSITES

4.1 Introduction

In this chapter xylan based composites reinforced with cellulose whiskers are studied. The goal was to understand the effects of cellulose whiskers addition on the mechanical properties of the composite and also to evaluate the effect of reinforcing xylan films with cellulose whiskers made from sulfuric acid hydrolysis and hydrochloric acid hydrolysis.

The majority of engineered plastic materials used today are made from synthetic polymers. The use of conventional petroleum-based polymer products creates potential problems due to their non-renewable nature and ultimate disposal. Cellulose and its derivatives, when used in bioplastic applications, often offer advantages with respect to ready availability and limited environmental impact [3-5]. Lignocellulosic fibers can also be used as a viable alternative to inorganic/mineral based reinforcing fibers in thermoplastic materials. During recent years, efforts have been made to use nanocrystals obtained from polysaccharides as reinforcing agents in polymer matrices. Studies by Pu et al. [43] have shown improvements in strength properties of acrylic films using cellulose whiskers and comparable results have been reported employing styrene and butyl acrylate, poly (vinylchloride) [36-38], polypropylene [39], and polyoxyethylene [40-42].

Xylan which is the most abundant of the hemicelluloses found in the cell wall of the land plants has also been used to enhance the strength properties of cellulosic fiber

networks [7]. A review of the literature indicates that surface xylans play an important role in a variety of physical strength properties of paper [7, 18, 210]. In addition, glucuronoxylan isolated from aspen have been used to produce films [8-9] that can be improved in strength properties when plasticized with xylitol or sorbitol. Dammström et al. [11] prepared composite films of glucuronoxylan reinforced with bacterial cellulose and showed that they formed transparent strong films. The objective of this study is to evaluate the effect of reinforcing xylan films with cellulose whiskers. The effect of adding cellulose whiskers to xylan is studied. Influence of cellulose whiskers made by hydrolysis via sulfuric acid and hydrochloric acid method are discussed and their effects on the mechanical properties are compared.

4.2 Results and discussion

An aqueous suspension of sulfonated cellulose whiskers was prepared following the literature procedures outlined by Pu et al. [43]. Cellulosic fibers were hydrolyzed with 64 wt % sulfuric acid at 45 °C for 45 min. The resultant hydrolyzed products were purified by ultracentrifugation, followed by dialysis with Spectra/Por membranes. Hydrochloride generated cellulose whiskers was prepared following the literature procedure outlined by Araki et al. [123-124]. Their studies demonstrated that HCl treatment of bleached softwood kraft pulp yielded 180 x 3.5 nm whiskers and the same procedure was used in this study. The charge on the cellulose whiskers was measured using conductometric titration. The bulk charge on the sulfonated whiskers was found to be 9.73 mmol acid groups/100 g which is contrasted to the charge of the starting kraft fibers being 3.82 mmol acid groups/100 g. This increase in acid groups is due to the strong acid groups introduced by esterification of cellulose hydroxyl groups to sulfonate groups [123] during

the sulfuric acid catalyzed hydrolysis of pulp fibers. In contrast, the HCl generated whiskers had an absence of strong acid groups but weak acid groups of 1.4 mmol/100 g. Due to the lack of bulk charge on the HCl whiskers, the rod like particles of cellulose whiskers can contact and interact extensively with each other leading to the formation of loose and bulky aggregates [124]. The average yield of sulfonated cellulosic whiskers was 35%. By AFM analysis, nanocrystalline cellulose was observed to have rod like structure with an average length of sulfuric nanocrystalline cellulose in range of 150–200nm and a width of less than 20nm while hydrochloric nanocrystalline cellulose had an average length of 200–300nm and a width slightly less than 20 nm.

Films prepared from xylan alone have poor film forming ability which has been attributed to high glass transition temperature or poor solubility [8]. Plasticizers such as sorbitol have been added to suppress the glass transition temperature [8]. Plasticizers work by embedding themselves between the chains of polymers, spacing them apart and thus significantly lowering the glass transition temperature for the plastic and making it softer.

4.2.1 Mechanical Properties

The effects of reinforcing xylan films with sulfonated and hydrochloride cellulosic whiskers were explored by varying the whisker content from 0 to 10% by mass and using 50 wt% of sorbitol. Plasticizer content was varied from 20% to 50 % (20, 40 and 50 wt %) and it was observed that films formed at low plasticizer levels, less than 50 wt%, were brittle with low tensile strength and no further studies were preformed on these samples.

We then maintained this level of addition of plasticizer for all of our experiments and just varied the whisker content from 0 and 10 wt % (i.e., 0, 2.5, 5, 7, 10 wt of whisker) to carry out an analysis of physical properties with variations in whisker content. The composites were characterized for tensile energy absorption (TEA), tensile strength and strain, as summarized in Figures 11-13. The evaluation of tensile testing of the xylan-whisker composite film showed that the addition of cellulose whiskers resulted in an improvement in the strength properties of the composite film. Addition of 7 % of sulfonated whisker increased the tensile energy absorption of the film increases by 445 % and tensile strength of the film increases by 141 %. The addition of 5% of HCl whisker resulted in almost the same improvement in tensile strength and tensile energy absorption of the composite film as sulfonated whisker, but the addition of more than 5% of HCl whisker, caused a gradual decrease in strength properties. The tensile energy absorption of the composite film made of sulfonated whisker increased rapidly up to 7% mass addition and then a gradual improvement in strength properties with further addition of sulfonated whiskers. We also studied the tensile stiffness of xylan films and found that tensile stiffness of control xylan was 5.50 N/mm as compared to 8.20 N/mm of xylan-5% sufonated whisker and 27.59 N/mm of xylan-10% sulfonated whisker. Favier reviewed that the increase in mechanical properties can be attributed to strong hydrogen-bonded fish net network which is created from a random distribution of whiskers as shown in Figure 14 [169].

As recently reviewed by Samir et al. [3], the improvements in mechanical properties of the composite can be attributed to the formation of a rigid hydrogen-bonded network of cellulose whiskers that is governed by percolation mechanism. These

considerations and the importance of the aspect ratio of whiskers are contributing factors to the mechanical properties reported in this study.

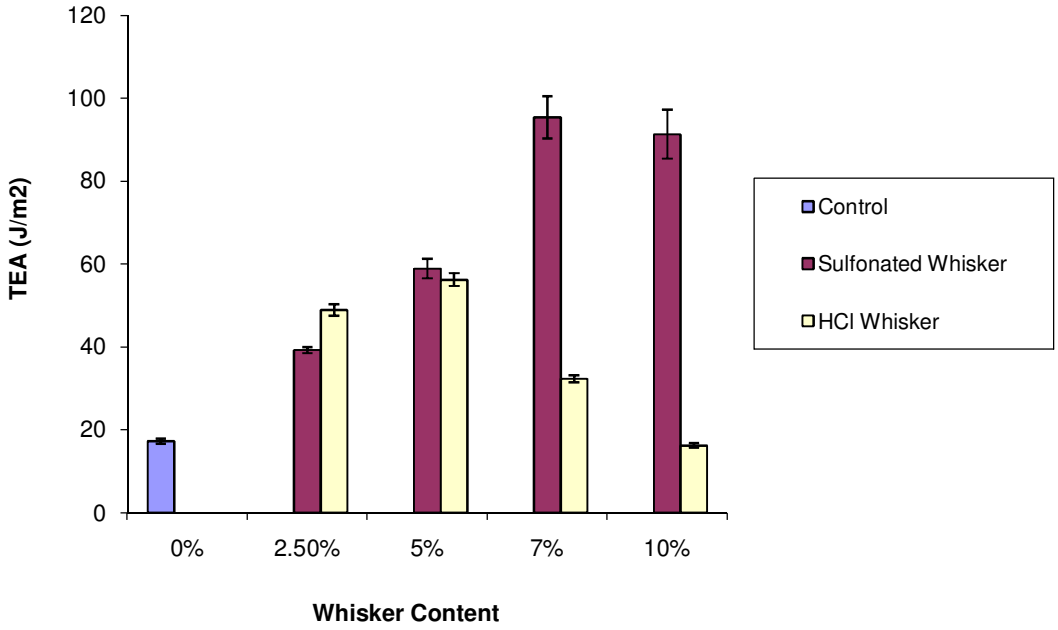

Figure 11. Effect of whisker on TEA of the xylan film

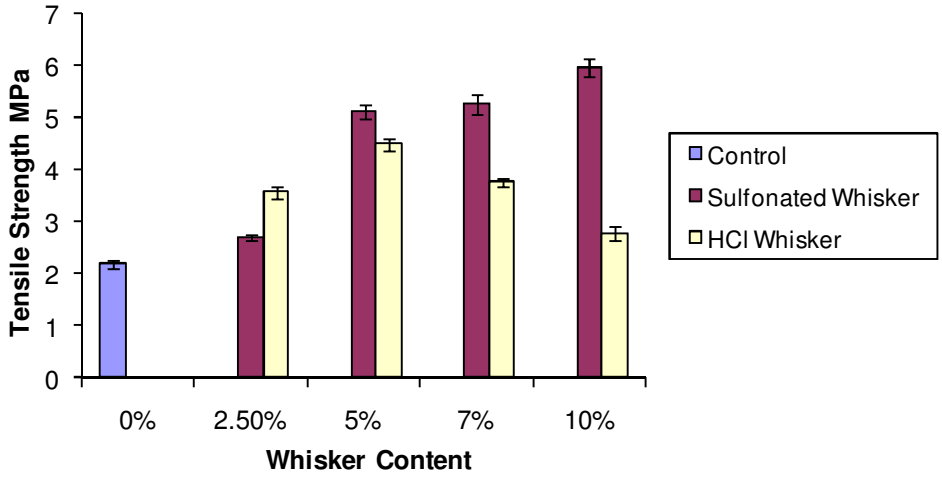

Figure 12. Effect of whisker on tensile strength of xylan film

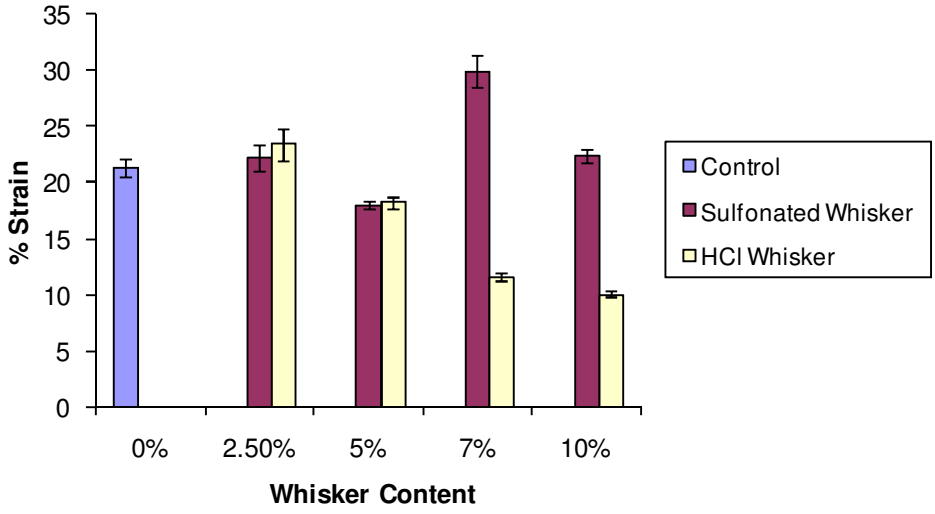

Figure 13. Effect of whisker on strain % on xylan film

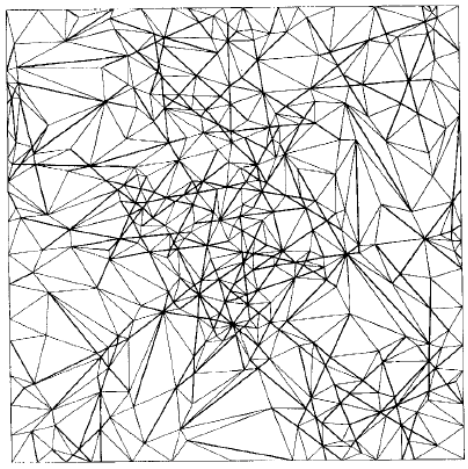

Figure 14. Piece of finite element mesh corresponding to an area fraction of whiskers, thick lines correspond to whiskers [169]

The specific density of xylan films was calculated and is summarized in Table 26.

Table 26. Specific density of xylan films.

Sample	Specific density of xylan films (g/cm^3)
Control (Xylan)	0.737
Xylan +5% sulfonated cellulose whiskers	0.756
Xylan+10% sulfonated cellulose whiskers	0.762

.
The resulting film thickness of xylan-sulfonated whisker film was 0.080±0.007 mm and for xylan-hydrochloride whiskers composite film was 0.087±0.005 mm.

4.2.2 Morphology of the composite films

The morphology of the composite films was analyzed by atomic force microscopy (AFM). The results are presented in Figure 15-16. AFM images of composite films show that the surface was not smooth instead composed of small nodules. The nodules were tightly connected to each other, forming a nodular structure. The functional pores were primarily the interstitial voids between closely packed nodules. Similar nodular structures were also reported for other hemicelluloses based films [211] as well as films from other polymers such as cellulose [212], cellulose acetate [213], starch [214]. Gabrielii et al. reported that the film obtained from xylan and chitosan showed a very smooth surface indicating a strong interaction between xylan and chitosan [215].

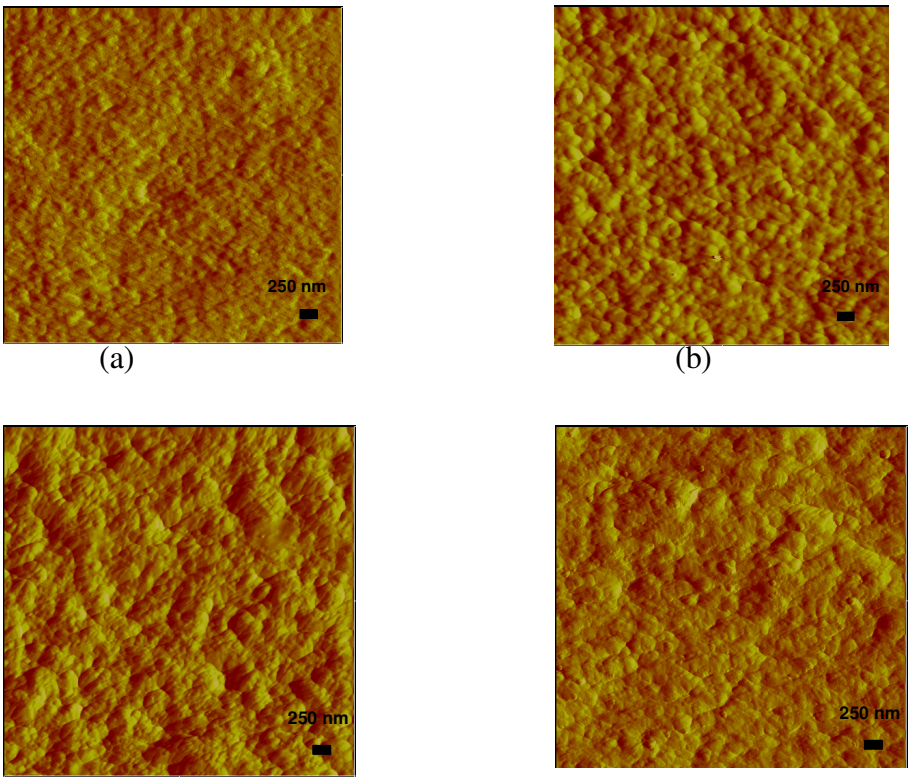

(a) (b)

(c) (d)

Figure 15. AFM images of film (a) control xylan from oat spelts (b) 7% sulfonated whisker reinforced (c) 10 % sulfonated whisker reinforced (d) 7% sulfonated whisker reinforced sample imaged after tensile testing.

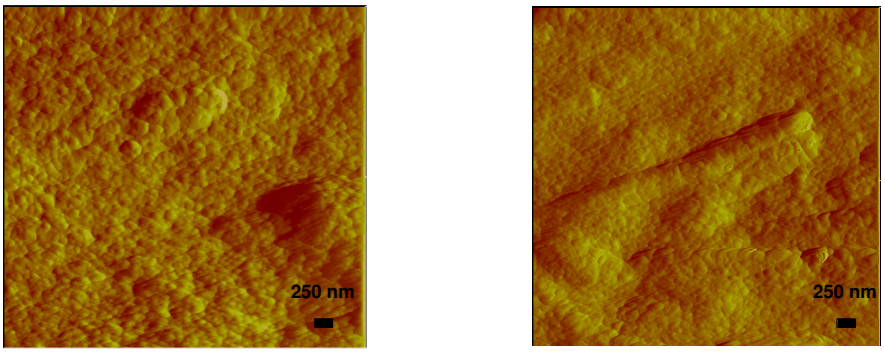

(a) (b)

Figure 16. AFM images of film (a) 2.5% hydrochloride whisker reinforced (b) 10 % hydrochloride whisker reinforced

AFM images were collected with tapping mode in air and are amplitude images. The roughness measurements in nm^2 for each sample is done by using Eq. (1)

$$R_{rms}=R\left(F\sum_{i=1}^{i=N}(Z_i-Z_{ave}),\ N\right)$$

where N is the number of points in the area examined, Z_i is the current height value,Z_{ave} is the average height value, and R_{rms}, is the root-mean square of the standard deviation for the height (Z) data.

Table 27. Statistical data for the composite films.

Sample	Roughness	Average	Standard Deviation
Control xylan	16.3, 20.2,22.3	19.6	3.0
+7% sulfonated whiskers	12.9,13.9,12.2	13.0	0.9
+5% hydrochloride whiskers	49.8,66.8,56.7	57.8	8.6
+10% hydrochloride whiskers	95.4,51.1,37.0	61.2	30.5
+7% sulfonated whiskers after tensile testing	23.3,28.4,27.5	26.4	2.7

The improvement in strength properties were attributed to a rigid hydrogen-bonded network of hydrogen bonded cellulose whiskers to form an integrated matrix as described by percolation theory integrated matrix. This trend is not, however, as evident with hydrochloride cellulose whiskers which shows poor dispersibility because of lack of strong acid groups on the HCl whiskers, which makes the rod like particles to contact and interact extensively with each other leading to the formation of loose and bulky aggregates as the loading of HCl whiskers was increased from 7% to 10%. Table 28 shows the statistical data of the composite films which shows that as the loading of HCl

whiskers increases from 2.5% to 10% the roughness of the films increases. The interpretation of the data was confirmed by surface roughness measurements which provided values of 19.59, 43.32, 57.75 and 61.15 for the control, 2.5%, 5%, 10% hydrochloride cellulose whiskers reinforced films, respectively. The surface roughness measurement of 7% xylan-sulfonated whiskers film shows the value of 12.97. The HCl generated whiskers had an absence of strong acid groups but weak acid groups of 1.4 mmol/100 g. Previous data from Akari et al. [123,124] reported that in the HCl treated fibers no strong acid groups were detected and <1.8 mmol/100 g weak acid groups were present which is comparable to our studies. The lack of strong acid groups presumably facilitates greater cellulose whisker–whisker interactions leading formation of aggregates [123,124].

4.3 Summary

Nanocellulosic-xylan films were prepared employing oat spelt xylan, cellulose whiskers and a plasticizer. The mechanical properties of the films were evaluated using tensile testing under controlled temperature and humidity conditions. The tensile data showed that the addition of sulfonated cellulose whiskers lead to a substantial improvement in strength properties. Addition of 7 wt% of sulfonated whiskers increased the tensile energy absorption of xylan films by 445 % and the tensile strength of the film by 141%. Furthermore, films to which 7% cellulose whiskers were added showed that nanocellulose whiskers produced with sulfuric acid (sulfonated whiskers) were significantly better at increasing film strength than cellulose whiskers produced by hydrochloric acid hydrolysis of cellulosic fibers. The formation of a continuous cellulosic network formed when the percolation threshold is reached is probably responsible for the unusual mechanical

properties of cellulose whisker reinforced nanocomposites. The interface between the matrix and reinforcement plays a critical role in determining the external load transfer within the films. The stiffness of this cellulosic network is due to strong interactions like hydrogen bonds between the cellulose whiskers and the matrix (xylan), similarly to what is observed for a paper sheet for which the hydrogen-bonding forces hold the percolating network of fibers. These interactions allow good interfacial adhesion between matrix and cellulose whiskers. Thus the improvement in the mechanical properties of the nanocomposite film as a consequence of the addition of cellulose whiskers could be ascribed to the high aspect ratio of cellulose whiskers, good mechanical strength of cellulose whiskers, and the strong interactions between cellulose whiskers and matrix.

CHAPTER 5

WATER TRANSMISSION BARRIER PROPERTIES OF BIODEGRADABLE FILMS BASED ON CELLULOSIC WHISKERS AND XYLAN

5.1 Introduction

In this chapter xylan based composites reinforced with sulfonated cellulose whiskers are discussed. The goal was to understand the effects of cellulose whiskers addition on the water vapor transmission properties of the composite and to compare the water transmission rate with softwood fiber reinforced composites.

The majority of engineered plastic materials used today are made from synthetic polymers. The use of conventional petroleum-based polymer products creates many potential problems due to their non-renewable nature and ultimate disposal. Cellulose and its derivatives, when used in such applications, offers advantages with respect to sustainability, limited environmental impact and simplified end-of-life disposal issues [3-5]. Of growing interest is the use of polysaccharide derived films as an alternative to petro-based materials such as polyvinyl alcohol and polyvinylidene chloride. Early studies examined the application of chitosan, starch and cellulose derivatives which were shown to have film forming properties [6]. Glucuronoxylan isolated from aspen has been used to produce films [8-9] that exhibit improved strength and oxygen barrier properties when plasticized with xylitol or sorbitol. Höije et al. [10] have shown that arabinoxylan film can be prepared from the extracts of barley husks without the need for plasticizers. The resulting films were stiff and rather brittle with high water content. Dammström et al.

[11] prepared composite films of glucuronoxylan reinforced with bacterial cellulose and showed that this biocomposite could form transparent strong films. The use of xylan for the production of biodegradable composite films in combination with wheat gluten has been investigated [12]. The presence of xylan did not adversely affect the film forming quality or the water vapor transmission rate, though the mechanical and solubility properties depended on the quantity of xylan in the wheat gluten. Recently, studies by Saxena et al. [181] have shown that oat-spelt xylan, plasticized with sorbital and reinforced with sulphuric acid generated cellulose whiskers exhibited enhanced strength properties [206]. For example, the addition of 7% sulfonated whiskers increased the tensile energy absorption of the xylan films by 445 % and the tensile strength of the film by 141%. As reviewed by Samir et al. [3], the improvements in mechanical properties of the composite can be attributed to the formation of a rigid hydrogen-bonded network of cellulose whiskers that is governed by percolation mechanism. The objective of this study is to evaluate the effect of reinforcing xylan films with cellulose whiskers with respect to water transmission properties.

5.2 Results and discussion

This study examines the reinforcement of xylan/sorbitol films with cellulose whiskers and its impact on water transmission. The films were prepared with varying amounts of cellulose whiskers which were prepared by sulfuric acid hydrolysis of softwood bleached kraft fibers.

By AFM analysis the cellulosic whiskers were observed to have rod like structure with an average length of 150-200 nm and a width of less than 20 nm. Previous studies

have indicated that AFM measurements of cellulose whiskers overestimated the width of the whiskers due to the tip broadening effects [216].

Prior studies have shown that the addition of 7% sulphonated whiskers increased the tensile energy absorption of the xylan films by 445 % and the tensile strength of the film by 141 % [206]. To determine if cellulose whiskers impact water transmission properties a series of xylan composite films were prepared and analyzed using optical microscope and scanning electron microscopy.

5.2.1 Water vapor transmission rate properties

The specific water transmission rate (WVTR) of the xylan films are shown in Fig 17. Because the thickness of the xylan-sulfonted whiskers and xylan-softwood fiber are different, the WVTR is sometimes normalized to film thickness (l) to obtain the specific water vapor transmission rate (Ŕ=WVTR*l) with units of gmil/hm^2 [217]. The technique used to measure water vapor transmission rate (WVTR) was a modification of the wet cup method described by ASTM E 96-95. The procedure involves using a Petri dish filled with distilled water and covered with a film. The mass of water lost from the dish was monitored as a function of time. Thickness measurements of the films were obtained with a digital gauge at a minimum of five positions on a test specimen. The glass petri dish was filled with distilled water (10.00 mL) and then the film was sealed to the petri dish with a 5-minute epoxy adhesive. After allowing the epoxy to cure for 30 min, the sample dish was weighed and placed in a convection oven at a setting of 37.0 ºC in the oven. The sample dish was periodically removed and weighed. The weight loss over a period of 24 h was determined. The water vapor transmission rate was calculated using: WVTR=mass of water lost/time*area = flux/area with units of g h $^{-1}$ m^{-2}.

The incorporation of sulfonated cellulose whiskers was found to reduce WVTR film properties. The composites were characterized for water vapor transmission rate, as summarized in Figure 17. For example, the incorporation of 10% sulfonated cellulose whiskers into a xylan film decreased the specific WVTR value from 304 g/hm^2 of the control to 174 g/hm^2 of xylan-cellulose whisker films. It appears that the high degree of crystallinity of cellulose whiskers, dense composite structure formed by the whiskers and rigid hydrogen bonded network of cellulose whiskers can causes cellulose whsikers to form integrated matrix which contribute to substantial benefit in the overall reduction of water transmission.

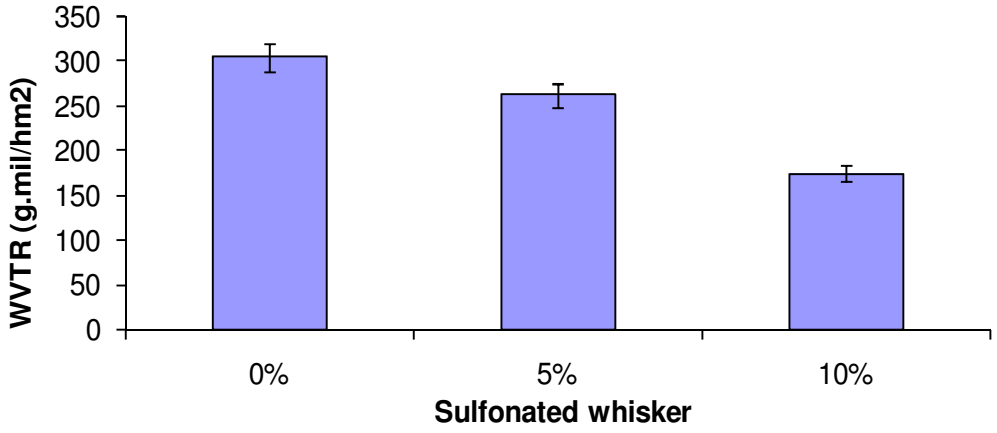

Figure 17. Effect of sulfonated whisker dosage on specific water vapor transmission rate of xylan films.

Similar experiments were performed using a softwood kraft fiber as reinforcement in a xylan film and it was found that with 5% pulp fibers specific water vapor transmission rate increases which increases further on addition of 10% pulp fibers to xylan as summarized in Table 28.

Table 28. Specific water vapor transmission rate of xylan films.

Sample	Specific water vapor transmission rate (gmil/hm^2)
Control (Xylan)	304
Xylan +5% softwood fiber	537
Xylan+10% softwood fiber	807
Xylan + 10% sulfonated cellulose whiskers	174

5.2.2 Morphology of xylan-cellulose whiskers and xylan-soft wood fibers composite films

Optical microscope images of xylan, xylan-softwood kraft fiber and xylan-cellulose whisker films were acquired both before and after the water transmission rate and these are summarized in Figure 18. The xylan control in Figure 18a shows hexagonal platelets like pattern [139]. The xylan-softwood kraft fiber films exhibited fiber aggregation as shown in Figure 18c; this can be reason of higher barrier properties of xylan-sulfonated whisker than xylan-softwood kraft fiber films which have a more open structure.

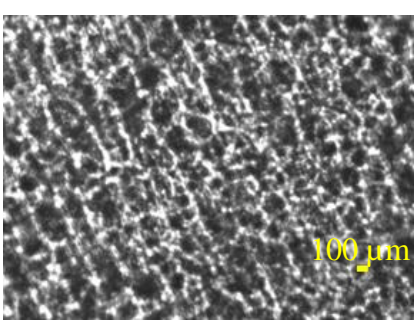

(a)

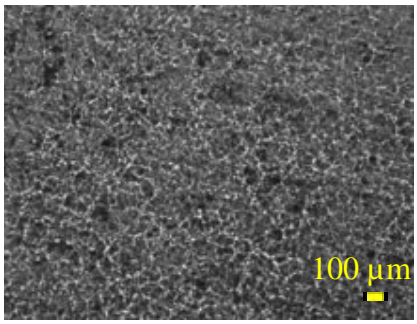

(b)

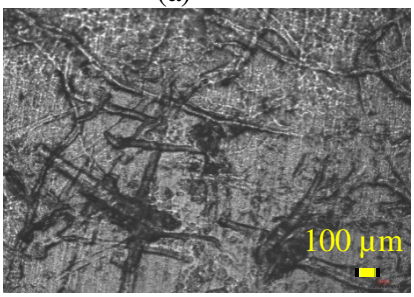

(c)

Figure 18. Optical microscope image of (a) control xylan (b) xylan reinforced with 10% sulfonated cellulose whiskers (c) xylan reinforced with softwood fibers

SEM images of fractured membrane surface of control xylan in Figure. 19(a) & (b) showed rough texture in comparison to smooth surface of fractured surface of xylan reinforced with cellulose whiskers in Figure 20(a) & (b). SEM images of control xylan film surface in Figure 19(c) shows agglomeration in comparison to well dispersed sulfonated cellulose whiskers on xylan surface in Figure 20(c). The uneven structure and agglomeration of the xylan can be the cause of higher water vapor transmission rate of control xylan film in comparison to xylan reinforced with sulfonated cellulose whiskers. It appears that pulp fibers cannot form an integrated matrix that cellulose whiskers can and this latter effect has a substantial benefit in the overall reduction of water transmission.

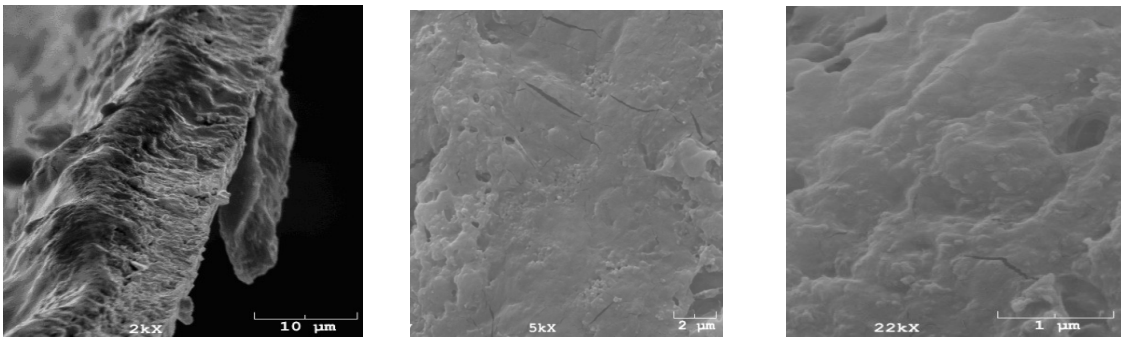

(a) (b) (c)

Figure 19. Scanning electron microscopic images of control xylan film (a) cross section images (b) and (c) surface image

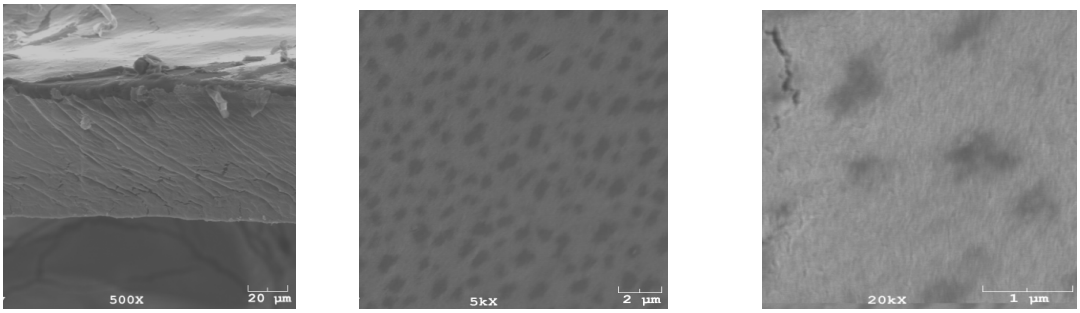

(a) (b) (c)

Figure 20. Scanning electron microscopic images xylan film reinforced with 10% sulfonated cellulose whiskers (a) cross section image (b) and (c) surface image.

The specific density of xylan films was calculated and is summarized in Table 29. The data shows that the xylan-10% cellulose whisker films were denser than the control and the xylan-10% softwood films.

Table 29. Specific density of xylan films.

Sample	Specific density of xylan films (g/cm^3)
Control (Xylan)	0.7272
Xylan +5% sulfonated cellulose whiskers	0.7560
Xylan+10% sulfonated cellulose whiskers	0.7616
Xylan + 16% sulfonated cellulose whiskers	0.7451
Xylan + 50% sulfonated cellulose whiskers	0.6600
Xylan + 10% softwood fiber	0.1780

Lagaron et al. [47] discussed the role of crystalline structure of plastics and emphasized that high crystallinity improves barrier properties. Cellulose whisker have high crystallinity [48] which is more than 60% together with the dense network held together by rigid hydrogen-bonded network of cellulose whiskers which causes more tortuous path for water molecules to follow and less water molecules to penetrate the crystalline part of cellulose whiskers and this may lower the water transmission rate.

5.3 Summary

The reinforcement of natural biopolymers with cellulosic whiskers has been shown to be beneficial for physical strength properties including xylan films. This study examines the water transmission properties of xylan films reinforced with cellulosic whiskers prepared from kraft pulp hydrolyzed with sulfuric acid. Measurements of water transmission rate (WVTR) were accomplished by a modification of wet cup method described by ASTM E 96-95. The results showed that films prepared by xylan reinforced by 10% sulfonated whiskers exhibited a 74% reduction in specific water transmission properties with respect to xylan film and a 362% improvement with respect to xylan films reinforced with 10% softwood kraft fibers. It appears that the high degree of crystallinity of cellulose whiskers,

dense composite structure formed by the whiskers and a rigid hydrogen-bonded network of cellulose whiskers that is governed by percolation mechanism can cause cellulose whiskers to form integrated matrix which contribute to substantial benefit in the overall reduction of water transmission. Optical microscopic images indicated that xylan incorporated with softwood kraft fiber films exhibit fiber aggregation in comparison to well dispersed sulfonated nanocrystalline cellulose on xylan surface. SEM images also support that xylan film contains well dispersed nanocrystalline cellulose as compared to rougher surface of control xylan due to aggregation. The aggregation in control xylan and xylan softwood kraft fiber films provides more open structure and channels for rapid permeation in the film leading to higher water vapor transmission rate as compared to xylan-sulfonated nanocrystalline cellulose films. This can be reason of higher barrier properties of xylan-sulfonated whisker than xylan-softwood kraft fiber and control xylan films which have a more open structure.

CHAPTER 6

MOISTURE BARRIER PROPERTIES OF XYLAN COMPOSITE FILMS

6.1 Introduction

In this chapter moisture barrier properties of films based on xylan reinforced with nanocrystalline cellulose, acacia bleached kraft pulp fibers and softwood kraft fibers have been evaluated. The goal has been to evaluate several cellulosic resources with wide range in size dimension and also to evaluate the effect of hydrochloric made nanocellulose and sulphonated based cellulose on water transmission rate properties. The goal was also to understand the interaction of the fillers with the matrix using FTIR studies.

Xylan is one the most common hemicelluloses and is the most abundant polysaccharide in nature after cellulose [146,178, 180]. Glucuronoxylan, isolated from aspen wood, when plasticized with xylitol or sorbitol has been used to produce films that exhibit improved strength and oxygen barrier properties with respect to control glucuronoxylan films [8-9]. Höije et al. [10] have shown that arabinoxylan films can be prepared from the extracts of barley husks without the need for plasticizers. Dammström et al. [11] showed that films based on glucuronoxylan reinforced with bacterial cellulose have tensile strength values ranging between 65 and 110 MPa. Xylan has also been used as an additive with wheat gluten for the production of biodegradable composite films [12]. The xylan did not adversely affect the film forming quality or water vapor transmission rate, although mechanical and solubility properties were dependent on the quantity of xylan in the wheat gluten. Water vapor transmission rate is an important

property for many film packaging applications influencing shelf life and product stability. Tock [17] reviewed some of the permeability and water vapor transmission rate properties of commercial polymeric films and provided an overview of how structural changes, such as crystallinity, and the presence of plasticizers and lamination can influence the barrier properties of polymer films. Miranda et al. [194] discussed water vapor transmission values of chitosan film plasticized with sorbitol, glycerol or polyethylene glycol reporting values from 1.3-1.5×10^{-3} [g/(m^2. h. Pa)]. Aydinli et al. [195] determined WVP of 6.3–11.6×10^{-8} [g/ (m. h. Pa)] for polyethylene glycol-plasticized locust bean gum as compared to 6.2-11.6 ×10^{-5}[g .mm/ (m^2. h. Pa)] reported by Mikkonen et al. [51]. The WVP of sorbitol-plasticized oat spelt arabinoxylan films studied using a fan-equipped desiccator was 4.5×10^{-5} [g. mm/ (m^2. h. Pa)] [197], while Péroval et al. [198] reported a value of 63.7×10^{-8} [g/ (m. h. Pa)] for corn arabinoxylan films. Saxena et al. [181] have shown that the addition of 7% sulfonated nanocellulose whiskers to xylan increased the tensile energy absorption of the resulting films by 445% and the tensile strength of the film by 141%. The improvements in mechanical properties of the composite film based on reinforcement with cellulose whiskers can be attributed to the formation of a rigid hydrogen-bonded network of cellulose whiskers that is governed by the percolation mechanism [3]. Recent studies by Saxena et al. [218] have also shown that xylan films reinforced with 10% sulfonated nanocrystalline cellulose exhibited a 74% reduction in specific water transmission properties with respect to control xylan film and 362% improvement with respect to xylan reinforced with 10% softwood kraft pulps. The objective of this study is to compare these previous results with xylan films reinforced with hydrochloric acid prepared nanocrystalline cellulose and films reinforced

with acacia and softwood bleached kraft fibers. The bleached acacia kraft fiber was selected because it is one of the shortest commercially available pulp fibers with a weight-weighted length of 0.62 mm and width of ~0.02 mm and yet is approximately 4000 orders of magnitude larger than the cellulosic whiskers employed.

6.2 Results and discussion

This study examines the reinforcement of xylan/sorbitol films with nanocrystalline cellulose, bleached acacia fiber and softwood kraft fibers and its impact on water transmission. By AFM analysis, nanocrystalline cellulose was observed to have rod like structure with an average length of sulfonated nanocrystalline cellulose in range of 150-200 nm and a width of less than 20 nm while hydrochloric nanocrystalline cellulose had an average length of 200-300 nm and a width slightly less than 20 nm. These results are consistent with literature reported for nanocrystalline cellulose prepared from softwood kraft pulps using sulfuric acid and hydrochloric acid. The differences in the organization between the two preparations can be seen sulfonated whiskers exhibiting more orderly, parallel arrangement compared to the aggregation of the hydrochloride whiskers (Figure 21).

Sulfonated whiskers Hydrochloride whiskers

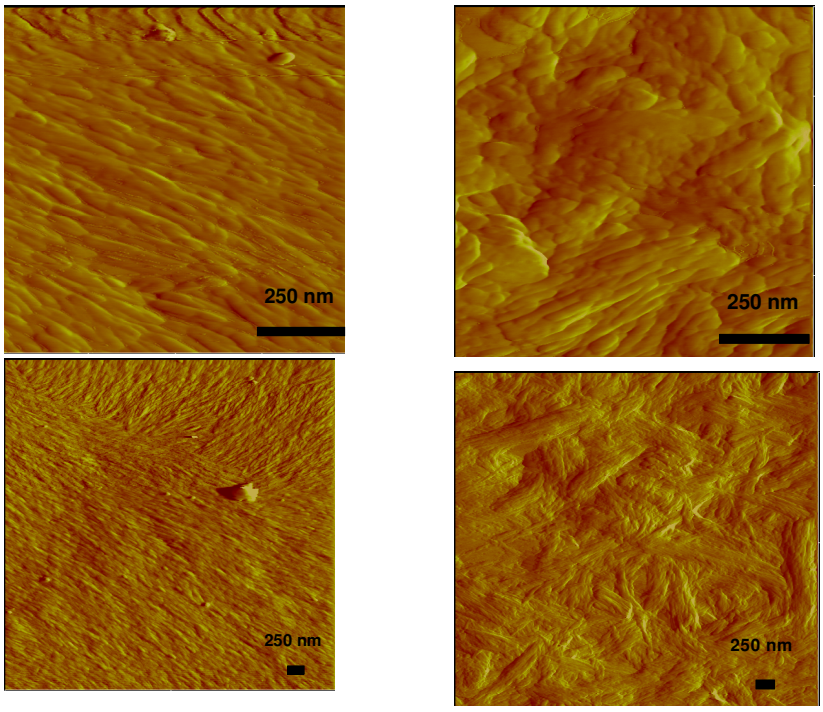

Figure 21. AFM images of sulfonated and hydrochloride whiskers

Saxena et al. [181] have shown that oat-spelt xylan, plasticized with sorbital and reinforced with 7% sulfonated nanocrystalline cellulose increased the tensile energy absorption of the xylan films by 445 % and the tensile strength of the film by 141% with respect to control xylan film. Saxena et al. [218] have also shown that when xylan film are reinforced with 10% sulfonated nanocrystalline cellulose, WVTR reduces from 304 g.mil/hm^2 for control to 174 g.mil/hm^2 for xylan-sulfonated nanocrystalline cellulose films.

6.2.1 Moisture barrier properties of xylan composite films

To determine the impact of alternative cellulosic fillers on water transmission properties, a series of xylan composite films were prepared and analyzed using the water vapor transmission test. In the current work, similar experiments were performed using acacia

fiber and hydrochloric prepared nanocrystalline cellulose as reinforcement in a xylan film. Because the thickness of the xylan-sulfonted nanocrystalline cellulose, xylan-softwood fiber and xylan-acacia fiber are different, the WVTR was normalized to film thickness (l) with units in mm to obtain the specific water vapor transmission rate ($\acute{R}$=WVTR×l) with units of g.mm/d.m^2 [217].

Table 30. Specific water vapor transmission rate of xylan films

Sample	Specific water vapor transmission rate (g.mil/h.m^2)
Control (Xylan)	304±15
Xylan + 10% acacia fiber	283±11
Xylan + 10% hydrochloric prepared nanocrystalline cellulose	281±9
Xylan+ 10% softwood fiber	807 ±24
Xylan + 10% sulfonated nanocrystalline cellulose	174±8

Xylan films reinforced with 10% acacia fiber and 10% hydrochloric nanocrystalline cellulose exhibited virtually no improvement in specific water vapor transmission rate in comparison to control. Xylan film reinforced with 10% sulfonated nanocrystalline cellulose exhibited lowest specific water transmission rate of 174 gmil/hm^2 and xylan film with softwood fiber exhibited highest water transmission rate as summarized in Table 30. The water transmission rate at other levels is summarized in Figure 22. It was found that the addition of 5% softwood kraft pulp fibers yielded a xylan film with increased specific water vapor transmission rate and a significant high water vapor transmission rate at 50% dosage with respect to control. The addition of softwood kraft fibers in the xylan film causes a significant high specific water vapor transmission

rate at any dosages (5%, 10%, and 50%). Addition of hydrochloric acid prepared nanocrystalline cellulose to xylan films was also analyzed for specific water transmission rate. The specific WVTR values decreased as the content of HCl generated nanocrystalline cellulose in the xylan film increased from 0% to 5% and further decreases at higher dosage of 50% addition in the xylan. WVTR values of xylan-50% hydrochloric nanocrystalline cellulose are almost similar to the values of xylan-10% sulfonated nanocrystalline cellulose.

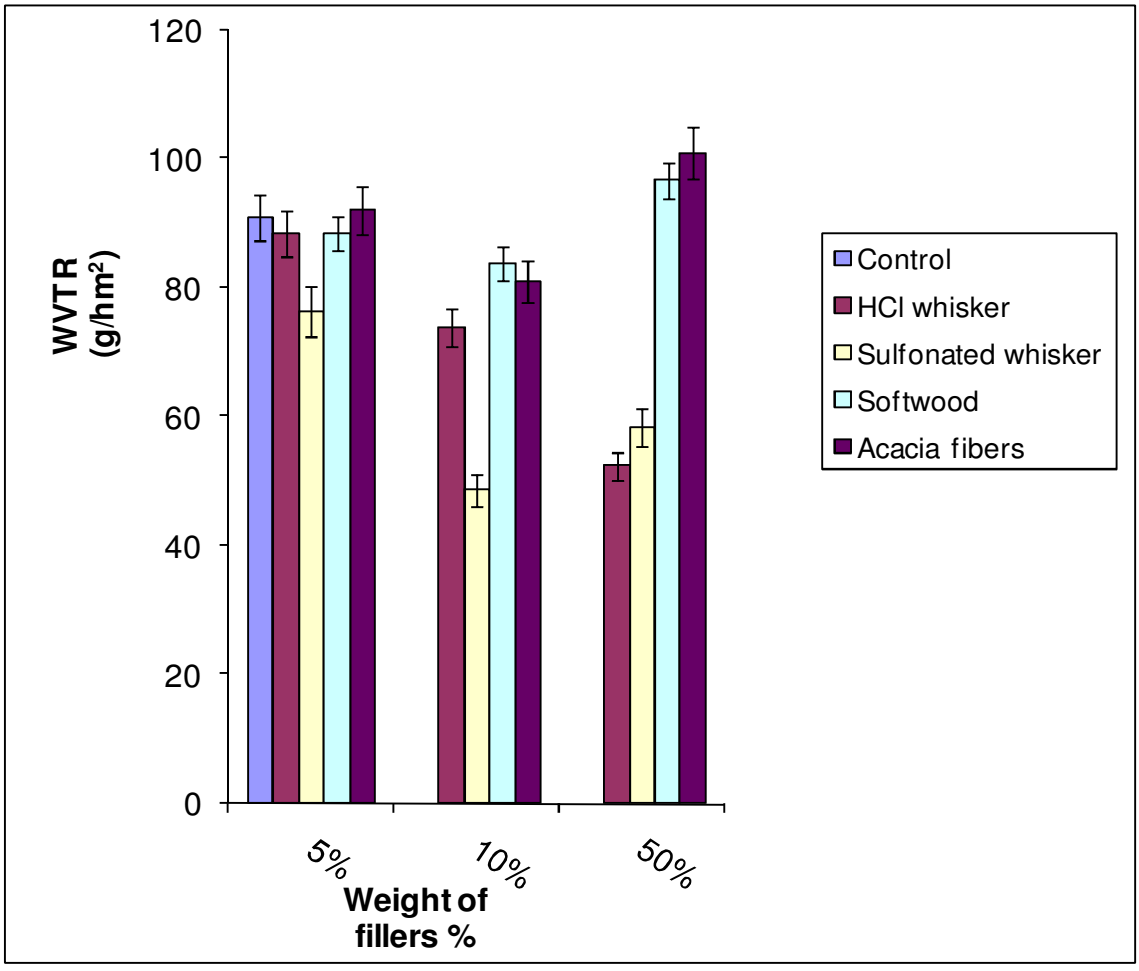

Figure 22. Water vapor transmission rate for xylan films

The rate of water transmission for the composite xylan and control films for first 24 hours is summarized in Figure 23. As can be seen, the control xylan film has a higher rate of weight of water loss per unit time whereas 10% sulfonated nanocrystalline cellulose and 50% hydrochloride generated nanocrsytalline cellulose reinforced xylan films have the lowest weight difference loss per unit time. The rate increases initially then remains constant for control, sulfuric nanocrystalline cellulose and hydrochloric nanocrystalline cellulose reinforced film but for acacia and softwood fiber reinforced film, the rate shows an increase trend.

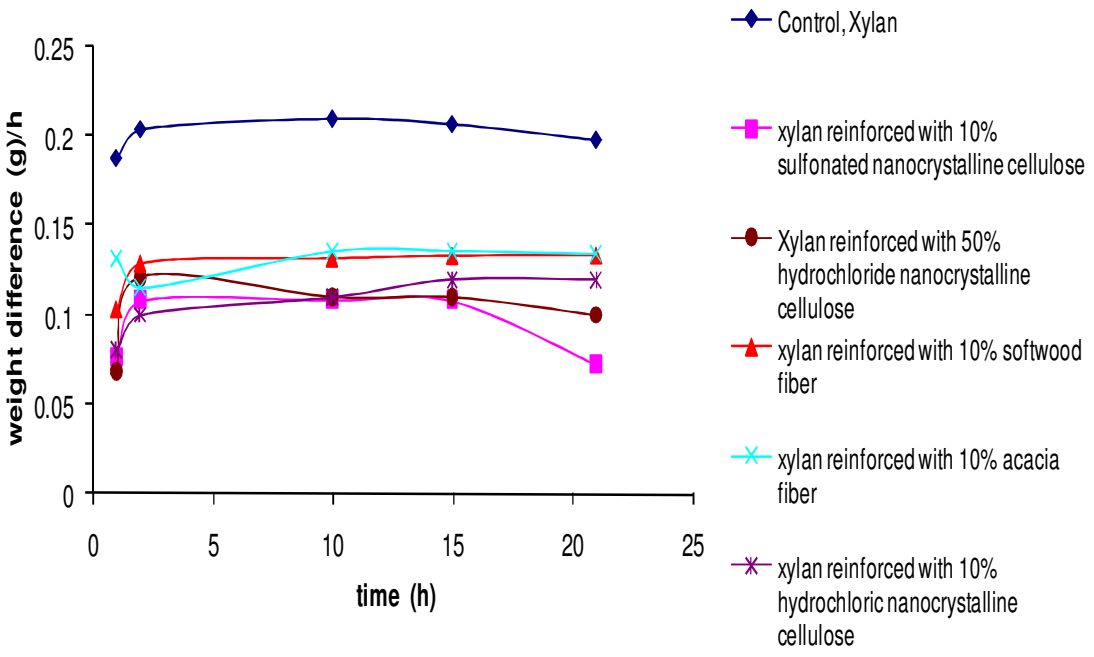

Figure 23. Rate of water vapor transmission of xylan films for 24 h

The mechanism of water transmission can be attributed to a diffusion process in which water vapor condenses and dissolves on film surface and then liquid water diffuses through the membrane and finally water vapor evaporates from the other side of film.

The low initial rate can be described as initial adsorption phase when water vapor condenses and dissolves on film surface and then liquid water diffuses through the membrane and finally water vapor evaporates from the other side of film. The incorporation of sulfonated cellulose whiskers was found to reduce WVTR properties which can be attributed to the tortuous path the water molecules have to travel around the cellulose whiskers to diffuse through the film. Since, the filler material is crystalline together with the dense, rigid hydrogen bonded network, it acts as a physical barrier to the transport of the diffusing molecules. Furthermore, since cellulose whisker and xylan are hydrophilic in nature, the diffusing water molecules could be absorbed via hydrogen bonding, which would also alter the flux. Once steady state equilibrium is attained, the flux remains constant. It appears that pulp fibers cannot form an integrated matrix that cellulose whiskers can and this latter effect has a substantial benefit in the overall reduction of water transmission. The uneven structure and agglomeration of the xylan can be the cause of higher water transmission rate of control xylan film in comparison to xylan reinforced with sulfuric nanocrystalline cellulose.

6.2.2 *Spectroscopy*

Figures 24 and 25 show the FT-IR spectra of xylan films containing sulfonated nanocrystalline cellulose, acacia fiber, softwood kraft pulp fibers and hydrochloric nano crystalline cellulose, respectively. Several characteristic bands of nanocrystalline cellulose can be readily assigned at 3340 cm^{-1} (OH stretch) and 2893 cm^{-1} (CH_2 stretch).A strong absorption band can be observed at 3330 cm^{-1} after addition of nanocrystalline cellulose for all concentrations, related to the typical O-H vibration of crystalline nanocellulose. The intensity of overall O-H band (3200–3450 cm^{-1}) increases

with the nanocellulose whiskers concentration, suggesting an increase of hydrogen bonding between xylan and nanocrystalline cellulose, suggesting the strong interactions occurred between the sulfates group of nanocrystalline cellulose surface and the matrix [219-220]. Other bands 1160 and 1070 cm^{-1} have their intensity increased after nanocrystalline cellulose addition and these bands are specific to cellulose, and some of them have been studied in detail to determine the crystalline organization [221] . Strong peaks around 1100 cm^{-1} assigned to secondary alcohol. The peak at 1205 cm^{-1} is sulfate peak of cellulose nanocrystalline cellulose from the esterification reaction. The peak at (3200–3450 cm^{-1}) of the nanocomposite moved to higher wavenumbers suggesting a strong interaction occurred between filler and the matrix [111]. The band in the spectrum near 1680 cm^{-1} is assigned mainly to C=O stretching vibration of carbonyl and acetyl groups in the xylan component of hemicellulose. The interactions between cellulose and xylan in a model system consisting of bacterial cellulose/glucuronoxylan have been studied in the past that showed strong interactions existed between cellulose and xylan [222].

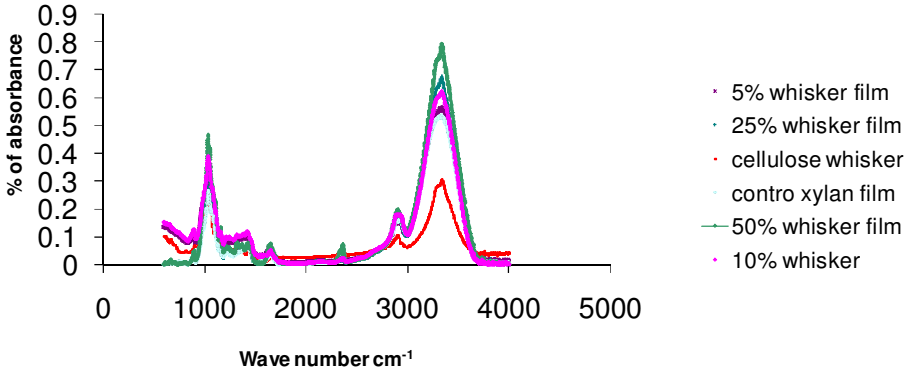

Figure 24. FTIR of xylan-sulfonated nanocrystalline cellulose film

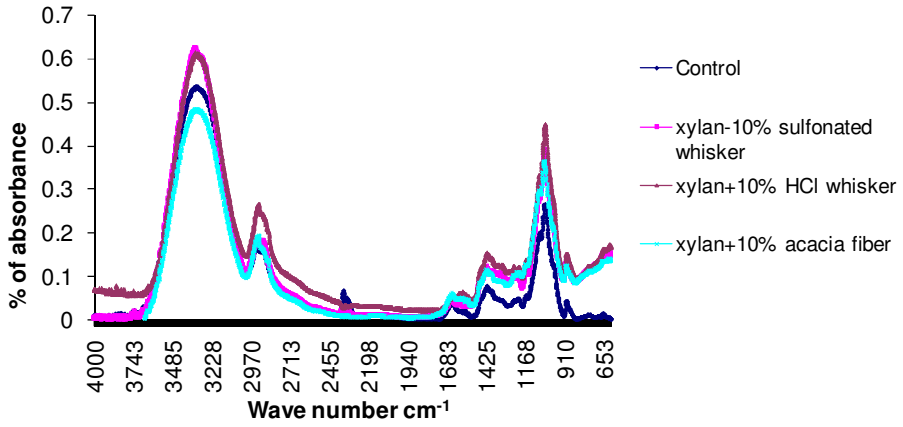

Figure 25. FTIR of xylan-10% different fillers composite film

6.2.3 Morphology of xylan composite films

Optical microscope images of xylan, xylan-softwood kraft fiber and xylan-nanocrystalline cellulose films were acquired both before and after the water transmission rate studies and these results are summarized in Figures 26-28. The xylan-sulfonated nanocrystalline cellulose film appears denser than control xylan film as seen in Figure 26. The xylan control film shown in Figure 26a exhibits hexagonal platelets like pattern [139]. Optical microscope images of xylan-acacia films were acquired before the WVTR test and immediately after and these results are summarized in Figure 27. Xylan-acacia films appear swollen after the water vapor transmission study as can be seen in Figure 27(a-b). The specific density of xylan films was also calculated and the result shows that the xylan-10% nanocrystalline cellulose films were denser than the control xylan, xylan-10% softwood and xylan-10% acacia films with specific densities of 0.7616, 0.7272, 0.1780, 0.1132 g/cm^3 respectively. The less dense structure of the control xylan, xylan-10% softwood and xylan-10% acacia films in comparison to the xylan-10%

nanocrystalline cellulose film leads to lower water transmission rates for the xylan-sulfonated nanocrystalline cellulose films in comparison to the other films.

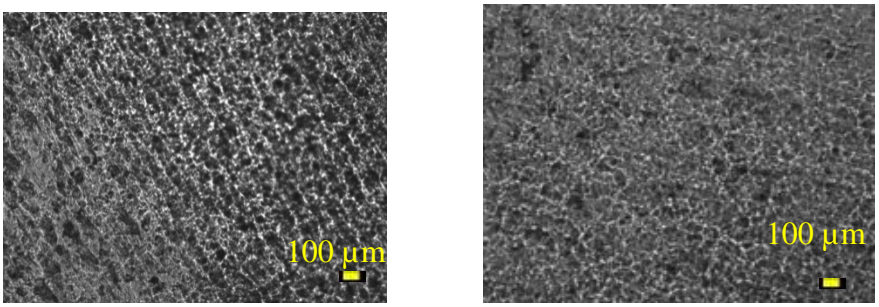

(a) (b)

Figure 26. Optical microscope image of (a) control xylan (b) xylan reinforced with sulfonated nanocrystalline cellulose

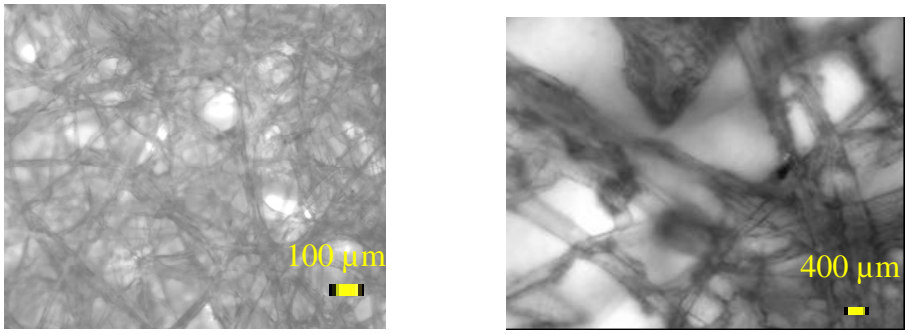

(a) (b)

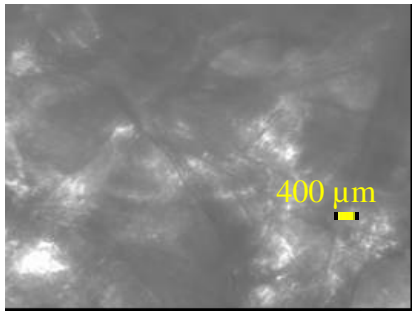

(c)

Figure 27. Optical images of (a) and (b) xylan reinforced with ECF bleached acacia kraft fibers before water vapor transmission rate showing more open structure (c) dense swollen film of xylan-acacia fibers after water vapor transmission rate test.

The optical micrograph of xylan film reinforced with softwood kraft fibers, exhibited in Figure 28c, shows fiber aggregation which may provides channels in the membrane that allow for more rapid permeation of water.

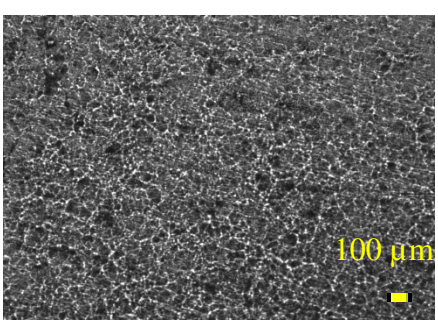

(a)

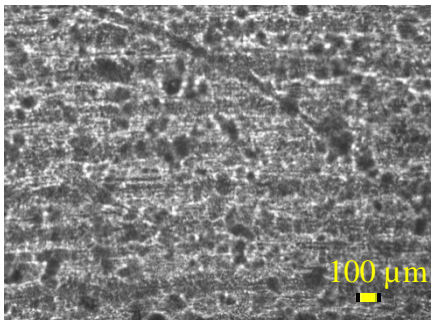

(b)

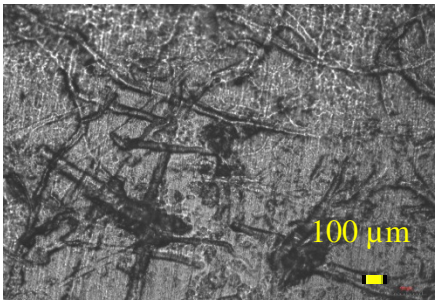

(c)

Figure 28. Optical images of xylan reinforced with (a) sulfonated nanocrystalline cellulose (b) hydrochloride nanocrystalline cellulose (c) softwood fibers.

Nanocrystalline cellulose has been reported to have crystallinity values greater than 60% [48,223]. This property, together with the resulting rigid hydrogen-bonded network of nanocrystalline cellulose was attributed to cause an increase in tortuousity [207] for water molecules to follow and the crystalline portion nanocellulose may further lower the water transmission rate as compared to more open structure of control xylan film as can be seen in Figure 29(a-d).

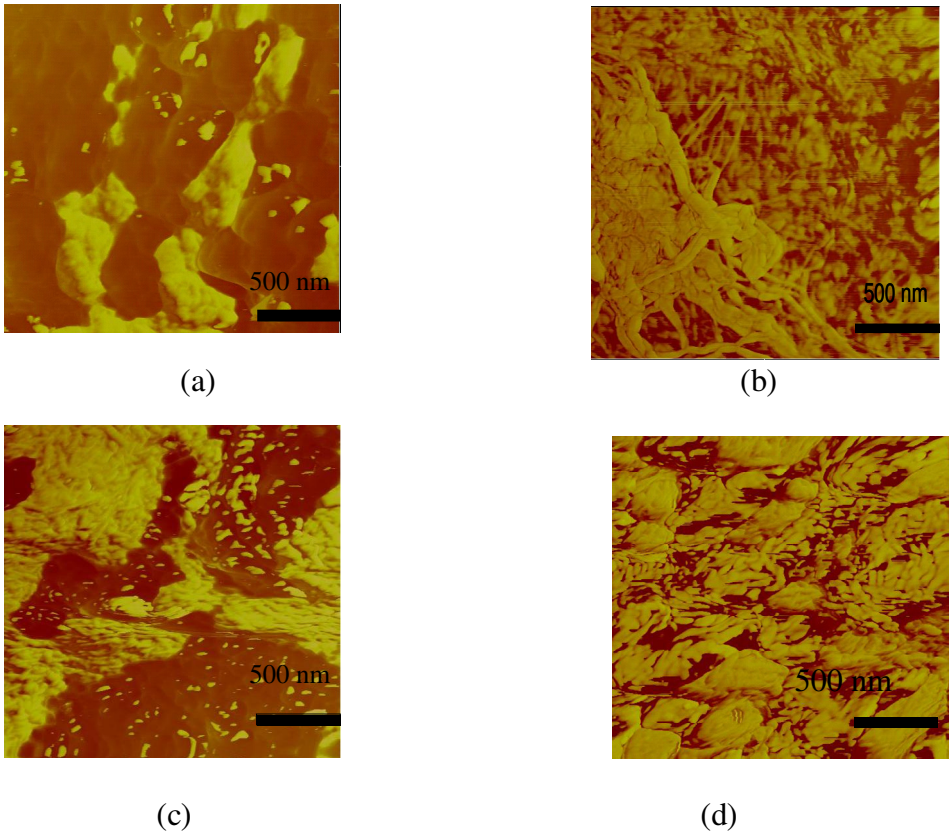

Figure 29. AFM images of fractured surface (a) control xylan (b) 10% (c) 25% and (d) 50% sulfonated nanocrystalline cellulose film

SEM images of control xylan film surface in Figure 30(a) shows agglomeration in comparison to well dispersed sulfonated nanocrystalline cellulose on xylan surface in Figure 30(b). Hydrochloric whiskers were observed to aggregate in the matrix as shown in Figure 30 (c). The uneven structure and agglomeration of the fibers can provide increase free volume of the matrix polymer leading to higher diffusivity of the permeating water molecules in the control xylan film which may cause higher water vapor transmission rate of control xylan in comparison to xylan reinforced with sulfonated nanocrystalline cellulose. It appears that pulp fibers cannot form an integrated matrix that nanocrystalline cellulose can and this latter effect has a substantial benefit in the overall reduction of water transmission.

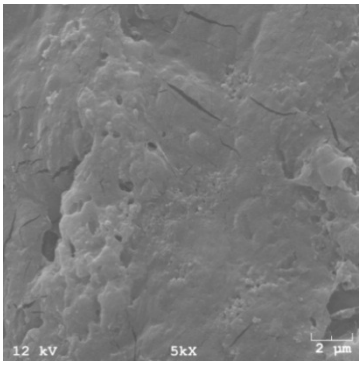

(a)

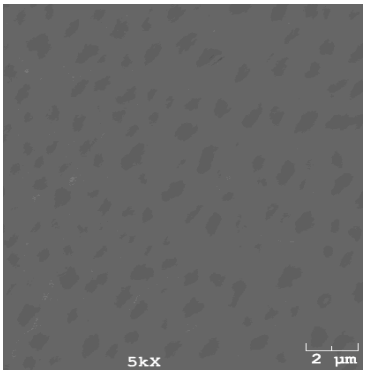

(b)

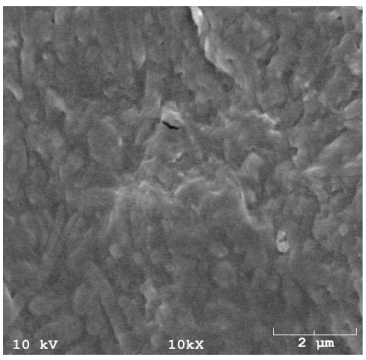

(c)

Figure 30. Scanning electron microscopic images of (a) surface image of control xylan (b) surface image of xylan sulfonated nanocrystalline composite film (c) surface image of xylan hydrochloric nanocrystalline composite film

6.3 Summary

Cellulose whiskers were incorporated into xylan slurry to prepare biodegradable films with improved water barrier properties. Measurements of water vapor transmission rate (WVTR) were performed by a modification of the wet cup method described by ASTM E 96-95, indicating that membranes with 10% nanocrystalline cellulose, prepared using a sulfuric acid, exhibited the lowest permeability 174 g.mil/h.m^2 among the composite films studied. Reinforcement of xylan with hydrochloric made nanocrystalline cellulose yielded films that showed a reduction in water transmission but the reduction was not as

significant as with the reinforcement of xylan with sulfonated nanocrystalline cellulose. Xylan films reinforced with 10% sulfonated nanocrystalline cellulose exhibited reductions in water transmission rates of 362%, 62% and 61% over films prepared with 10% softwood kraft fibers, 10% acacia fiber and 10% hydrochloric acid prepared nanocrystalline cellulose, respectively. It appears that the high degree of crystallinity of nanocellulose, the dense composite structure of the formed films with nanocrystalline cellulose and xylan leads to a film that has reduced moisture transmission properties. These effects were attributed to a rigid hydrogen-bonded network of hydrogen bonded nanocellulose to form an integrated matrix as described by percolation theory. Both the acacia and softwood kraft pulp fibers when used for xylan film formation exhibited higher water vapor transmission rates at addition levels of 50% and no improvement at lower levels of 5% and 10%, in comparison to control xylan films. Optical microscopic images indicated that xylan incorporated with softwood kraft fiber and acacia fiber exhibit fiber aggregation in comparison to well dispersed sulfonated nanocrystalline cellulose on xylan surface as indicated in optical and SEM images of xylan-sulfonated nanocrystalline cellulose film. This provides more open structure for more rapid permeation in control xylan, xylan-softwood kraft fiber and xylan-acacia fibers leading to higher water vapor transmission rate as compared to xylan- sulfonated nanocrystalline cellulose films which have substantially lower water vapor transmission rate. The results from FT-IR showed strong interactions occurred between the nanocrystalline cellulose and the matrix and explain the synergistic xylan-10% sulfonated nanocrystalline cellulose which performed well and show potential for the development of improved biodegradable barrier membranes.

CHAPTER 7

OXYGEN BARRIER PROPERTIES OF XYLAN COMPOSITE FILMS

7.1 Introduction

In this chapter xylan based composites reinforced with cellulose whiskers are studied. The goal of this work is to produce nanocomposite film with low oxygen permeability by casting an aqueous solution containing xylan, sorbitol and nanocrystalline cellulose. Biobased plastics have generated increasing interest to replace petrochemical based polymers in light of their ready availability, sustainability, limited environmental impact and simplified end-of-life disposal issues [2-5]. High barrier packaging materials require low oxygen permeability with good mechanical strength. Replacing existing oxygen barriers such as aluminium and synthetic polymers with biopolymers is a research topic of increased interest. Early studies examined the use of chitosan, starch and cellulose derivatives to address these challenges and were shown to have good film forming properties [5].

Acetylated galactoglucomannan (AcGGM) hemicellulose was found to be an excellent candidate for making new renewable barrier materials [6]. The oxygen barrier permeability of the AcGGM films were found to be similar to, or lower than, the values reported for oxygen barrier films made from glucuronoxylan [7] and other polysaccharides, such as starch [8], chitosan [9] and mixtures of various polysaccharides [10]. Hartman reported oxygen permeability of 2.0 (cm^3 μm)/ (m^2 d kPa) for GGM-sorbitol film [6]. The oxygen barrier properties of films obtained from a mixture of *O*-

acetyl-galactoglucomannan and either alginate or carboxymethylcellulose were also studied. The reported values of oxygen permeability of GGM/alginate/glycerol blend were 4.6 (cm^3 μm)/ (m^2 d kPa) [6]. The oxygen permeability of the GGM films was lower than that of glycerol-plasticized amylose and amylopectin films [11], but not as low as that of sorbitol-plasticized aspen glucuronoxylan films [7,12]. The oxygen permeability of oat spelt arabinoxylan films plasticized with 40% sorbitol was 4.7 (cm^3 μm)/ (m^2 d kPa), which is slightly lower than that of GGM films [13]. Biobased free-standing films and coatings with low oxygen permeability of 1 (cm^3 μm)/ (m^2 d kPa) have been also prepared from a wood hydrolysate [14]. Films made from these polysaccharides are brittle and therefore to form cohesive films requires plasticizers such as sorbitol and xylitol. However, even with the plasticizers, the mechanical properties of these films have been considered to be poor. Nanocrystalline cellulose have been studied as reinforcements of various synthetic and some natural polymer matrices [15-17] to improve the strength properties owing to their high bending strength of 10 GPa, and elastic modulus of 143 GPa [18-19]. Lagaron et al. [20] discussed the role of crystalline structure of polymers and emphasized that high crystallinity improves barrier properties. Nanocrystalline cellulose are greater than 60% crystalline [21-22] and this property together with the resulting rigid hydrogen-bonded network of nanocrystalline cellulose can cause an increase in tortuousity and smaller pore size for nanocomposites which may be utilized to create high barrier materials. In a recent study, spruce galactoglucomannans (GGM) and konjac glucomannan (KGM) were mixed with nanocrystalline cellulose (NCC) to study the mechanical and barrier properties of the films [23-24]. The tensile strength of unplasticized KGM films increased by 30% but the mechanical properties of

the plasticized films were not affected with increased in nanocrystalline cellulose. The presence of 5% of nanocrystalline cellulose did not significantly affect the oxygen permeability of the films. Xylan is one the most common hemicelluloses, is the most abundant polysaccharide in nature after cellulose, and is an attractive resource for film production [25-27]. Prior studies by Saxena et al. [28] have shown that the addition of 7% nanocrystalline cellulose to xylan-sorbital films increased the tensile energy absorption of the resulting films by 445% and the tensile strength of the film by 141%. Recent studies demonstrated that films with 10% nanocrystalline cellulose exhibited a 74% reduction in specific water transmission properties with respect to films prepared solely from xylan/sorbitol, and a 362% reduction in water transmission rate with respect to xylan films reinforced with 10% softwood kraft fibers [29]. The objective of the current study is to evaluate the oxygen barrier properties of xylan-nanocrystalline cellulose composite films.

7.2 Results and discussion

This study examines the oxygen barrier properties of xylan-nanocrystalline cellulose composite films.

7.2.1 Oxygen transmission rate studies of nanocomposite films

The specific oxygen transmission rate of the xylan nanocomposite films are shown in Table 31. The transmission rate decreased drastically upon reinforcement with nanocrystalline cellulose. The measured oxygen permeability is lower or comparable to the often used barrier plastic ethylene vinyl alcohol (EVOH) [33] and the films made from microfibrillar cellulose [34], see Table 31.

Table 31. Effect of sulfonated nanocrystalline cellulose dosage on oxygen transmission rate of xylan film.

Sample	Specific oxygen transmission rate (cm^3/m^2day)
Control (Xylan)	354.95
Xylan + 5% sulfonated nanocrystallinecellulose	1.44
Xylan + 10% sulfonated nanocrystalline cellulose	1.36
Xylan + 25% sulfonated nanocrystalline cellulose	1.04
Xylan + 50% sulfonated nanocrystalline cellulose	0.14
EVOH	3-5 [33]
Polyester, oriented, Polyvinylidene chloride (PVdC) coated	9-15 [224]
MFC film	17.0-18.5 [34]

Oxygen permeability values were calculated by dividing the oxygen transmission rates by the differential partial pressure of oxygen across the film (1 atm or 101.3 kPa) and multiplying by the film thickness in microns [5]. Table 32 summarized the oxygen permeability of some of the literature work and current work. The oxygen transmission rates as summarized in Table 31 at 25% and 50% dosage of nanocrystalline cellulose decreased drastically with respect to control xylan films and are the two lowest values that we obtained in this study. It will be an interesting subject to explore the porosity, bulk density and tortuosity factor at these two levels and the control xylan films. As summarized in Table 33, the density and tortuosity factor of the composite film increased while the pore diameter and porosity decreased as the loading of sulfonated nanocrystalline cellulose increased in the xylan-based films.

Table 32. Oxygen Permeability of biopolymer films.

Sample	Oxygen Permeability (cm^3 μm)/ (m^2 d kPa)	
GGM-sorbitol	2.0	[6]
GGM/alginate/glycerol blend	4.6	[6]
Oat spelt arabinoxylan films plasticized with 40% sorbitol	4.7	[13]
Biobased free-standing films and coatings from a wood hydrolysate	1.0	[14]
Xylan + 50% sulfonated cellulose whiskers	0.2 (current study)	

Table 33. Mercury intrusion porosimetry measurements of control xylan and nano-composite films

Sample	Average pore diameter (μm)	Bulk density (g/mL)	Porosity %	Tortuosity factor
Control (Xylan)	0.17	0.6	53.0	1.3
Xylan+25% sulfonated nanocrystalline cellulose	0.13	0.9	41.0	1.7
Xylan+50% sulfonated nanocrystalline cellulose	0.06	1.2	23.0	2.0

Nanocrystalline cellulose have been reported to have crystallinity values greater than 60% [21] which would further reduce the transmission of oxygen molecules through these nanocomposite films. The tortuosity factor measurements from mercury porosimetry techniques showed that the control xylan films have a tortuosity factor of 1.258 whereas the xylan films containing 50% nanocrystalline cellulose had a tortuosity

factor of 2.005. The combination of 50% nanocrystalline cellulose and xylan showed the lowest oxygen transmission rate of 0.139 cm3/m2•day). Figures (31 and 32) show the rate of oxygen transmission rate for the control xylan and xylan reinforced with 50% nanocrystalline cellulose respectively. Control xylan films have much higher rate of oxygen transmission than xylan reinforced with nanocrystalline cellulose films.

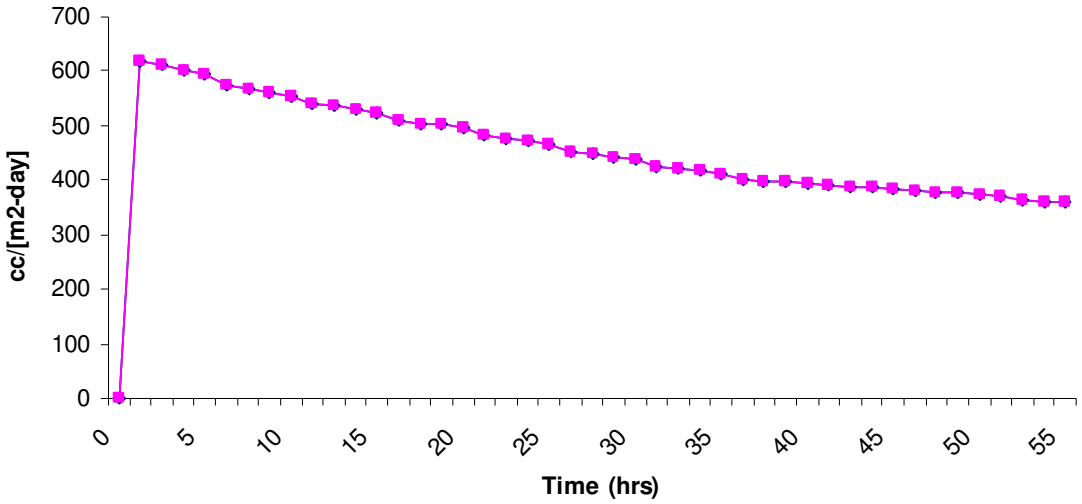

Figure 31. Oxygen transmission rate for control xylan films.

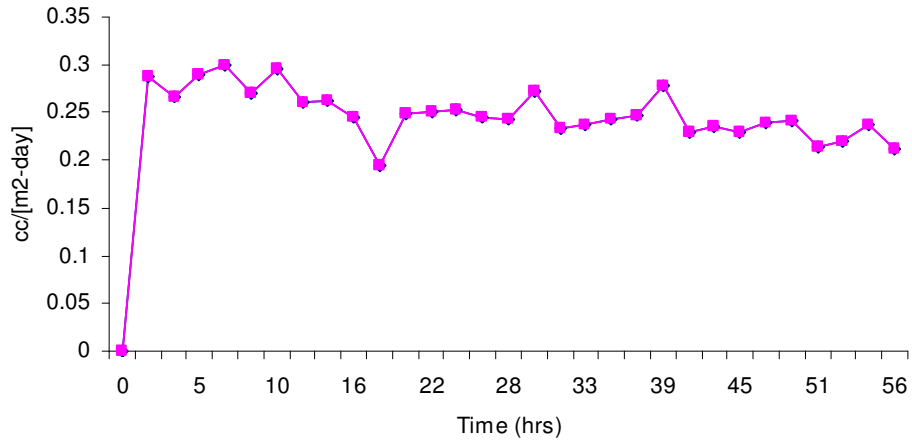

Figure 32. Oxygen transmission rate for control xylan reinforced with 50% nanocrystalline cellulose.

7.2.2 Morphology of cross section and surface images of composite films

By AFM analysis, the sulfonated nanocrystalline cellulosic were observed to have rod like structure with an average length of 150-200 nm and a width of less than 20 nm (Figure 33). AFM images, acquired using tapping mode, of the xylan/sorbitol films reinforced with nanocrystalline cellulose show well dispersed sulfonated nanocrystalline cellulose on xylan surface in comparison to more open structure of xylan/sorbitol control films (Figure 34).

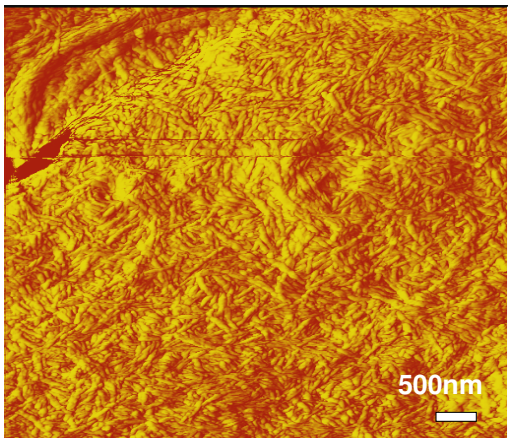

Figure 33. AFM image of sulfonated nanocrystalline cellulose with a concentration of 0.7% by weight.

SEM images of the control xylan film surface showed agglomerated structures on the surface in comparison to a more uniform surface for the nanocrystalline cellulose-xylan films (Figure 35 (a) and 35(b)).

Oxygen transmission rate at 5% and 10% charge of nanocrystalline cellulose doesn't differ much but a significant drop of transmission rate as compared to control. We studied xylan-10% nanocrystalline cellulose film under SEM (Figure 35) and AFM (Figure 34b) and found that control xylan film surface in Figure 35 (a) shows agglomeration in comparison to well dispersed sulfonated nanocrystalline cellulose on

xylan surface in Figure 35 (b). The uneven structure and agglomeration of the xylan can be the cause of higher oxygen transmission rate of control xylan film in comparison to xylan reinforced with 10% sulfonated nanocrystalline cellulose.

SEM cross-section images of freeze fracture of control xylan films showed a rough texture with small cracks in the film as summarized in Figure 36(a) and 36(b). The same analysis for the xylan film reinforced with nanocrystalline cellulose exhibited smooth fractured surface and less porous structure (see Figure 36(c) and Figure 36(d)).

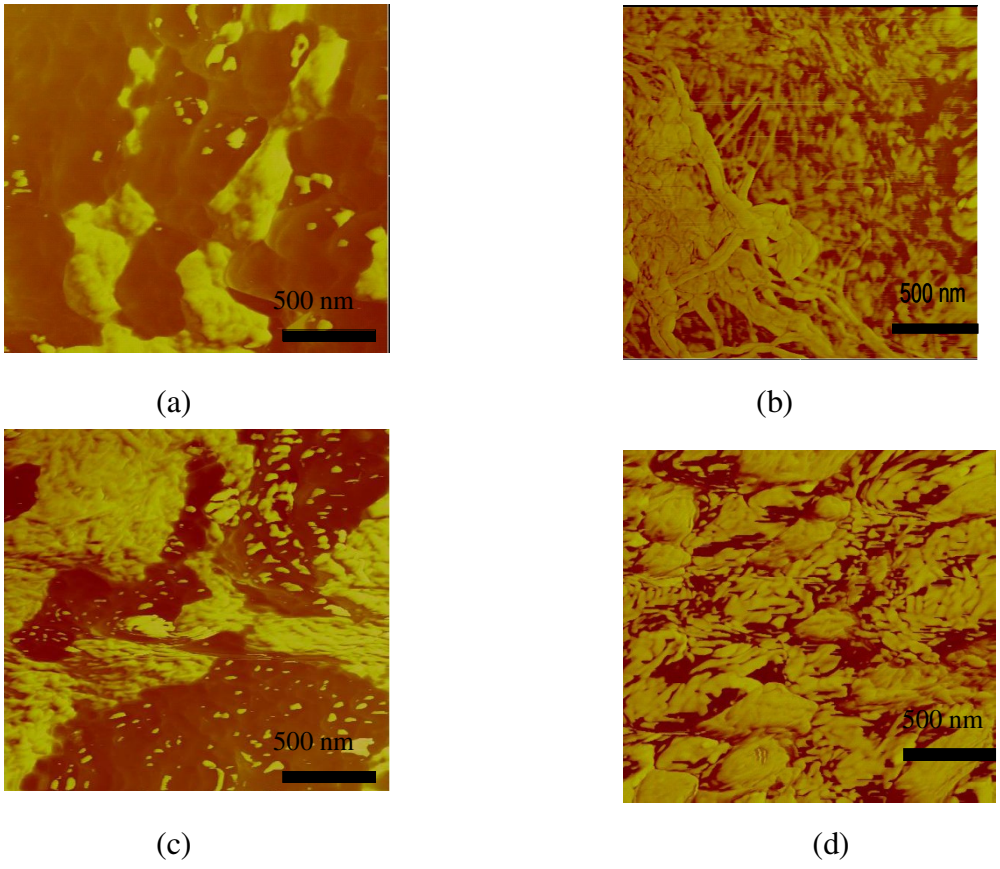

(a) (b)

(c) (d)

Figure 34. AFM images of (a) control xylan (c) 10% sulfonated nanocrystalline cellulose film (d) 25% % sulfonated nanocrystalline cellulose (e) 50% sulfonated nanocrystalline cellulose film.

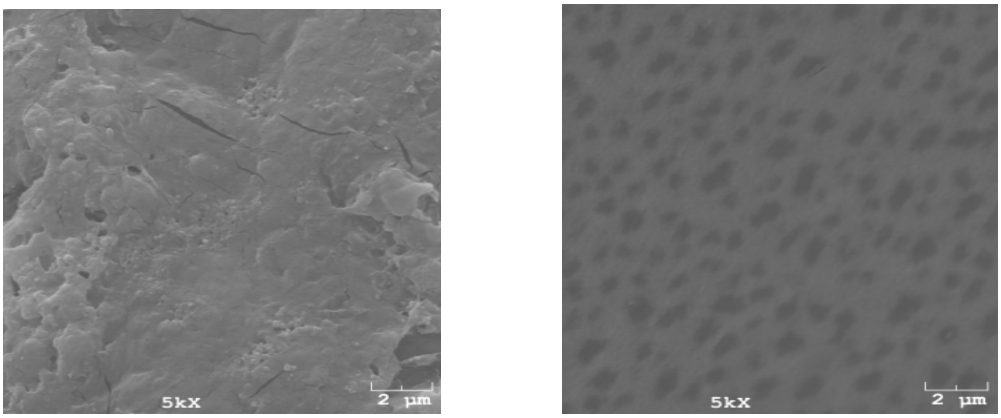

(a) (b)

Figure 35. SEM surface images of the (a) control xylan, (b) xylan reinforced with 10% sulfonated nanocrystalline cellulose

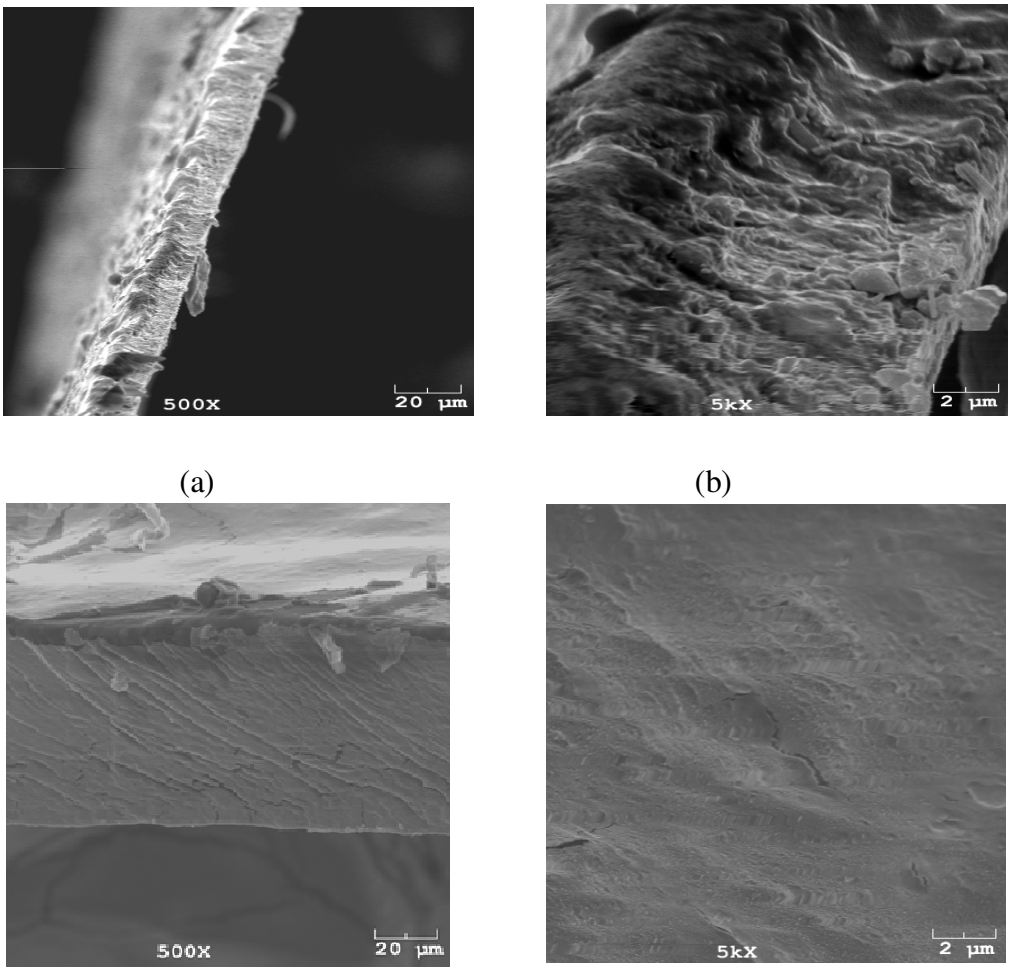

(a) (b)

(c) (d)

Figure 36. SEM fracture images of the cross-sections of membranes of (a) and (b) control xylan, (c) and (d) xylan reinforced with sulfonated nanocrystalline cellulose.

The dense structure of composite films with reduced surface porosity is due to the combination of the nanocrystalline cellulose and the resulting rigid hydrogen-bonded network within the nanocrystalline cellulose and with the matrix [3]. This causes an increase in the tortuosity factor and bulk density with decrease in porosity and average pore diameter of the composite films resulting in lower oxygen transmission rates of composite films in comparison to the control

7.3 Summary

Nanocrystalline cellulose was incorporated into xylan slurry to prepare high oxygen barrier biodegradable films. The morphology of the resulting nanocomposite films was examined by scanning electron microscopy and atomic force microscopy which showed that control films containing xylan and sorbitol had a more open structure as compared to xylan-sorbitol films containing sulfonated nanocrystalline cellulose.

The average pore diameter, bulk density, porosity and tortuosity factor measurements of control xylan films and nanocomposite xylan films were examined by mercury intrusion porosimetry techniques. Xylan films reinforced with nanocrystalline cellulose films were denser and exhibited higher tortuosity factor than the control xylan films. Control xylan films had average pore diameter, bulk density, porosity and tortuosity factor of 0.1730 μm, 0.6165 g/mL , 53.0161 % and 1.258 respectively as compared to xylan films reinforced with 50% nanocrystalline cellulose with average pore diameter of 0.0581 μm, bulk density of 1.1513 g/mL, porosity of 22.8906 % and tortuosity factor of 2.005. Oxygen transmission rate tests demonstrated that films prepared with xylan, sorbitol and 5%, 10%, 25% and 50% sulfonated nanocrystalline cellulose exhibited a significantly reduced oxygen permeability of 1.1387, 1.0933, 0.8986

and 0.1799 (cm^3 μm)/ (m^2 d kPa) respectively with respect to films prepared solely from xylan and sorbitol with a oxygen permeability of 189.1665 (cm^3 μm)/ (m^2 d kPa).

It appears that the high degree of crystallinity of nanocrystalline cellulose and the dense composite structure of the formed films with nanocrystalline cellulose and xylan leads to a film that has reduced transmission properties. These effects were attributed to a rigid hydrogen-bonded network of hydrogen bonded nanocrystalline cellulose to form an integrated matrix as described by percolation theory.

CHAPTER 8

FUNDAMENTAL STUDIES ON XYLAN-CELLULOSE WHISKERS COMPOSITE FILMS

8.1 INTRODUCTION

Environmental concerns arising from the use of nondegradable petroleum-based plastics have resulted in the search for suitable substitutes [2-5]. In recent years, increasing societal concerns have accelerated efforts to develop new ways to utilize biopolymers such as polysaccharides, proteins and lipids to create biodegradable films due to their ready availability, sustainability and reduced end-of-life environmental concerns [2-5]. Many naturally occurring polysaccharides and their derivatives such as starch, cellulose, chitosan, alginates, carrageenan, pectinate, and various naturally occurring gums have been proposed for use in coating and film formulations.

Typically, polysaccharide films possess poor mechanical and barrier properties, [173-174] and plasticizers are normally added to improve the strength of the films and aid in stabilizing the film network [175-176]. Xylan, which is one the most common hemicelluloses and the most abundant polysaccharide in nature after cellulose, is an attractive resource for film production [178-180]. Recently, acetylated galactoglucomannan (AcGGM) hemicellulose was found to be an alternative material for making new renewable barrier materials [13]. The oxygen barrier permeability of the AcGGM films was found to be similar to, or lower than, the values reported for oxygen barrier films made from glucuronoxylan [8] and other polysaccharides, such as starch [14], chitosan [186] and mixtures of various polysaccharides [16]. Glucuronoxylan,

isolated from aspen wood, when plasticized with xylitol or sorbitol has been used to produce films that exhibit improved strength and oxygen barrier properties with respect to control glucuronoxylan films [8-9]. Hartman et al. reported oxygen permeability values of 2.0 cm^3 μm m^{-2} day^{-1} kPa^{-1} for GGM-sorbitol film [13]. Miranda et al. studied water vapor transmission values of chitosan film plasticized with sorbitol, glycerol or polyethylene glycol reporting values from 1.3-1.5×10^{-3} [g/(m^2. h. Pa)] [194].The goal was to decrease the water vapor permeability and to improve the mechanical properties of chitosan films. Miranda et al. also discussed that in hydrophilic films, water molecules interact with polar groups in the film structure, causing plasticization or swelling, which, in turn results in varying permeability [194]. Films made from these polysaccharides are brittle and therefore to form cohesive films requires plasticizers such as sorbitol and xylitol. However, even with the plasticizers, the mechanical properties of these films have been considered to be poor. Nanocellulose whiskers (NCW) have been studied as reinforcements of various synthetic and natural polymer matrices [3, 200,201] to improve the strength properties of the nanocomposites. They have a high bending strength of 10 GPa, an elastic modulus of 143 GPa [202-203] and forms a rigid hydrogen-bonded network [3]. The properties of nanocomposite materials and the enhancement of these properties, depend not only on their individual components but also on the interaction between the matrix and the reinforcing phases and their morphology [34-35]. Recent studies by Saxena et al. have shown that xylan films reinforced with NCWs can reduce water and oxygen permeability by greater than +70% while increasing physical strength properties by +50% with respect to control xylan/sorbitol film by the addition of 5-10% of NCWs [181,206-207].

X-ray diffraction (XRD) and nuclear magnetic resonance (NMR) techniques was used to study the structure-property relationships of xylan films reinforced with NCWs. A critical issue to probe is the interactions of NCWs with the film matrix because of the significantly increased matrix-filler interfacial area typically associated with nanocomposite. In addition, we used NMR T_2 relaxation experiments to investigate the change in the nature of carbohydrate–water interactions as a result of NCW incorporation. These results will facilitate an improved understanding of the mechanisms involved in the superior barrier and mechanical properties of xylan-NCW nanocomposite films previously reported [181,206-207].

8.2 RESULTS AND DISCUSSION

This study utilizes X-ray diffraction (XRD) and nuclear magnetic resonance (NMR) techniques to study the structure-property relationships of xylan films reinforced with NCWs which will facilitate an improved understanding of the mechanisms involved in the superior barrier and mechanical properties of rigid hydrogen bonded xylan-whisker nanocomposite films previously reported [181,206-207]. A control xylan/sorbitol film was prepared from a 1:1 weight ratio of xylan and sorbitol. The morphology of the nanocomposite films and the size distribution of nanocellulose whiskers were fully characterized using SEM and AFM and previously reported by Saxena et al. [181,206-207]. The surface morphology of nanocrsyatlline cellulose was evaluated by TEM. TEM images of cellulose nanowhiskers (CNW) are shown in Figure 37. Sulfonated nanocrystalline cellulosic were observed to have rod like structure with an average length of 150-200 nm and a width of less than 20 nm.

Figure 37. Transmission Electron Microscopy (TEM)

8.2.1 Solid-state ^{13}C CP/MAS NMR analysis on xylan nanocomposite films

To characterize the interaction of NCWs with the matrix, NMR analysis on the nanocomposite films were performed. Solid-state ^{13}C CP/MAS NMR analysis of a control xylan/sorbitol film, NCW and NCW/xylan nanocomposite films is shown in Figure 38. ^{13}C NMR chemical shifts of the starting xylan and NCWs agreed with literature values [225-228] and could be readily assigned in the spectra of the nanocomposite films. The ^{13}C CP/MAS NMR spectra of the NCWs showed the typical spectra of crystalline cellulose and based on the integration of the cellulose C_4 peak region, the NCWs had a crystallinity of ~ 64%. Newman et al. has made specific assignments for the cellulose C_4 spectral resonances arising from cellulose crystallite interiors, crystallite surfaces and amorphous regions [229]. Recent results reported by Lopez et al. suggested that the enthalpic interaction exists in xyloglucan-cellulose whiskers system [230]. The results also suggested that the strong xyloglucan-cellulose

interactions are governed by several types of interactions, including hydrogen bonding and hydrophobic interactions [230].

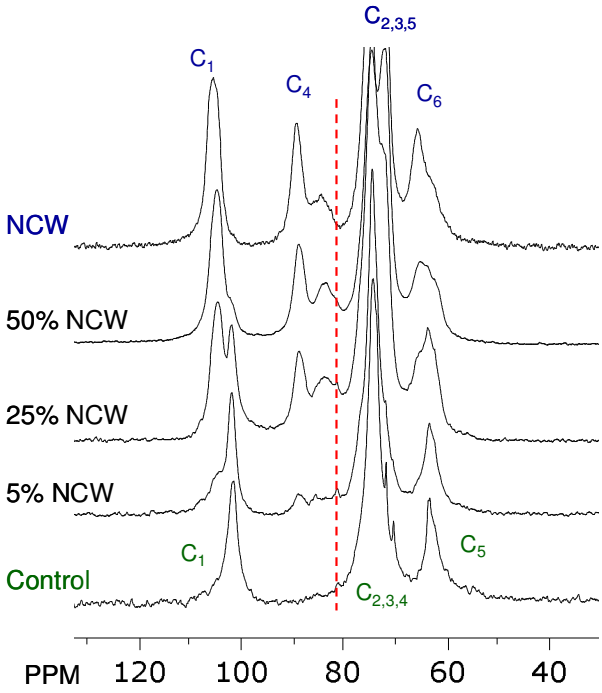

Figure 38. ^{13}C spectra of NCW/xylan nanocomposite films of increasing NCW content conditioned under 100% RH for 48 h.

As shown in both Figure 38 and Figure 39, the C_1 peak of cellulose and xylan is ~ 105 and 102 ppm, respectively. The analysis of the both the C_4 and C_1 peak regions of xylan/cellulose are unobstructed by resonances from sorbitol which only appear ~ 74-63 ppm. Figure 39 shows the non-linear least-squared line-fitting of the C_1 region for the ^{13}C spectra of 25% NCW/xylan nanocomposite film. A primarily Gaussian line-shape was applied to the carbon signal attributed to the C_1 peak of cellulose with a constant line-width of 294 Hz (based on the neat NCW spectrum), while a Lorentzian weighted line seemed to describe the signal from the C_1 peak of xylan. Though the spectrum in

Figure 39 suggests these peaks are well-resolved, the other nanocomposite films required deconvolution by line-fitting due to the highly reduced contribution of either NCWs or xylan in the 5 and 50% NCW nanocomposite films. Larsson et al. reviewed the interaction of cellulose and hemicellulose using CP/MAS ^{13}C-NMR spectroscopy [225] and our results are consistent with this report with respect to the types of line-shape and peak chemical shifts.

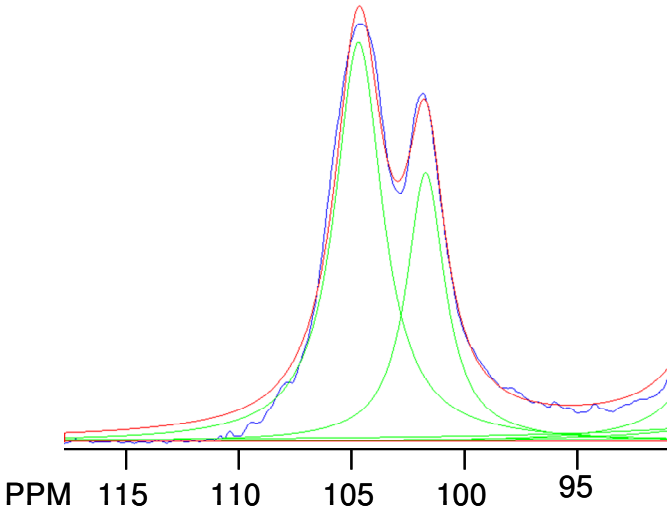

Figure 39. The non-linear, least-squared, spectral fitting of the C_1 region for the ^{13}C spectra of 25% NCW/xylan nanocomposite film conditioned under 100% RH for 48 h. Green lines = C_1 peak of cellulose and xylan; Red lines = C_1 peak summed fit of cellulose and xylan and; Blue line = real spectra

Larsson et al. reported that for 70/30% (w/w) mixture of cellulose and xylan, when heated in the presence of water an additional resonance not present in either the spectra of cellulose or xylan appeared [225]. It appears that cellulose-xylan interactions increase as water is removed from the system in the heating process which may cause a formation of a strong hydrogen bonding between xylan and cellulose [225]. This signal was observed at ~ 82 ppm, slightly overlapping the signal from inaccessible cellulose fibril surfaces at ~ 84 ppm. The authors concluded that this additional peak must be

attributed to xylan adsorbed to cellulose and would be accompanied by a loss of signal intensity from cellulose at accessible fibril surfaces and an increase in signal intensity from cellulose at inaccessible fibril surfaces due to the 'coverage' by xylan [225]. Qualitatively, the obtained spectra of the NCW/xylan nanocomposite films seen in Figure 38 demonstrate a similar affect. The relative signal intensity at ~ 81.7 ppm is appreciably higher in the spectra of all the nanocomposite films with respect to the spectra of the control xylan/sorbitol film or neat nanocellulose whisker. In an attempt to quantify this effect, non-linear least-squared spectral line fitting was used to deconvolute the adsorbed xylan peak at ~ 82 ppm. The results are presented in Table 34, as a ratio of δ_{82ppm}:δ_{102ppm} with respect to the xylan C_1 peak, which represents the total amount of xylan present in the nanocomposite. The ratio seen in Table I has been adjusted, subtracting intensity from the 82 ppm region based on the deconvoluted intensity of cellulose C_1 peak and a predetermined peak intensity ratio at δ_{82ppm}:δ_{105ppm} for neat NCW. This was done in an effort to account for the overlapping the signal from inaccessible cellulose fibril surfaces. This ratio suggests that upon the addition of 50% NCW, the amount of adsorbed xylan increases by a factor of three.

Table 34. Non-linear least-squared spectral fitting results of the C_1 of cellulose and xylan region for the ^{13}C spectra of the NCW/xylan nanocomposite films conditioned under 100% RH for 48 h.

Sample	Peak at 104.9 ppm			Peak at 101.9 ppm			Adjusted δ_{82ppm}:δ_{102ppm}
	Relative Intensity	FWHM (Hz)	% Lorentzian	Relative Intensity	FWHM (Hz)	% Lorentzian	
Control Film					231	100	0.17
NCW		295	36				
5% NCW	32	295	36	68	186	57	0.17
25% NCW	56	295	36	54	208	90	0.34
50% NCW	92	295	36	8	126	67	0.49

8.2.2 NMR T_2 relaxation experiments on xylan nanocomposite films

NMR T_2 relaxation experiments can provide information pertaining to the molecular mobility within a system. ^1H Carr–Purcell–Meiboom–Gill (CPMG) experiments were used to investigate the change in the nature of carbohydrate–water interactions as a result of NCWs incorporation. T_2 relaxation values probe how fast a nuclei loses transverse magnetization. In this experiment, the signal intensity decays as a function of local inhomogeneities in the magnetic field mainly due to perturbation by nuclei through space or dipolar interactions, and this signal attenuation or the characteristic relaxation rate for this process is called the spin-spin relaxation (i.e. T_2). Basically, the faster the rate of the decay, the more rigid or fewer degrees of freedom the chemical group associated with that decay has [231]. Spin-spin (T2) relaxation of water adsorbed in western red cedar

and Douglas fir sapwood have been studied in the past [232, 233] and recently Marcus et al. [234] used spin-spin (T2) relaxation to study the interaction of cellulose and water. We used a similar method to study the ^{1}H T_2 relaxation of water adsorbed into the NCW nanocomposite system to infer the structure-property relationships with respect to the enhanced strength and barrier properties observed for these xylan-nanocomposite films. The analysis of wide T_2 distributions using a single model can be difficult. One technique to resolve this issue, while also showing any change in T_2 relaxation, is to extract the distribution of relaxers or exponential decays from the T_2 data using an inverse Laplace transform (ILT) routine [9]. Figure 40 shows the relaxation rate distributions of adsorbed water in the control xylan/sorbitol film, NCWs and nanocomposite films. The T_2 distribution for the control xylan /sorbitol film indicates at least two distributions of water exist. There are peaks centered at ~ 12 and 130 ms. The shorter relaxation time distribution suggests this water is on average less mobile, having less degrees of freedom. This can be interpreted as meaning the water associated with this distribution is either within a much more confined volume or pore space and/or there exist increased interactions with the xylan substrate which adequately retards the molecular dynamics of the water with respect to the water associated with the peaks found at 130 ms [234,235].

Between 10 and 25% whisker content the major distribution of peaks originally centered at 10 ms shifts to larger T_2 times indicating the strength of the carbohydrate-water interactions in the xylan matrix are becoming weaker [234,235]. However, the water adsorbed into the 50% NCW film has significantly shorter relaxation time with respect to the control xylan/sorbitol, 5, 10 and 25% CNW/xylan nanocomposite films with a very

narrow distribution. This shift strongly correlates with the change in the amount of adsorbed xylan discussed previously. This would suggest that either the carbohydrate-water interactions in this system are dominated by that of CNWs, a radical reduction in the pore size distribution [207] and/or there was a significant change in strength of the carbohydrate-water interactions in the xylan matrix for the 50% NCW film with respect to all the other films.

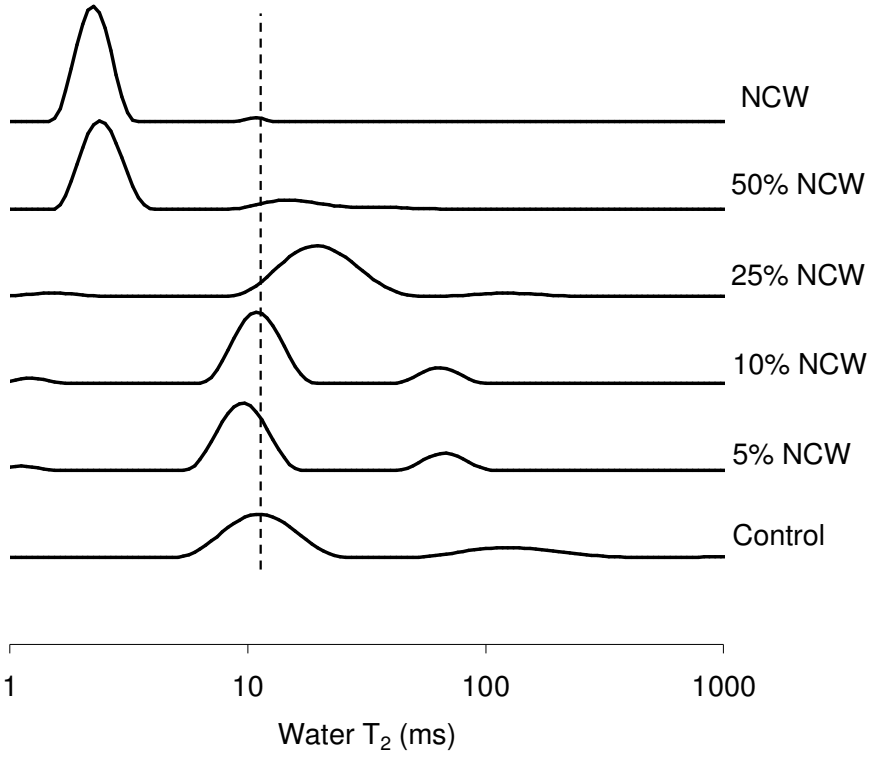

Figure 40. Distribution of spin-spin relaxation times of absorbed water within control xylan/sorbitol, pure NCW and nanocomposite films reinforced with 10%, 17%, 25%, 35% and 50% NCW produced via ILTs of ^{1}H CMPG NMR T_2 experiments conditioned under 100% RH for 48 h. The vertical dotted lines serve to visually demonstrate shifts in peak position.

8.2.3 Crystallinity of nanocomposite films

X-ray diffraction (XRD) studies on the nanocomposite system can also be used to infer the structure-property relationships with respect to the observed physical properties previously observed for these nanocomposite films [111,8] Lagaron et al. discussed the role of crystalline structure of polymers and emphasized that high crystallinity in semi-crystalline polymer systems improves barrier properties for polymers used in packaging application [47] The present paper uses XRD technique to study xylan films reinforced with NCWs, initially comparing XRD results of dry mechanically mixed film components (xylan, sorbitol and NCWs) with a nanocomposite film formed by dissolution and solution casting (as described in the experimental section) which facilitates intimate blending and the formation of a strong hydrogen bonded structures [3,9].

In Figure 41, the effect of film formation on the overall film crystallinity is shown. Xylan particles show distinctive semi-crystalline characteristics with a broad peak around 19.3°. The sorbitol particles, used as stabilizer in making the xylan film, are very crystalline (see Figure 41). The diffractograms of sorbitol show sharp individual peaks, whereas the pure xylan polymer has broader peaks (see Figure 41) which is in agreement with literature [8] which shows pure low molecular weight plasticizers give rise to sharp distinct peaks, whereas the xylan has broader peaks resulting from scattering from the amorphous parts. The XRD pattern of the mechanically mixed particles of xylan and sorbitol shows a very comparable pattern with sorbitol particles (see Figure 41 and 42). The observed intensity for this mixture drops significantly compared to sorbitol pattern, because of the semi-crystalline nature of xylan particles. After solution casting the

control xylan/sorbitol film, the crystallinity decreases significantly with respect to the xylan and sorbitol particle mixture.

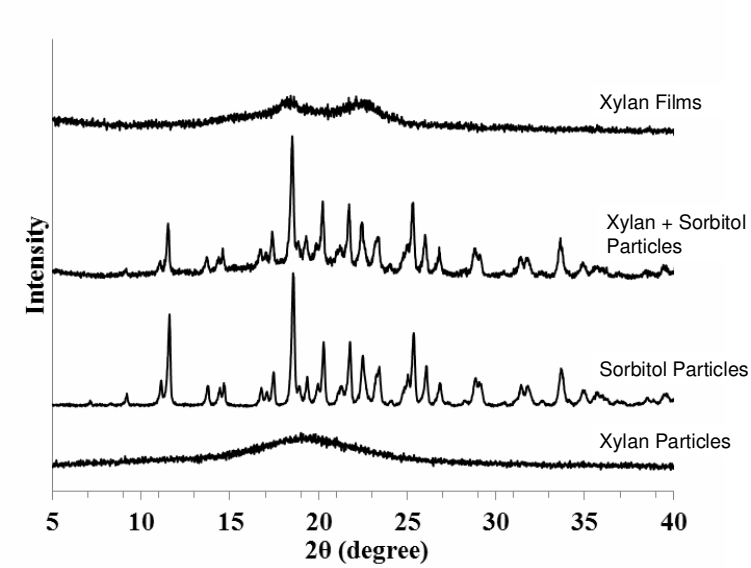

Figure 41. Wide-angle X-ray diffraction patterns of xylan particles, sorbitol particles, mechanical mix of 1:1 mass ratio of xylan and sorbitol particles, and control xylan/sorbitol film.

In Figure 42, the effects of making the 25% xylan/NCW nanocomposite film, on crystallinity of the initial components, have been shown. XRD patterns of xylan/sorbitol particles show the strong sorbitol crystallinity. In Figure 42, 25% NCW has been added to the mixture of xylan-sorbitol and the peaks near 22° have been enhanced due to the NCW crystalline peak at 22.2°. The nanocomposite film with 25% CNW shows a much lower crystallinity than the sample of mechanically mixed components, but its dominant peaks come from NCW peaks. The XRD of mechanically mixed xylan, sorbitol, NCWs shows a superposition of the diffraction patterns from crystalline sorbitol, NCW and semi-crystalline xylan. This result indicates that dry mixing does not affect the individual film components on the atomic scale whereas the film formation procedure of the xylan film with NCW does.

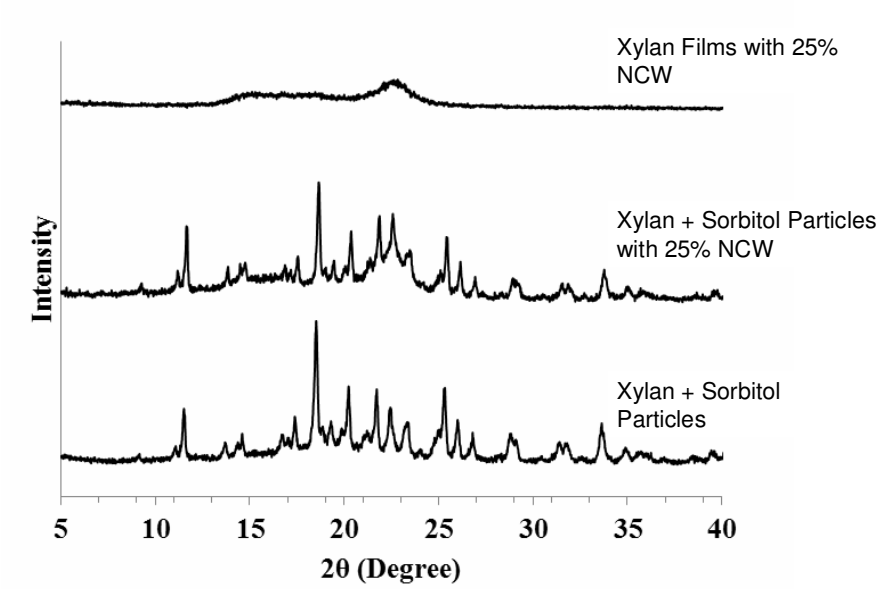

Figure 42. Wide Angle X-Ray Diffraction patterns of mechanically mixed 1:1 xylan and sorbitol, mechanically mixed 1:1 xylan and sorbitol with 25% NCW, and xylan/sorbitol film with 25% NCW generated by stirring, heating and solution casting.

The morphology of xylan-NCW nanocomposite films was then further studied using XRD focusing on specific crystalline peaks associated with cellulose and xylan. The diffractograms of xylan-NCW nanocomposite films with different whisker contents are shown in Figure 43. The control xylan/sorbitol film shows weak crystalline peaks at $2\theta = 17.9$ and 22.2° which is in agreement with literature [8,236]. Similar to the control xylan/sorbitol film, the nanocomposite of 10% NCW shows weak and broad diffraction pattern. As the NCW concentration increases, the patterns show characteristic diffractions of cellulose I at $2\theta = 16.1$ and 22.6° that correspond to (110) and (200) planes [111, 8]. The diffraction peak at 22.2° has contribution from both xylan in the film matrix and NCWs, so it becomes noticeably sharper as the loading increases. However, a second peak attributed to xylan in the control xylan/sorbitol film occurs at a slightly higher angle (~ 17.9°) than the diffraction peak associated with the 110 planes in NCWs. This second

peak appears as a very broad signal in the nanocomposite films and seems to increase with NCW loading, suggesting an increase in crystallinity of the xylan in the matrix film may be related to increased NCW incorporation.

An overall increase in the relative amount of crystalline material in the nanocomposite films, a indicated by the change in the diffraction peak at 22.2°, with increased whisker incorporation was expected and consistent with work by other researchers [111,47,236]. Accordingly, we believe that the higher relative amount of crystalline material in the nanocomposites results in less penetration of water molecules into the film. This would then result in lower water transmission rate and may in part explain the observed improved barrier properties of the nanocomposite film. The angle of the xylan crystalline peak at ~ 17.9° in the diffractograms of the nanocomposite films also seems to change to lower values when compared to the control xylan/sorbitol film. The distance between the lattice planes, d, can be related to the Bragg angle, θ, using Bragg's law: $2\,d \sin\theta = n\lambda$, where n is an integer and λ is the wavelength of the X-ray radiation. A lower angle correlates to a larger distance between the lattice planes. This may be to due to an altering of the crystal structure of xylan in the nanocomposite during film formation and/or more likely, changed contributions of overlapping diffraction peaks for NCWs and xylan at 16.1 and 17.9°, respectively.

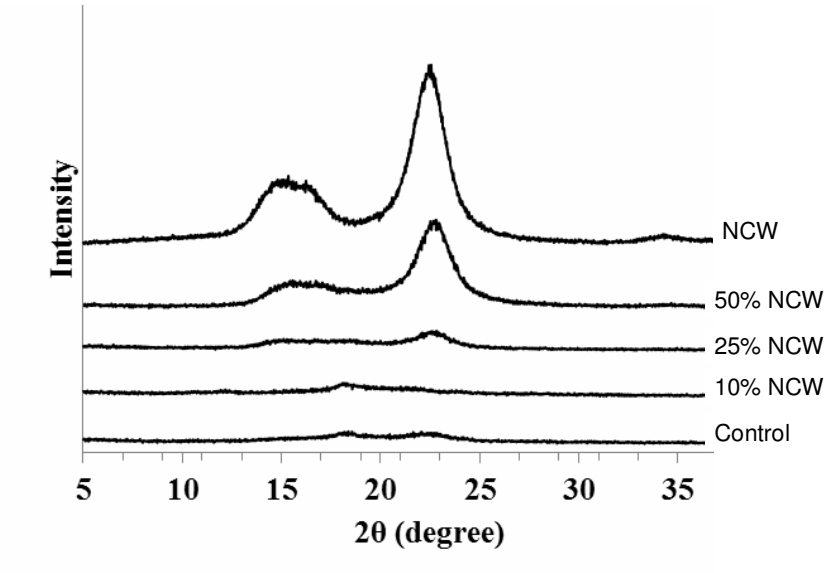

Figure 43. Wide-angle X-ray diffraction patterns of NCW/xylan nanocomposite films of increasing whisker content.

Crystallinity Index (CI) has been calculated for the xylan/sorbitol films with different NCW loading using the XRD amorphous subtraction method [237]. The basis for this method was outlined by Ruland et al. (1961) who determined crystallinity by subtracting the amorphous contribution from diffraction spectra using an amorphous standard [238]. Various materials have been used as an amorphous standard, such as ball-milled cellulose, and xylan powder. Sathitsuksannoh et al. used amorphous subtraction method using amorphous xylan as a standard to calculate crystallinity of cellulosic materials [239]. Gumuskaya et al. used xylan as an amorphous standard to calculate crystallinity of bleached wheat straw-oxygen soda pulp [240].Xylan powder was used as the standard in our measurements to measure crystallinity of xylan composite films. We used XRD subtraction method similar to the one used in the referenced papers [237-241]. A scale factor is applied to the spectrum of the amorphous material, so that after subtraction of the amorphous spectrum from the original spectrum, no part of the residual

spectrum contains a negative signal. We used ball-milled cellulose as a cellulose standard for calculating cellulose whiskers crystallinity as shown in Figure 44 (e). Figure 44 (a-d) shows the XRD spectrum of xylan films containing 0 (control xylan/sorbitol), 10, 25, 50% NCW along with their scaled amorphous spectrum. The difference between the XRD spectrum and the amorphous spectrum denotes the crystalline contribution part of the spectrum. CI is calculated as the ratio between the area of the crystalline contribution and the total area of the spectrum from 5-40°.

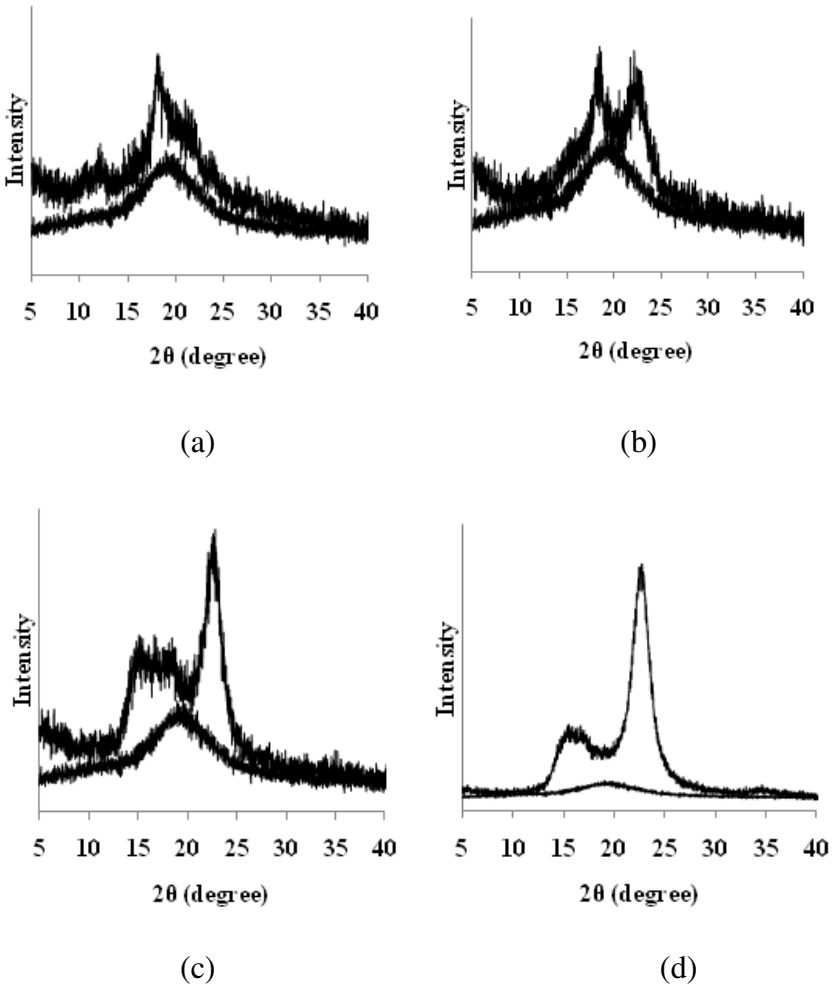

Figure 44. XRD spectrum of NCW and xylan films containing (a) 0 (control xylan/sorbitol), (b) 10, (c) 25, (d) 50% NCW and (e) pure NCW (100%) along with their scaled amorphous spectrum.

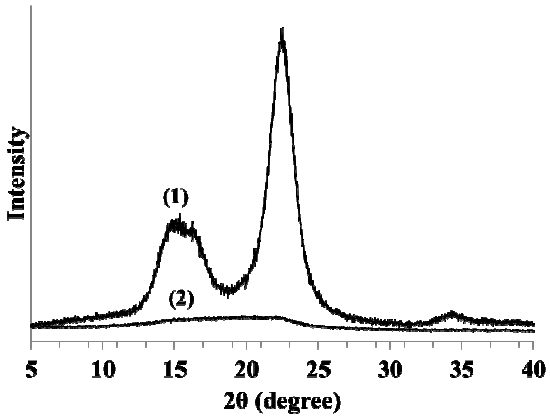

(e)

Figure 44. continued

Table 35 shows the calculated crystallinity index for xylan films containing 0 (control xylan/sorbitol), 10, 25, 50% NCW and pure NCW (100%). The CI values are 26, 32, 42, 61, and 70% respectively. Control xylan/sorbitol film with no NCW loading shows some crystallinity (26%) most likely a consequence of the film formation procedure. Table 35 also shows that a pure NCW film has a CI ~ 67%, very comparable to that determined by NMR, attributed to unhydrolyzed amorphous cellulose and cellulose at crystallite surfaces. Assuming film formation causes no change to the xylan/sorbitol matrix, one may expect to calculate the CI of the composite based on a simple additive rule of mixtures, the NCW volume fraction and the CI of pure NCW and control xylan/sorbitol film.

Table 35. Crystallinity index (CI) for xylan/sorbitol nanocomposites with different NCW contents

Sample	CI by XRD amorphous subtraction method	Expected CI by mixing rule	Difference
Control film	26%	--	--
10% NCW	32%	30%	+2%
25% NCW	42%	37%	+5%
50% NCW	61%	48%	+13%
NCW	70%	--	--

In Table 35, as expected, the crystallinity index of the films increases as the NCW loading increases in the films. The results seem to suggest that there is more crystalline material in the nanocomposite than can be directly correlated with the addition of NCWs and that the nanocomposite deviates from the rule of mixtures. This is significant because these results suggest that there are significant interactions between the xylan film and NCW that increases the crystallinity specifically in the matrix of the film.

8.3 Summary

A processing-structure-property relationship study of xylan-NCWs nanocomposites was done and the effectiveness of nanocellulose as reinforcement was demonstrated. Degradable polymer nanocomposites from renewable resources based on xylan and nano cellulose whiskers were synthesized by solution processing techniques. The spectral data obtained for the NCW/xylan nanocomposite films showed that the amount of xylan

adsorbed to cellulose increases with the addition of NCW in the matrix. In addition, NMR T_2 relaxation experiments studies were conducted to investigate the change in the nature of carbohydrate–water interactions as a result of NCW incorporation. These results will facilitate an improved understanding of the mechanisms involved in the superior barrier and mechanical properties of rigid hydrogen bonded xylan-whisker nanocomposite films previously reported. XRD studies show that when a xylan-whisker nanocomposite films is formed the mixing occurs on the atomic scale and NCW loading increases the matrix crystallinity.

CHAPTER 9

OVERALL CONCLUSIONS

The thesis deals with new nanostructured composites, where both the reinforcement and the matrix are biobased. It reports that incorporation of nanocellulose whiskers can act as a reinforcing additive to ultimately derive new properties especially strength and barrier, when incorporated with the traditional "green" polymers such as xylan. The unique molecular attractions between cellulose fibrils and xylan provided enhanced structural and physical properties. Xylan films were prepared using oat-spelt xylan, sulfuric acid generated cellulose whiskers with sorbitol as plasticizer. Degradable polymer nanocomposites films were synthesized by solution processing techniques. Xylan films reinforced with the whiskers showed an improvement in strength properties especially using the sulfonated whiskers. Xylan incorporated with low dosages of cellulose whiskers films providedwith improved water barrier properties. It appears that the high degree of crystallinity of cellulose whiskers, dense composite structure formed by the whiskers and a rigidly hydrogen-bonded cellulose whiskers that is governed by percolation mechanism can cause cellulose whiskers to form integrated matrix which contribute to substantial benefit in the overall reduction of water transmission. The xylan–softwood kraft fiber films exhibited fiber aggregation; this can be reason of higher barrier properties of xylan–sulfonated whisker than xylan–softwood kraft fiber films which have a more open structure. Optical microscopic images indicated that xylan incorporated with softwood kraft fiber and acacia fiber exhibit fiber aggregation in comparison to well dispersed sulfuric nanocrystalline cellulose on xylan surface as indicated in optical and SEM images of xylan–sulfuric nanocrystalline cellulose film. This provides more open

structure for more rapid permeation in control xylan, xylan–softwood kraft fiber and xylan–acacia fibers leading to higher water vapor transmission rate as compared to xylan–sulfuric nanocrystalline cellulose films which have substantially lower water vapor transmission rate. The synergistic xylan–10% sulfuric nanocrystalline cellulose performed well and shows potential for the development of improved biodegradable barrier membranes. Nanocrystalline cellulose was also incorporated into xylan slurry to prepare high oxygen barrier biodegradable films. The morphology of the resulting nanocomposite films was examined by scanning electron microscopy and atomic force microscopy which showed that control films containing xylan and sorbitol had a more open structure as compared to xylan-sorbitol films containing sulfonated nanocrystalline cellulose. Xylan films reinforced with nanocrystalline cellulose were denser and exhibited higher tortuosity factor than the control xylan films. A processing-structure-property relationship study of xylan-NCWs nanocomposites was done and the effectiveness of nanocellulose as reinforcement was demonstrated. The spectral data obtained for the NCW/xylan nanocomposite films showed that the amount of xylan adsorbed to cellulose increases with the addition of NCW in the matrix. In addition, NMR T_2 relaxation experiments studies were conducted to investigate the change in the nature of carbohydrate–water interactions as a result of NCW incorporation. These results facilitated an improved understanding of the mechanisms involved in the superior barrier and mechanical properties of rigid hydrogen bonded xylan-whisker nanocomposite films previously reported. XRD studies show that when a xylan-whisker nanocomposite films is formed the mixing occurs on the atomic scale and NCW loading increases the matrix crystallinity.

APPENDIX A

COPYRIGHT PERMISSIONS

Copyright Clearance Center

LICENSE YOUR CONTENT | PRODUCTS AND SOLUTIONS | PARTNERS | EDUCATION | ABOUT US

1 PAYMENT 2 REVIEW 3 CONFIRMATION

Step 3: Order Confirmation

Thank you for your order! A confirmation for your order will be sent to your account email address. If you have questions about your order, you can call us at 978-646-2600, M-F between 8:00 AM and 6:00 PM (Eastern), or write to us at info@copyright.com.

Confirmation Number: 10418151
Order Date: 07/05/2011

If you pay by credit card, your order will be finalized and your card will be charged within 24 hours. If you pay by invoice, you can change or cancel your order until the invoice is generated.

Payment Information

AMIT SAXENA
Georgia Institute of Technology
amitech2007@gmail.com
+1 (770)9063536
Payment Method: n/a

Order Details

Composites. Part B, Engineering

Order detail ID:	55211194
Order License Id:	2702680606265
Article Title:	Novel nanocellulosic xylan composite film
Author(s):	Saxena, Amit
DOI:	10.1016/J.COMPOSITESB.2009.05.003
Date:	Dec 01, 2009
ISSN:	1359-8368
Publication Type:	Journal
Volume:	40
Issue:	8
Start page:	727
Publisher:	PERGAMON

Permission Status: Granted
Permission type: Republish or display content
Type of use: reuse in a thesis/dissertation
View details

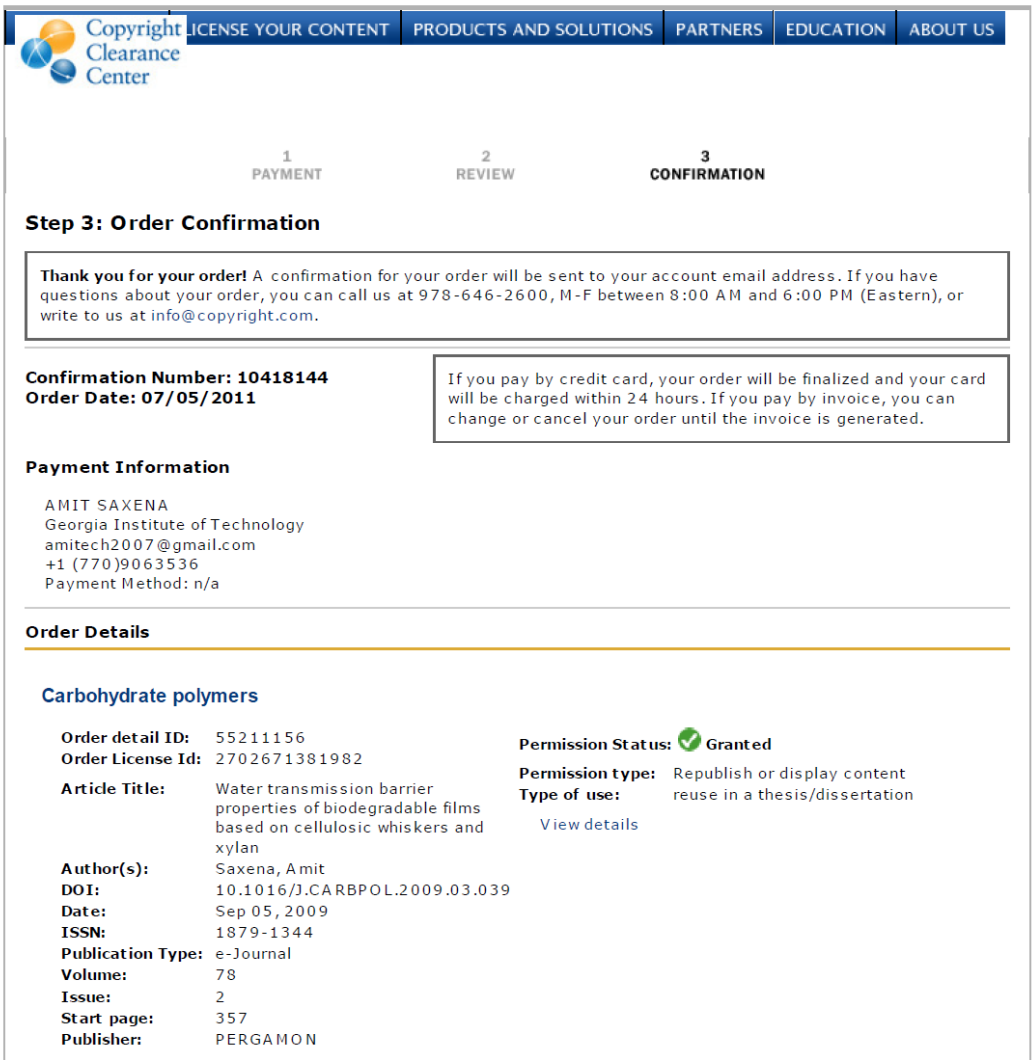
Copyright Clearance Center
ICENSE YOUR CONTENT
PRODUCTS AND SOLUTIONS
PARTNERS
EDUCATION
ABOUT US
1 PAYMENT
2 REVIEW
3 CONFIRMATION
Step 3: Order Confirmation
Thank you for your order! A confirmation for your order will be sent to your account email address. If you have questions about your order, you can call us at 978-646-2600, M-F between 8:00 AM and 6:00 PM (Eastern), or write to us at info@copyright.com.
Confirmation Number: 10418144
Order Date: 07/05/2011
If you pay by credit card, your order will be finalized and your card will be charged within 24 hours. If you pay by invoice, you can change or cancel your order until the invoice is generated.
Payment Information
AMIT SAXENA
Georgia Institute of Technology
amitech2007@gmail.com
+1 (770)9063536
Payment Method: n/a
Order Details
Carbohydrate polymers
Order detail ID: 55211156
Order License Id: 2702671381982
Article Title: Water transmission barrier properties of biodegradable films based on cellulosic whiskers and xylan
Author(s): Saxena, Amit
DOI: 10.1016/J.CARBPOL.2009.03.039
Date: Sep 05, 2009
ISSN: 1879-1344
Publication Type: e-Journal
Volume: 78
Issue: 2
Start page: 357
Publisher: PERGAMON
Permission Status: Granted
Permission type: Republish or display content
Type of use: reuse in a thesis/dissertation
View details

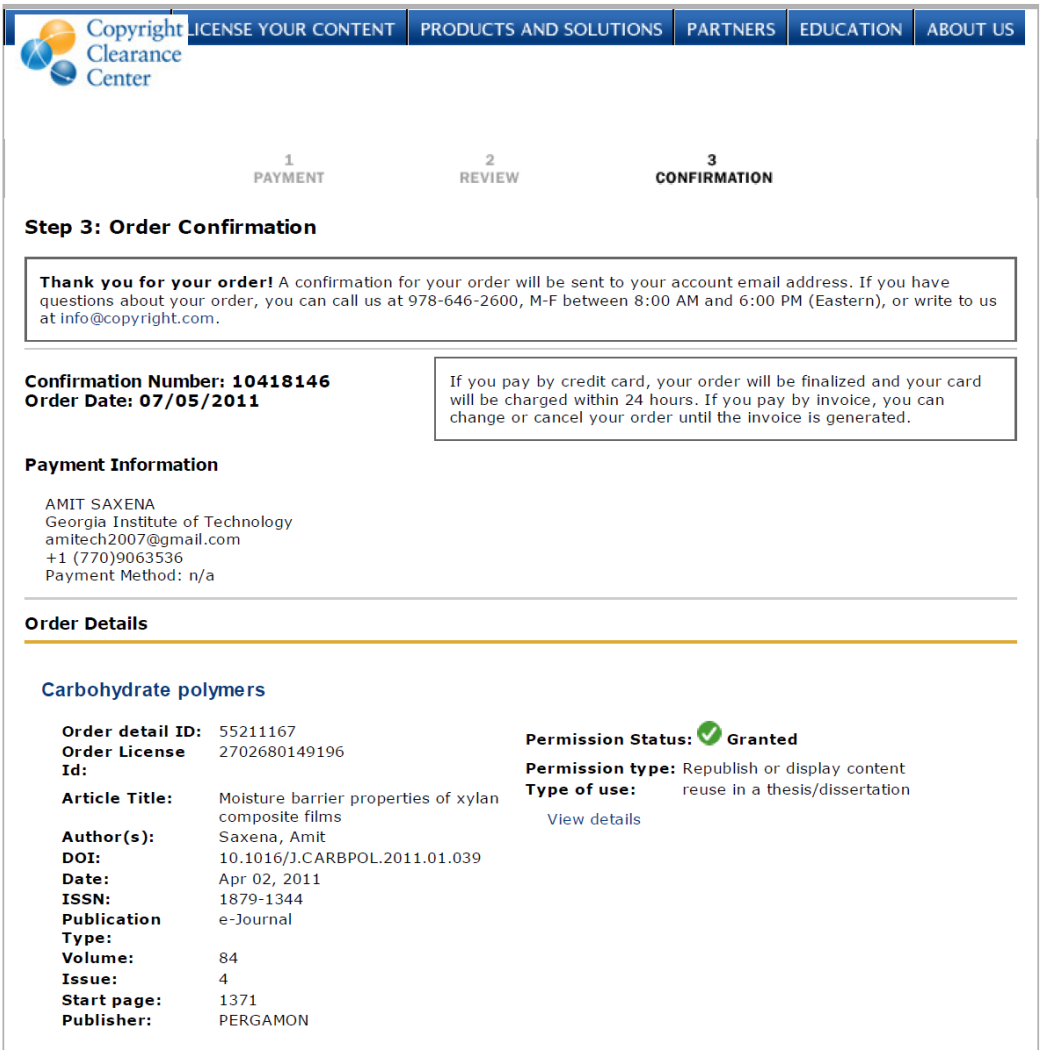
Copyright Clearance Center
LICENSE YOUR CONTENT
PRODUCTS AND SOLUTIONS
PARTNERS
EDUCATION
ABOUT US
1 PAYMENT
2 REVIEW
3 CONFIRMATION
Step 3: Order Confirmation
Thank you for your order! A confirmation for your order will be sent to your account email address. If you have questions about your order, you can call us at 978-646-2600, M-F between 8:00 AM and 6:00 PM (Eastern), or write to us at info@copyright.com.
Confirmation Number: 10418146
Order Date: 07/05/2011
If you pay by credit card, your order will be finalized and your card will be charged within 24 hours. If you pay by invoice, you can change or cancel your order until the invoice is generated.
Payment Information
AMIT SAXENA
Georgia Institute of Technology
amitech2007@gmail.com
+1 (770)9063536
Payment Method: n/a
Order Details
Carbohydrate polymers
Order detail ID: 55211167
Order License Id: 2702680149196
Article Title: Moisture barrier properties of xylan composite films
Author(s): Saxena, Amit
DOI: 10.1016/J.CARBPOL.2011.01.039
Date: Apr 02, 2011
ISSN: 1879-1344
Publication Type: e-Journal
Volume: 84
Issue: 4
Start page: 1371
Publisher: PERGAMON
Permission Status: Granted
Permission type: Republish or display content
Type of use: reuse in a thesis/dissertation
View details

On Sun, Sep 9, 2012 at 2:12 PM, AMIT SAXENA <amitech2007@gmail.com> wrote:

Dear Ann,

How are you? Actually I would like to place an order to get copyright permission of my own published work to be used in my thesis. The article I am looking is
"High oxygen nanocomposite barrier films based on xylan and nanocrystalline cellulose.Nano-Micro Lett. 2, 235-241 (2010)" The link is
http://nmletters.org/index.php?journal=nml&page=article&op=view&path%5B%5D=118
Can you please place an order for this?

Thanks
Best regards,
Amit Saxena

On Mon, Sep 10, 2012 at 1:55 PM, Ann Delacey <adelacey@copyright.com> wrote:

Dear Amit,
This is not covered by Copyright Clearance Center. Please access the link that you provided, scroll to the bottom of the pages, click on the logo for Creative Commons and read the material and licensing information attached.

Best regards,
Ann
Ann DeLacey
Customer Service Representative
Copyright Clearance Center
222 Rosewood Drive
Danvers, MA 01923
info@copyright.com
1.877.622.5543 Toll Free
+1.978.646.2600 Main
+1.978.646.8633Fax
www.copyright.com

Creative Commons

Creative Commons License Deed

Attribution 3.0 Unported (CC BY 3.0)

This is a human-readable summary of the Legal Code (the full license).
Disclaimer

You are free:

to Share — to copy, distribute and transmit the work

to Remix — to adapt the work

to make commercial use of the work

Under the following conditions:

Attribution — You must attribute the work in the manner specified by the author or licensor (but not in any way that suggests that they endorse you or your use of the work).

With the understanding that:

Waiver — Any of the above conditions can be waived if you get permission from the copyright holder.

Public Domain — Where the work or any of its elements is in the public domain under applicable law, that status is in no way affected by the license.

Other Rights — In no way are any of the following rights affected by the license:

- Your fair dealing or fair use rights, or other applicable copyright exceptions and limitations;
- The author's moral rights;
- Rights other persons may have either in the work itself or in how the work is used, such as publicity or privacy rights.

- **Notice** — For any reuse or distribution, you must make clear to others the license terms of this work. The best way to do this is with a link to this web page.

About The Licenses

What our licenses do

The Creative Commons copyright licenses and tools forge a balance inside the traditional "all rights reserved" setting that copyright law creates. Our tools give everyone from individual creators to large companies and institutions a simple, standardized way to grant copyright permissions to their creative work. The combination of our tools and our users is a vast and growing digital commons (http://creativecommons.org/videos/a-shared-culture), a pool of content that can be copied, distributed, edited, remixed, and built upon (http://creativecommons.org/videos/wanna-work-together), all within the boundaries of copyright law.

License design and rationale

All Creative Commons licenses have many important features in common. Every license helps creators — we call them licensors if they use our tools — retain copyright while allowing others to copy, distribute, and make some uses of their work — at least non-commercially. Every Creative Commons license also ensures licensors get the credit for their work they deserve. Every Creative Commons license works around the world and lasts as long as applicable copyright lasts (because they are built on copyright). These common features serve as the baseline, on top of which licensors can choose to grant additional permissions when deciding how they want their work to be used.

A Creative Commons licensor answers a few simple questions on the path to choosing a license — first, do I want to allow commercial use or not, and then second, do I want to allow derivative works or not? If a licensor decides to allow derivative works, she may also choose to require that anyone who uses the work — we call them licensees — to make that new work available under the same license terms. We call this idea "ShareAlike" and it is one of the mechanisms that (if chosen) helps the digital commons grow over time. ShareAlike is inspired by the GNU General Public License, used by many free and open source software projects.

Our licenses do not affect freedoms that the law grants to users of creative works otherwise protected by copyright, such as exceptions and limitations to copyright law like fair dealing. Creative Commons licenses require licensees to get permission to do any of the things with a work that the law reserves exclusively to a licensor and that the license does not expressly allow. Licensees must credit the licensor, keep copyright notices intact on all copies of the work, and link to the license from copies of the work. Licensees cannot use technological measures to restrict access to the work by others.

Try out our simple *License Chooser* (http://creativecommons.org/choose).

Three "Layers" Of Licenses

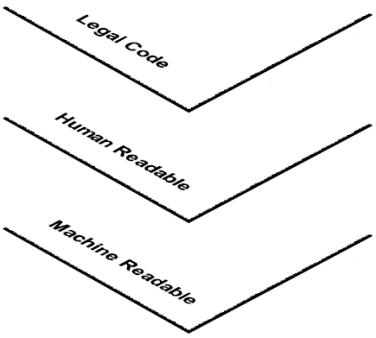

Our public copyright licenses incorporate a unique and innovative "three-layer" design. Each license begins as a traditional legal tool, in the kind of language and text formats that most lawyers know and love. We call this the Legal Code layer of each license.

But since most creators, educators, and scientists are not in fact lawyers, we also make the licenses available in a format that normal people can read — the Commons Deed (also known as the "human readable" version of the license). The Commons Deed is a handy reference for licensors and licensees, summarizing and expressing some of the most important terms and conditions. Think of the Commons Deed as a user-friendly interface to the Legal Code beneath, although the Deed itself is not a license, and its contents are not part of the Legal Code itself.

The final layer of the license design recognizes that software, from search engines to office productivity to music editing, plays an enormous role in the creation, copying, discovery, and distribution of works. In order to make it easy for the Web to know when a work is available under a Creative Commons license, we provide a "machine readable" version of the license — a summary of the key freedoms and obligations written into a format that software systems, search engines, and other kinds of technology can understand. We developed a standardized way to describe licenses that software can understand called CC Rights Expression Language (http://wiki.creativecommons.org/Ccrel) (CC REL) to accomplish this.

Searching for open content is an important function enabled by our approach. You can use Google (http://www.google.com/support/websearch/bin/answer.py?&answer=29508&hl=) to search for Creative Commons content, look for pictures at Flickr (http://www.flickr.com/creativecommons/), albums at Jamendo (http://www.jamendo.com/en/creativecommons), and general media at spinxpress (http://spinxpress.com/). The Wikimedia Commons (http://commons.wikimedia.org/wiki/Main_Page), the multimedia repository of Wikipedia (http://wikipedia.org), is a core user of our licenses as well.

Taken together, these three layers of licenses ensure that the spectrum of rights isn't just a legal concept. It's something that the creators of works can understand, their users can understand, and even the Web itself can understand.

The Licenses

Attribution
CC BY

This license lets others distribute, remix, tweak, and build upon your work, even commercially, as long as they credit you for the original creation. This is the most accommodating of licenses offered. Recommended for maximum dissemination and use of licensed materials.

View License Deed (http://creativecommons.org/licenses/by/3.0) | View Legal Code (http://creativecommons.org/licenses/by/3.0/legalcode)

Attribution-ShareAlike
CC BY-SA

This license lets others remix, tweak, and build upon your work even for commercial purposes, as long as they credit you and license their new creations under the identical terms. This license is often compared to "copyleft" free and open source software licenses. All new works based on yours will carry the same license, so any derivatives will also allow commercial use. This is the license used by Wikipedia, and is recommended for materials that would benefit from incorporating content from Wikipedia and similarly licensed projects.

View License Deed (http://creativecommons.org/licenses/by-sa/3.0) | View Legal Code (http://creativecommons.org/licenses/by-sa/3.0/legalcode)

Attribution-NoDerivs
CC BY-ND

This license allows for redistribution, commercial and non-commercial, as long as it is passed along unchanged and in whole, with credit to you.

View License Deed (http://creativecommons.org/licenses/by-nd/3.0) | View Legal Code (http://creativecommons.org/licenses/by-nd/3.0/legalcode)

Attribution-NonCommercial
CC BY-NC

This license lets others remix, tweak, and build upon your work non-commercially, and although their new works must also acknowledge you and be non-commercial, they don't have to license their derivative works on the same terms.

View License Deed (http://creativecommons.org/licenses/by-nc/3.0) | View Legal Code (http://creativecommons.org/licenses/by-nc/3.0/legalcode)

Attribution-NonCommercial-ShareAlike
CC BY-NC-SA

This license lets others remix, tweak, and build upon your work non-commercially, as long as they credit you and license their new creations under the identical terms.

View License Deed (http://creativecommons.org/licenses/by-nc-sa/3.0) | View Legal Code (http://creativecommons.org/licenses/by-nc-sa/3.0/legalcode)

Attribution-NonCommercial-NoDerivs
CC BY-NC-ND

This license is the most restrictive of our six main licenses, only allowing others to download your works and share them with others as long as they credit you, but they can't change them in any way or use them commercially.

View License Deed (http://creativecommons.org/licenses/by-nc-nd/3.0) | View Legal Code (http://creativecommons.org/licenses/by-nc-nd/3.0/legalcode)

We also provide tools that work in the "all rights granted" space of the public domain (http://wiki.creativecommons.org/Public_domain). Our CC0 tool (http://creativecommons.org/about/cc0) allows licensors to waive all rights and place a work in the public domain, and our Public Domain Mark (http://creativecommons.org/about/pdm) allows any web user to "mark" a work as being in the public domain.

This page is available in the following languages:
Castellano (?lang=es) Castellano (España) (?lang=es_ES) Català (?lang=ca) Deutsch (?lang=de) English (?lang=en) Esperanto (?lang=eo) français (?lang=fr) hrvatski (?lang=hr) Italiano (?lang=it) Nederlands (?lang=nl) Norsk (?lang=no) polski (?lang=pl) Português (?lang=pt) Português (BR) (?lang=pt_BR) Suomeksi (?lang=fi) svenska (?lang=sv) Ελληνικά (?lang=el) русский (?lang=ru) українська (?lang=uk) 華語 (台灣) (?lang=zh_TW) 한국어 (?lang=ko)

(http://www.facebook.com/creativecommons)
(http://twitter.com/creativecommons)
(http://identi.ca/creativecommons)

(http://creativecommons.org/licenses/by/3.0/

Except where otherwise noted (/policies#license), content on this site is licensed under a Creative Commons Attribution 3.0 License (http://creativecommons.org/licenses/by/3.0/).

Policies (http://creativecommons.org/policies)

Privacy (http://creativecommons.org/privacy)

Copyright Clearance Center | LICENSE YOUR CONTENT | PRODUCTS AND SOLUTIONS | PARTNERS | EDUCATION | ABOUT US

1 PAYMENT 2 REVIEW 3 CONFIRMATION

Step 3: Order Confirmation

Thank you for your order! A confirmation for your order will be sent to your account email address. If you have questions about your order, you can call us at 978-646-2600, M-F between 8:00 AM and 6:00 PM (Eastern), or write to us at info@copyright.com.

Confirmation Number: 11026226
Order Date: 09/04/2012

If you pay by credit card, your order will be finalized and your card will be charged within 24 hours. If you pay by invoice, you can change or cancel your order until the invoice is generated.

Payment Information

AMIT SAXENA
Georgia Institute of Technology
amitech2007@gmail.com
+1 (770)9063536
Payment Method: invoice

Billing address:
Georgia Institute of Technology
500 NORTHSIDE CIRCLE NW #BB2
Atlanta, GA 30309
US

Order Details

Special Orders

Learn more about how Special Orders work

Journal of nanoscience and nanotechnology

Order detail ID:	62876851
ISSN:	1533-4880
Publication year:	2012
Publication Type:	Journal
Publisher:	AMERICAN SCIENTIFIC PUBLISHERS
Rightsholder:	AMERICAN SCIENTIFIC PUBLISHERS
Author/Editor:	Amit Saxena

Permission Status: Special Order
Special Order Update: Checking availability

Permission type:	Republish or display content
Type of use:	Dissertation
Republication title:	omposites based on nanocellulose whiskers
Republishing organization:	Amit Saxena/Georgia Institute of Technology
Organization status:	Non-profit 501(c)(3)
Republication date:	12/03/2012
Circulation/ Distribution:	3
Type of content:	Figure/ diagram/ table
Description of requested content:	Biopolymer Nanocomposite Films Reinforced with Nanocellulose Whiskers
Page range(s):	218-226
Translating to:	No Translation
Requested content's publication date:	01/02/2012

$TBD

Total order items: 1

Dear Mr. Saxena:

This is to your request for permission to use the following material from American Scientific Publishers (ASP).

Saxena A, Foston M, Kassaee M, Elder TJ, Ragauskas AJ. Biopolymer Nanocomposite films reinforced with nanocellulose whiskers, J.Nanosci. Nanotechnol., 2012, 12, 218-226
American Scientific Publishers (ASP) is pleased to grant you permission for using whole article in your forthcoming Ph.D. dissertation at Georgia Institute of Technology in print and online editions.

H. S. Nalwa, PhD
AMERICAN SCIENTIFIC PUBLISHERS
26650 The Old Road, Suite 208
Valencia, California 91381, USA
Tel. 661-799-7200
Fax: 661-799-7230
Email: order@aspbs.com

Step 3: Order Confirmation

Thank you for your order! A confirmation for your order will be sent to your account email address. If you have questions about your order, you can call us at 978-646-2600, M-F between 8:00 AM and 6:00 PM (Eastern), or write to us at info@copyright.com.

Confirmation Number: 11027865
Order Date: 09/10/2012

If you pay by credit card, your order will be finalized and your card will be charged within 24 hours. If you pay by invoice, you can change or cancel your order until the invoice is generated.

Payment Information

AMIT SAXENA
Georgia Institute of Technology
amitech2007@gmail.com
+1 (770)9063536
Payment Method: n/a

Order Details

Carbohydrate polymers

Order detail ID:	62884903
Order License Id:	2985680890135
Article Title:	Isolation, preparation and characterization of cellulose microfibers obtained from bagasse
Author(s):	Bhattacharya, Deepanjan ; Germinario, Louis T. ; Winter, William T.
DOI:	10.1016/J.CARBPOL.2007.12.005
Date:	Jan 01, 2008
ISSN:	0144-8617
Publication Type:	Journal
Volume:	73
Issue:	3
Start page:	371
Publisher:	PERGAMON

Permission Status: Granted
Permission type: Republish or display content
Type of use: reuse in a thesis/dissertation
View details

Note: This item will be invoiced or charged separately through CCC's **RightsLink** service. More info **$ 0.00**

Total order items: 1 **Order Total: 0.00 USD**

SPRINGER ORDER DETAILS

Sep 08, 2012

Order Number	500695610
Order date	Sep 04, 2012
Licensed content publisher	Springer
Licensed content publication	Nanoscale Research Letters
Licensed content title	Cellulose fibres, nanofibrils and microfibrils: The morphological sequence of MFC components from a plant physiology and fibre technology point of view
Licensed content author	Gary Chinga-Carrasco
Licensed content date	Jan 1, 2011
Volume number	6
Issue number	1
Type of Use	Thesis/Dissertation
Portion	Figures
Author of this Springer article	No
Order reference number	cao2722
Title of your thesis / dissertation	Nanocomposites based on nanocellulose whiskers
Expected completion date	Dec 2012
Estimated size(pages)	150
Total	0.00 USD

1 PAYMENT 2 REVIEW 3 CONFIRMATION

Step 3: Order Confirmation

Thank you for your order! A confirmation for your order will be sent to your account email address. If you have questions about your order, you can call us at 978-646-2600, M-F between 8:00 AM and 6:00 PM (Eastern), or write to us at info@copyright.com.

Confirmation Number: 11026123
Order Date: 09/04/2012

If you pay by credit card, your order will be finalized and your card will be charged within 24 hours. If you pay by invoice, you can change or cancel your order until the invoice is generated.

Payment Information

AMIT SAXENA
Georgia Institute of Technology
amitech2007@gmail.com
+1 (770)9063536
Payment Method: n/a

Order Details

Journal of polymers and the environment

Order detail ID:	62876570
Order License Id:	2982021027312
Article Title:	Nanocomposites of Cellulose Acetate Butyrate Reinforced with Cellulose Nanocrystals
Author(s):	Winter, William T. ; Grunert, Maren
DOI:	10.1023/A:1021065905986
Date:	Apr 01, 2002
ISSN:	1566-2543
Publication Type:	Journal
Volume:	10
Issue:	1
Start page:	27
Publisher:	SPRINGER NEW YORK LLC

Permission Status: Granted
Permission type: Republish or display content
Type of use: use in a thesis/dissertation
View details

Note: This item will be invoiced or charged separately through CCC's **RightsLink** service. More info **$ 0.00**

Total order items: 1 **Order Total: 0.00 USD**

JOHN WILEY AND SONS LICENSE TERMS AND CONDITIONS

Sep 04, 2012

This is a License Agreement between Georgia Institute of Technology ("You") and John Wiley and Sons ("John Wiley and Sons") provided by Copyright Clearance Center ("CCC"). The license consists of your order details, the terms and conditions provided by John Wiley and Sons, and the payment terms and conditions.

All payments must be made in full to CCC. For payment instructions, please see information listed at the bottom of this form.

License Number	2982071360504
License date	Sep 04, 2012
Licensed content publisher	John Wiley and Sons
Licensed content publication	Polymer Engineering & Science
Licensed content title	Mechanical percolation in cellulose whisker nanocomposites
Licensed content author	V. Favier,J. Y. Cavaille,G. R. Canova,S. C. Shrivastava
Licensed content date	Apr 8, 2004
Start page	1732
End page	1739
Type of use	Dissertation/Thesis
Requestor type	University/Academic
Format	Print and electronic
Portion	Figure/table
Number of figures/tables	1
Number of extracts	None
Original Wiley figure/table number(s)	figure 6
Will you be translating?	No
Order reference number	cao2722
Total	0.00 USD
Terms and Conditions	

TERMS AND CONDITIONS

This copyrighted material is owned by or exclusively licensed to John Wiley & Sons, Inc. or one of its group companies (each a "Wiley Company") or a society for whom a Wiley Company has exclusive publishing rights in relation to a particular journal (collectively WILEY"). By clicking "accept" in connection with completing this licensing transaction, you agree that the following

terms and conditions apply to this transaction (along with the billing and payment terms and conditions established by the Copyright Clearance Center Inc., ("CCC's Billing and Payment terms and conditions"), at the time that you opened your Rightslink account (these are available at any time at http://myaccount.copyright.com)

Terms and Conditions

1. The materials you have requested permission to reproduce (the "Materials") are protected by copyright.

2. You are hereby granted a personal, non-exclusive, non-sublicensable, non-transferable, worldwide, limited license to reproduce the Materials for the purpose specified in the licensing process. This license is for a one-time use only with a maximum distribution equal to the number that you identified in the licensing process. Any form of republication granted by this licence must be completed within two years of the date of the grant of this licence (although copies prepared before may be distributed thereafter). The Materials shall not be used in any other manner or for any other purpose. Permission is granted subject to an appropriate acknowledgement given to the author, title of the material/book/journal and the publisher. You shall also duplicate the copyright notice that appears in the Wiley publication in your use of the Material. Permission is also granted on the understanding that nowhere in the text is a previously published source acknowledged for all or part of this Material. Any third party material is expressly excluded from this permission.

3. With respect to the Materials, all rights are reserved. Except as expressly granted by the terms of the license, no part of the Materials may be copied, modified, adapted (except for minor reformatting required by the new Publication), translated, reproduced, transferred or distributed, in any form or by any means, and no derivative works may be made based on the Materials without the prior permission of the respective copyright owner. You may not alter, remove or suppress in any manner any copyright, trademark or other notices displayed by the Materials. You may not license, rent, sell, loan, lease, pledge, offer as security, transfer or assign the Materials, or any of the rights granted to you hereunder to any other person.

4. The Materials and all of the intellectual property rights therein shall at all times remain the exclusive property of John Wiley & Sons Inc or one of its related companies (WILEY) or their respective licensors, and your interest therein is only that of having possession of and the right to reproduce the Materials pursuant to Section 2 herein during the continuance of this Agreement. You agree that you own no right, title or interest in or to the Materials or any of the intellectual property rights therein. You shall have no rights hereunder other than the license as provided for above in Section 2. No right, license or interest to any trademark, trade name, service mark or other branding ("Marks") of WILEY or its licensors is granted hereunder, and you agree that you shall not assert any such right, license or interest with respect thereto.

5. NEITHER WILEY NOR ITS LICENSORS MAKES ANY WARRANTY OR REPRESENTATION OF ANY KIND TO YOU OR ANY THIRD PARTY, EXPRESS, IMPLIED OR STATUTORY, WITH RESPECT TO THE MATERIALS OR THE ACCURACY OF ANY INFORMATION CONTAINED IN THE MATERIALS, INCLUDING, WITHOUT LIMITATION, ANY IMPLIED WARRANTY OF MERCHANTABILITY, ACCURACY, SATISFACTORY QUALITY, FITNESS FOR A PARTICULAR PURPOSE, USABILITY, INTEGRATION OR NON-INFRINGEMENT AND ALL SUCH WARRANTIES ARE HEREBY EXCLUDED BY WILEY AND ITS LICENSORS AND WAIVED BY YOU.

6. WILEY shall have the right to terminate this Agreement immediately upon breach of this Agreement by you.

7. You shall indemnify, defend and hold harmless WILEY, its Licensors and their respective directors, officers, agents and employees, from and against any actual or threatened claims, demands, causes of action or proceedings arising from any breach of this Agreement by you.

8. IN NO EVENT SHALL WILEY OR ITS LICENSORS BE LIABLE TO YOU OR ANY OTHER PARTY OR ANY OTHER PERSON OR ENTITY FOR ANY SPECIAL, CONSEQUENTIAL, INCIDENTAL, INDIRECT, EXEMPLARY OR PUNITIVE DAMAGES, HOWEVER CAUSED, ARISING OUT OF OR IN CONNECTION WITH THE DOWNLOADING, PROVISIONING, VIEWING OR USE OF THE MATERIALS REGARDLESS OF THE FORM OF ACTION, WHETHER FOR BREACH OF CONTRACT, BREACH OF WARRANTY,

TORT, NEGLIGENCE, INFRINGEMENT OR OTHERWISE (INCLUDING, WITHOUT LIMITATION, DAMAGES BASED ON LOSS OF PROFITS, DATA, FILES, USE, BUSINESS OPPORTUNITY OR CLAIMS OF THIRD PARTIES), AND WHETHER OR NOT THE PARTY HAS BEEN ADVISED OF THE POSSIBILITY OF SUCH DAMAGES. THIS LIMITATION SHALL APPLY NOTWITHSTANDING ANY FAILURE OF ESSENTIAL PURPOSE OF ANY LIMITED REMEDY PROVIDED HEREIN.

9. Should any provision of this Agreement be held by a court of competent jurisdiction to be illegal, invalid, or unenforceable, that provision shall be deemed amended to achieve as nearly as possible the same economic effect as the original provision, and the legality, validity and enforceability of the remaining provisions of this Agreement shall not be affected or impaired thereby.

10. The failure of either party to enforce any term or condition of this Agreement shall not constitute a waiver of either party's right to enforce each and every term and condition of this Agreement. No breach under this agreement shall be deemed waived or excused by either party unless such waiver or consent is in writing signed by the party granting such waiver or consent. The waiver by or consent of a party to a breach of any provision of this Agreement shall not operate or be construed as a waiver of or consent to any other or subsequent breach by such other party.

11. This Agreement may not be assigned (including by operation of law or otherwise) by you without WILEY's prior written consent.

12. Any fee required for this permission shall be non-refundable after thirty (30) days from receipt.

13. These terms and conditions together with CCC's Billing and Payment terms and conditions (which are incorporated herein) form the entire agreement between you and WILEY concerning this licensing transaction and (in the absence of fraud) supersedes all prior agreements and representations of the parties, oral or written. This Agreement may not be amended except in writing signed by both parties. This Agreement shall be binding upon and inure to the benefit of the parties' successors, legal representatives, and authorized assigns.

14. In the event of any conflict between your obligations established by these terms and conditions and those established by CCC's Billing and Payment terms and conditions, these terms and conditions shall prevail.

15. WILEY expressly reserves all rights not specifically granted in the combination of (i) the license details provided by you and accepted in the course of this licensing transaction, (ii) these terms and conditions and (iii) CCC's Billing and Payment terms and conditions.

16. This Agreement will be void if the Type of Use, Format, Circulation, or Requestor Type was misrepresented during the licensing process.

17. This Agreement shall be governed by and construed in accordance with the laws of the State of New York, USA, without regards to such state's conflict of law rules. Any legal action, suit or proceeding arising out of or relating to these Terms and Conditions or the breach thereof shall be instituted in a court of competent jurisdiction in New York County in the State of New York in the United States of America and each party hereby consents and submits to the personal jurisdiction of such court, waives any objection to venue in such court and consents to service of process by registered or certified mail, return receipt requested, at the last known address of such party.

Wiley Open Access Terms and Conditions

All research articles published in Wiley Open Access journals are fully open access: immediately freely available to read, download and share. Articles are published under the terms of the Creative Commons Attribution Non Commercial License. which permits use, distribution and reproduction in any medium, provided the original work is properly cited and is not used for commercial purposes. The license is subject to the Wiley Open Access terms and conditions: Wiley Open Access articles are protected by copyright and are posted to repositories and websites in accordance with the terms of the Creative Commons Attribution Non Commercial License. At

the time of deposit, Wiley Open Access articles include all changes made during peer review, copyediting, and publishing. Repositories and websites that host the article are responsible for incorporating any publisher-supplied amendments or retractions issued subsequently.
Wiley Open Access articles are also available without charge on Wiley's publishing platform, **Wiley Online Library** or any successor sites.

Use by non-commercial users

For non-commercial and non-promotional purposes individual users may access, download, copy, display and redistribute to colleagues Wiley Open Access articles, as well as adapt, translate, text- and data-mine the content subject to the following conditions:

- The authors' moral rights are not compromised. These rights include the right of "paternity" (also known as "attribution" - the right for the author to be identified as such) and "integrity" (the right for the author not to have the work altered in such a way that the author's reputation or integrity may be impugned).
- Where content in the article is identified as belonging to a third party, it is the obligation of the user to ensure that any reuse complies with the copyright policies of the owner of that content.
- If article content is copied, downloaded or otherwise reused for non-commercial research and education purposes, a link to the appropriate bibliographic citation (authors, journal, article title, volume, issue, page numbers, DOI and the link to the definitive published version on Wiley Online Library) should be maintained. Copyright notices and disclaimers must not be deleted.
- Any translations, for which a prior translation agreement with Wiley has not been agreed, must prominently display the statement: "This is an unofficial translation of an article that appeared in a Wiley publication. The publisher has not endorsed this translation."

Use by commercial "for-profit" organisations

Use of Wiley Open Access articles for commercial, promotional, or marketing purposes requires further explicit permission from Wiley and will be subject to a fee. Commercial purposes include:

- Copying or downloading of articles, or linking to such articles for further redistribution, sale or licensing;
- Copying, downloading or posting by a site or service that incorporates advertising with such content;
- The inclusion or incorporation of article content in other works or services (other than normal quotations with an appropriate citation)

that is then available for sale or licensing, for a fee (for example, a compilation produced for marketing purposes, inclusion in a sales pack)
• Use of article content (other than normal quotations with appropriate citation) by for-profit organisations for promotional purposes
• Linking to article content in e-mails redistributed for promotional, marketing or educational purposes;
• Use for the purposes of monetary reward by means of sale, resale, licence, loan, transfer or other form of commercial exploitation such as marketing products
• Print reprints of Wiley Open Access articles can be purchased from: corporatesales@wiley.com

Other Terms and Conditions:

BY CLICKING ON THE "I AGREE..." BOX, YOU ACKNOWLEDGE THAT YOU HAVE READ AND FULLY UNDERSTAND EACH OF THE SECTIONS OF AND PROVISIONS SET FORTH IN THIS AGREEMENT AND THAT YOU ARE IN AGREEMENT WITH AND ARE WILLING TO ACCEPT ALL OF YOUR OBLIGATIONS AS SET FORTH IN THIS AGREEMENT.

v1.7

If you would like to pay for this license now, please remit this license along with your payment made payable to "COPYRIGHT CLEARANCE CENTER" otherwise you will be invoiced within 48 hours of the license date. Payment should be in the form of a check or money order referencing your account number and this invoice number RLNK500851229.
Once you receive your invoice for this order, you may pay your invoice by credit card. Please follow instructions provided at that time.

Make Payment To:
Copyright Clearance Center
Dept 001
P.O. Box 843006
Boston, MA 02284-3006

For suggestions or comments regarding this order, contact RightsLink Customer Support: customercare@copyright.com or +1-877-622-5543 (toll free in the US) or +1-978-646-2777.

Gratis licenses (referencing $0 in the Total field) are free. Please retain this printable

REFERENCES

1. Tharanathan RN, Saroja N. Hydrocolloid-based packaging films - alternate to synthetic plastics. J. Sci. Ind. Res. 2001; 60(7):547-559.

2. Sheen L, Worrell E, Patel M. Present and future development in plastics from biomass Befoul Bipod. Bior. 2010; 4(1):25-40.

3. Samir A, Alloin F, Dufresne A. Review of recent research into cellulosic whiskers, their properties and their application in nanocomposite field. Biomacromolecules 2005; 6(2):612-626.

4. Ragauskas AJ, Williams CK, Davison BH, Britovsek G, Cairney J, Eckert CA, Frederick WJ,Hallett JP, Leak DJ, Liotta CL, Mielenz JR, Murphy R, Templer R, Tschaplinski T. The path forward for biofuels and biomaterials. Science 2006; 311(5760):484-489.

5. Petersson L, Oksman K. Biopolymer based nanocomposites: Comparing layered silicates and microcrystalline cellulose as nanoreinforcement. Compos. Sci. Technol.2006; 66(13): 2187-2196.

6. Krochta JM, Baldwin EA, Nisperos-Carriedo MO. Edible coatings and films to improve food quality. Lancaster: Technomic (1994).

7. Roberts JC, El-Karim AS. The behavior of surface adsorbed xylans during the beating of a bleached kraft pine pulp. Cellul. Chem. Technol. 1983; 17(4):379-386.

8. Gröndahl M, Eriksson L, Gatenholm P. Material properties of plasticized hardwood xylans for potential application as oxygen barrier films. Biomacromolecules 2004; 5 (4):1528 -1535.

9. Linder A, Bergman R, Bodin A, Gatenholm P. Mechanism of assembly of xylan onto cellulose surfaces. Langmuir 2003; 19(12):5072 -5077

10. Höije A, Gröndahl M, Tømmeraas K, Gatenholm P. Isolation and characterization of physicochemical and material properties of arabinoxylans from barley husks. Carbohyd. Polym. 2005; 61(3):266-275.

11. Dammström S, Salmén L, Gatenholm P. The effect of moisture on the dynamical mechanical properties of bacterial cellulose/glucuronoxylan nanocomposites. Polymer 2005; 46(23):10364-10371

12. Kayserilioglu, BS, Bakir U, Yilaz L, Akkas N. Use of xylan, an agricultural product, in wheat gluten based biodegradable films: mechanical, solubility and water vapor transmission rate properties. Bioresource Technol. 2003; 87(3):239-246.

13. Hartman J, Albertsson AC, Lindblad MS, Sjöberg J. Oxygen barrier materials from renewable sources: Material properties of softwood hemicellulose-based films. J. Appl. Polym. Sci. 2006; 100(4):2985-91.

14. Dole P, Joly C, Espuche E, Alric I, Gontard N. Gas transport properties of starch based films. Carbohyd. Polym. 2004; 58(3):335-43.

15. Butler BL, Vergano PJ, Testin RF, Bunn JM, Wiles JL. Mechanical and barrier properties of edible chitosan films as affected by composition and storage. J. Food Sci. 1996; 61(5):953-56.

16. Arvanitoyannis I, Biliaderis CG. Physical properties of polyol-plasticized edible blends made of methyl cellulose and soluble Carbohyd. Polym. 1999; 38(1):47-58.

17. Tock R. Permeabilities and water vapor transmission rates for commercial polymeric films. Adv. Polym. Technol. 1983; 3(3): 223-231.

18. Schönberg C, Oksanen T, Suurnäkki A, Kettunen H, Buchert J. The importance of xylan for the strength properties of spruce kraft pulp fibres. Holzforschung 2001; 5(6):639-644.

19. Dufresne A. Polysaccharide nanocrystals reinforced nanocomposites. Can. J. Chem. 2008; 86:484-494.

20. Beck-Candanedo S, Roman M, Gray D. Effect of reaction conditions on the properties and behavior of wood cellulose nanocrystal suspensions. Biomacromolecules 2005; 6(2):1048-52.

21. Chanzy H. Cellulose sources and exploitation, Aspects of cellulose structure. Kennedy, JF, Phillips, GO, Williams PA. Eds.; Ellis Horwood Ltd. New York 1990:3-12.

22. Thomas A, Antonietti M. Silica nanocating of simple cellulose derivatives: towards chiral pore systems with long-range order and chiral optical coatings. Adv. Functional Materials. 2003; 13:763-766.

23. Beck-Candanedo S, Roman M, Gray DG. Effect of reaction conditions on the properties and behavior of wood cellulose nanocrystal suspensions Biomacromolecules 2005; 6(2): 1048-1054.

24. Zhang J, Elder TJ, Pu Y, Ragauskas AJ. Polymer clay self-assembly complexes on paper. Carbohyd. Polymers 2007; 69(3): 607 – 611.

25 Elazzouzi-Hafraoui S , Nishiyama Y Putaux J-L, Heux L, Dubreuil F, Rochas C. The shape and size distribution of crystalline nanoparticles prepared by acid hydrolysis of native cellulose. Biomacromolecules 2008; 9 (1):57-65.

26 Chanzy, H. Cellulose Sources and Exploitation. J.F. Kennedy, G.O. Phillips, P.A. Williams Eds., Ellis Horwood Ltd, New York, 1990.

27. Sugiyama J, Chanzy H, Revol JF. On the polarity of cellulose in the cell wall of Valonia. Planta 1994; 193(2):260-265.

28. Revol, JF, Godbout L, Dong XM, Gray DG, Chanzy H, Maret G. Chiral nematic suspensions of cellulose crystallites; phase separation and magnetic field orientation. Liq. Cryst. 1994; 16(1):127-134.

29. Favier V, Chanzy H, Cavaille J. Polymer Nanocompsoites reinforced by cellulose whiskers. Macromolecules 1995; 28(18): 6365-6367.

30. Dufresne A, Kellerhals M, Witholt B. Transcrystallinization in MclPHAs/Cellulose whiskers composites. Macromolecules 1999; 32(22): 7396-7401.

31. Eichhorn S, Baillie C, Zafereiropoulos N, Mwaikambo L, Ansell M, Dufresne A, Entwistle K, Herrera-Franco P, Escamilla G, Groom L, Hughes M, Hill C, Rials T.Current international research into cellulosic fibres and composites. J. Mater. Sci. 2001; 36(9): 2107-2131.

32. Marks R., Cell wall mechanics of trachieds. Cell wall mechanics of trachieds; Yale University press: New Haven, 1967.

33. Hon D., Chemical modification of lignocellulosic materials; Marcel Dekker Inc.: New York, 1996, 36.

34. Oriakhi CO. Nano Sandwiches. Chem. Br. 1998; 34(11):59-62.

35. Imai Y, Nishimura S, Abe E, Tateyama H, Abiko A, Yamaguchi A, Aoyama T, Taguchi H. High-modulus poly(ethylene terephthalate)/expandable fluorine mica nanocomposites with a novel reactive compatibilizer. Chem. Mater. 2002; 14(2):477-479.

36. Chazeau L, Paillet M and Cavaille JY. Plasticized PVC reinforced with cellulose whiskers.Linear viscoelastic behavior analyzed through the quasi-point defect theory. J. Polym. Sci. Polym. Phys. 1999A; 37 (16):2151–2164.

37. Chazeau L, Cavaille JY, Terech P. Mechanical behavior above Tg of a plasticized PVC reinforced with cellulose whiskers; a SANS structural study. Polymer 199b; 40 (19): 5333–5344.

38. Chazeau L, Cavaille JY, Canova G, Dendievel R, Boutherin B. Viscoelastic properties of plasticized PVC reinforced with cellulose whiskers. J. Appl. Polym. Sci. 1999c; 71 (11):1797–1808.

39. Ljungberg N, Bonini C, Bortolussi F, Boisson C, Heux L, Cavaille JY. New nanocomposite materials reinforced with cellulose whiskers in atactic polypropylene: effect of surface and dispersion characteristics. Biomacromolecules 2005; 6 (5):2732–2739

40. Samir MASA, Alloin F, Gorecki W, Sanchez JY, Dufresne A. Nanocomposite polymer electrolytes based on poly (oxyethylene) and cellulose nanocrystals. J. Phys. Chem. B 2004a; 108 (30):10845–10852.

41. Samir MASA, Alloin F, Sanchez JY, Dufresne A. Cross-linked nanocomposite polymer electrolytes reinforced with cellulose whiskers. Macromolecules 2004b; 37(13): 4839–4844.

42. Samir MASA, Alloin F, Sanchez JY, Dufresne A. Cellulose nanocrystals reinforced poly (oxyethylene). Polymer 2004c; 45 (12): 4149–4157.

43. Pu Y, Zhang J, Elder T, Deng Y, Gatenholm P, Ragauskas A. Investigation into acrylic films reinforced with nanocellulosics versus acacia. Composite. Eng. 2007; 38B (3): 360-366.

44. Mathew AP, Dufresne A. Morphological Investigation of Nanocomposites from sorbitol plasticized starch and tunicin whiskers Biomacromolecules 2002; 3(3):609-617.

45. Grunert M, Winter WT. Nanocomposites of cellulose acetate butyrate reinforced with cellulose nanocrystals. J. Polym. Environ. 2002; 10(1):27-30.

46. Kvien I, Oksman K. Orientation of cellulose nanowhiskers in polyvinyl alcohol (PVA). Appl. Phys. A: Mater. Sci. Processing. 2007; 87(4): 641-643.

47. Lagaron JM, Catala R and Gavaa R. Structural characteristics defining high barrier properties in polymeric materials. Mater. Sci. Technol. 2004; 20(1): 1-7.

48. De Souza Lima MM and Borsali R. Rodlike cellulose microcrystals: structure, properties, and applications. Macromol. Rapid Commun. 2004; 25(7): 771-87.

49. Ioelovich M. Cellulose as a nanostructured polymer: a short review. BioRes. 2008; 3(4):1403

50. Sturcova A, His I., Apperley DC, Sugiyma J, Jarvis MC. Structural details of crystalline cellulose from higher plants. Biomacromolecules 2004; 5(4): 1333-1339.

51. Mikkonen KS, Heikkilä MI, Helén H, Hyvönen L and Tenkanen M. Spruce galactoglucomannan films show promising barrier properties. Carbohyd. Polym. 2010; 79(4):1107-12.

52. Dufresne A. Polymer nanocomposites from Biological Sources. In Encyclopedia of Nanoscience and Nanotechnology, 2nd ed.; Nalwa, H.S., Ed.; American Scientific Publisher: Valencia, CA, USA; in press.

53. Krässig HA. Cellulose: structure, accessibility, and reactivity. Carbohyd. Polym. 1995; 26(4):313-314.

54. Eyerer P, Weller M, Hübner C, Augusto Agnelli J. Polymers - Opportunities and Risks II: Sustainability, Product Design and Processing 2010, 2.

55. Kumar R, Mago G, Balan V, Wymand CE. Physical and chemical characterizations of corn stover and poplar solids resulting from leading pretreatment technologies. Bioresource Technol. 2009; 100 (17):3948-3962.

56. Pan X, Xie D, Kang KY, Yoon SL, Saddler JN. Effect of organosolv ethanol pretreatment variables on physical characteristics of hybrid poplar substrates. Appl. Biochem. Biotech. 2007; 137-140 (1-12):367-377.

57. Martínez JM, Reguant J, Montero MÁ, Montané D, Salvadó J, Farriol X. Hydrolytic pretreatment of softwood and almond shells. Degree of polymerization and enzymatic digestibility of the cellulose fraction. Ind. Eng. Chem. Res. 1997; 36 (3):688-696.

58. Jahan MS, Mun SP. Studies on the macromolecular components of nonwood available in Bangladesh. Ind. Crop. Prod. 2009; 30 (3):344-350.

59. Sweet MS, Winandy JE. Influence of degree of polymerization of cellulose and hemicellulose on strength loss in fire-retardant-treated southern pine. Holzforschung 1999; 53 (3):311-317.

60. Jahan MS, Mun SP. Effect of tree age on the cellulose structure of Nalita wood (Trema orientalis). Wood Sci. Technol. 2005; 39 (5):367-373.

61. Coffey DG, Bell DA, Henderson A. Cellulose and cellulose derivatives. In: Food polysaccharides and their applications. Stephen AM, editors. Marcel Dekker: New York City, New York, 1995:125.

62. Sjöholm E. Size exclusion chromatography of cellulose and cellulose derivatives In: Handbook of size exclusion chromatography and related techniques. Wu C, editors. Marcel Dekker: New York, 2004: 311-354.

63. Hallac BB, Ragauskas AJ. Analyzing cellulose degree of polymerization and its relevancy to cellulosic ethanol. Biofuels, Bioprod. Bior. 2011; 5(2):215-225.

64. Feller RL, Lee SB, Bogaard J. The kinetics of cellulose deterioration. Historic textile and paper materials 1986; 18 (212):329-347.

65. Alemdar A, Sain M. Biocomposites from wheat straw nanofibers: Morphology, thermal and mechanical properties. Composites Sci. Technol. 2008; 68(2): 557-565.

66. Jahan MS, Mun SP. Studies on the macromolecular components of nonwood available in Bangladesh. Ind Crop Prod 2009; 30 (3):344-350.

67. Sweet MS, Winandy JE. Influence of degree of polymerization of cellulose and hemicellulose on strength loss in fire-retardant-treated southern pine. Holzforschung 1999; 53 (3):311-317.

68. Jahan MS, Mun SP. Effect of tree age on the cellulose structure of Nalita wood (Trema orientalis). Wood Sci Technol 2005; 39 (5):367-373

69. Xu W, Reddy N, Yang Y. Extraction, characterization and potential applications of cellulose in corn kernels and Distillers‘ dried grains with solubles (DDGS). Carbohyd. Polym. 2009; 76 (4):521-527.

70. Gilberto Siqueira 1, 2, Julien Bras 1 and Alain Dufresne Cellulosic Bionanocomposites: A
Review of Preparation, Properties and Applications. Polymers 2010; 2:728-765.

71. Preston RD. The Physical Biology of Plant Cell Walls (Wiley, New York) 1974.

72. Kuga S and Brown RM.Jr. Silver labeling of the reducing ends of bacterial cellulose. Carbohyd. Res.1988; 180(2):345-50.

73. Brown, RM. The biosynthesis of cellulose. Pure Appl. Chem. 1996: 10: 1345-1373.

Ranby BG. The mercerisation of cellulose III. A phase transition study using electron diffraction. Acta Chemica Scand. 1952; 6:128-133.

74. Atalla R, VanderHart DL. Native cellulose: a composite of two distinct crystalline forms. Science 1984; 223(4633): 283-85.

75. Wada M, Sugiyama J, Okano T. Native celluloses on the basis of the two crystalline phase (Iα/Iβ) system. App. Polym. Sci. 1993; 49(8): 1491-96

76. Imai T, Sugiyama J. Nanodomains of Iα and Iβ cellulose in algal microfibrils. Macromolecules 1998; 31(18):6275-6279.

77. Wada M, Heux L, Sugiyama J. Polymorphism of Cellulose I Family: Reinvestigation of Cellulose IVI .Biomacromolecules 2004; 5(4): 1385-91.

78 Horii F, Yamamoto H, Kitamaru R., Tanahashi M., Higuchi T. Transformation of native cellulose crystals induced by saturated steam at high temperatures. Macromolecules 1987; 20(11): 2946-2949.

79. Yamamoto H, Horii F, Odani H. Structural changes of native cellulose crystals induced by annealing in aqueous alkaline and acidic solutions at high temperatures. Macromolecules 1989; 22(10): 4130-32.

80. Sugiyama J, Okano T, Yamamoto H, Horii, F. Transformation of valonia cellulose crystals by an alkaline hydrothermal treatment. Macromolecules; 1990; 23(12): 3196-98.

81. Ioelovich MY. A study on formation of supermolecular structure of cotton cellulose. Vysokomolekulyarnye Soedineniya Seriya a & Seriya B 1993; 35(5): B268-B271.

82. Ioelovich M. & Larina E. Parameters of crystalline structure and their influence on the reactivity of cellulose I. Cellulose Chem. Technol. 1999; 33(1-2): 3-12.

83. Ioelovich M. Accessibility and crystallinity of cellulose. Bioresources 2009; 4(3): 1168-1177.

84. Ioelovich M, Leykin A. Accessibility and supramolecular structure of cellulose. Cellulose Chem. Technol. 2009; 43(9-10):379-85.

85. O'Sullivan AC. Cellulose: the structure slowly unravels. Cellulose; 1997; 4(3):173-207.

86. Bhattacharya D, Germinario LT, Winter WT. Isolation, preparation and characterization of cellulose microfibers obtained from bagasse. Carbohydr. Polym. 2008; 73(3):371-377.

87. Li R, Fei J, Cai Y, Li Y, Feng J and Yao J. Cellulose whiskers extracted from mulberry: A novel biomass production. Carbohyd. Polym.2009; 76(1):94-99.

88. www.fpl.fs.fed.us/documnts/pdf2009/fpl_2009_moon001.pdf.

89. Fink HP, Hofmann D, Purz HJ. On the fibrillar structure of native cellulose. Acta Polymerica 1990; 41(2):131-137.

90. Zimmermann T, Pöhler E, Geiger T. Cellulose fibrils for polymer reinforcement. Adv. Eng. Mater. 2004; 6(9): 754-61.

91. Chinga-Carrasco G. Cellulose fibers, nanofibrils and microfibrils: The morphological sequence of MFC components from a plant physiology and fiber technology point of view Nanoscale Res. Lett. 2011; 6(1):417.

92. Sources: Wood Handbook; Danforth International; W.S.U., WMEL; Columbus, Institute of Natural Fibres, U.S.D.A., A.R.S.; The BioComposite Centre (1996)).

93. Heyn AN. The elementary fibril and supermolecular structure of cellulose in softwood fiber. J. Ultrastruct. Res. 1969; 26(1-2):52-68.

94. Ranby G. The colloidal properties of cellulose micelles. Discussions Faraday Society 1951; 11: 158-164.

95. Aqueous colloidal solutions of cellulose micelles. Acta Chemica Scand. 1949; 3:649 – 650.

96. Ranby G.The colloidal properties of cellulose micelles. Discussions Faraday Society 1951; 11: 158-164

97. Ranby BG. Aqueous colloidal solutions of cellulose micelles. Acta Chemica Scand. 1949; 3:649–665.

98. Angles M.N, Dufresne A. Plasticized/tunicin whiskers nanocomposites materials. 2. mechanical behaviour. Macromolecules 2000; 34(9): 2921-2931.

99. Hamad W. On the development and applications of cellulosic nanofibrillar and nanocrystalline materials. The Canadian Journal of Chemical Eng. 2006; 84(5): 513 – 519.

100. Wong EW, Sheehan PE, Lieber CM. Nanobeam mechanics: Elasticity, strength, and toughness of nanorods and nanotubes. Science 1997(Washington, DC); 277(5334):1971–1975.

101. Yu MF, Lourie O, Dyer MJ, Moloni K, Kelly TF, Ruoff RS. Strength and breaking mechanism of multiwalled carbon nanotubes under tensile load. Science 2000; 287(5453):637–640.

102. Araki J, Kuga S. Effect of trace electrolyte on liquid crystal type of cellulose microcrystals Langmuir 2001; 17 (15):4493-4496.

103. Roman M, Winter WT. Effect of sulfate groups from sulfuric acid hydrolysis on the thermal degradation behavior of bacterial cellulose. Biomacromolecules 2004; 5(5) 1671-1677.

104. Grunnert M, Winter WT. Nanocomposites of cellulose acetate butyrate reinforced with cellulose nanocrystals. J. Polym. Environ. 2002; 10(1-2): 27-30.

105. Araki J, Wada M, Kuga S. Steric stabilization of a cellulose microcrystal suspension by poly (ethylene glycol) grafting. Langmuir 2001; 17(1): 21–27.

106. Dong XM, Kimura T, Revol JF, Gray DG. Effects of ionic strength on the isotropic-chiral nematic phase transition of suspensions of cellulose crystallites. Langmuir 1996; 12(8):2076-82.

107. Heux L, Chauve G, Bonini C. Nonflocculating and chiral-nematic self-ordering of cellulose microcrystals suspensions in nonpolar solvents. Langmuir 2000, 16(21), 8210-8212.

108. de Souza Lima MM, Wong J T, Paillet M, Borsali R, Pecora R.Translational and rotational dynamics of rodlike cellulose whiskers. Langmuir 2003; 19(1): 24-29.

109. Miller AF, Donald AM. Imaging of anisotropic cellulose suspensions using environmental scanning electron microscopy. Biomacromolecules 2003; 4(3): 510-517.

110. Roohani, M, Habibi Y, Belgacem NM, Ebrahim G, Karimi AN, Dufresne A. Cellulose whiskers reinforced polyvinyl alcohol copolymers nanocomposites. Eur. Polym. J. 2008; 44(8):2489–2498.

111. Li Q, Zhou J, Zhang L. Structure and properties of the nanocomposite films of chitosan reinforced with cellulose whiskers. J. Polym. Sci. Part B: Polym. Phys. 2009; 47(11): 1069-1077.

112. Capadona JR, Shanmuganathan K, Trittschuh S, Seidel S, Rowan SJ, Weder C. Polymer nanocomposites with microcrystalline cellulose. Biomacromolecules 2009; 10(4):712-716.

113. Pranger L, Tannenbaum R. Biobased nanocomposites prepared by in situ polymerization of furfuryl alcohol with cellulose whiskers or montmorillonite clay. Macromolecules 2008; 41(22): 8682–8687.

114. Habibi Y, Goffin AL, Schiltz N, Duquesne E, Dubois P, Dufresne, A. Bionanocomposites based on poly (ε-caprolactone)-grafted cellulose nanocrystals by ring-opening polymerization. J. Mater. Chem. 2008, 18(41):5002-5010.

115. Junior de Menezes A, Siqueira G, Curvelo AAS, Dufresne A. Extrusion and characterization of functionalized cellulose whiskers reinforced polyethylene nanocomposites Polymer 2009, 50(19): 4552-4563.

116. Garcia de Rodriguez NL, Thielemans W, Dufresne, A. Sisal cellulose whiskers reinforced polyvinyl acetate nanocomposites. Cellulose 2006; 13(3): 261–270.

117. Siqueira G, Bras J, Dufresne A. Cellulose whiskers versus microfibrils: Influence of the nature of the nanoparticle and its surface functionalization on the thermal and mechanical properties of nanocomposites. Biomacromolecules 2009; 10(2):425-432.

118. Angles MN, Dufresne A. Plasticized/tunicin whiskers nanocomposites materials. 1. structural analysis. Macromolecules 2000; 33:8344-8353.

119. Terech P, Chazeau L, Cavaille JY. A Small-Angle Scattering Study of Cellulose Whiskers in Aqueous Suspensions Macromolecules 1999; 32(6):1872-75.

120. Kimura F, Kimura T, Tamura M, Hirai A, Ikuno M, Horii F. Magnetic alignment of the chiral nematic phase of a cellulose microfibril suspension. Langmuir 2005; 21(5):2034-2037.

121. Ashby MF, Jones DRH Engineering materials 1: an introduction to their properties and applications. Pergamon Press, Oxford 1989.

122. Sakurada I, Nukushina Y, Ito T. Experimental Determination of Elastic Modulus of Crystalline Regions in Oriented Polymers. J. Polym. Sci. 1962; 57(165): 651-660.

123. Araki J, Wada M, Kuga S, Okano T. Flow properties of microcrystalline cellulose suspension prepared by acid treatment of native cellulose. Colloids Surf. A 1998; 142(1):75-82.

124. Araki J, Wada M, Kuga S, Okano T. Influence of surface charge on viscosity behavior of cellulose microcrystal suspension. J. Wood Sci. 1999; 45(3):258-261.

125. Araki J, Wada M, Kuga S, Okano T. Birefringent glassy phase of cellulose microcrystal suspension. Langmuir 2000; 16(6): 2413-2415.

126. Lu P, Hsieh Y. Preparation and properties of cellulose nanocrystals: Rods, spheres, and network, Carbohyd. Polym. 2010; 82(2):329-336.

127. Hasani M, Cranston ED, Westman G, Gray DG. Cationic surface functionalization of cellulose nanocrystals. Soft Matter 2008; 4(11):2238-2244.

128. Bondeson D, Oksman K. Polylactic acid/cellulose whisker nanocomposites modified by polyvinyl alcohol. Composites Part a-Applied Science and Manufacturing 2007; 38(12): 2486-2492.

129. Bai W, Holbery J, Li KC. A technique for production of nanocrystalline cellulose with a narrow size distribution. Cellulose 2009; 16(3): 455-465.

130. Siqueira G, Bras J, Dufresne A. New process of chemical grafting of cellulose nanoparticles with a long chain isocyanate. Langmuir 2010; 26(1):402-411.

131. Dong X, Revol J, Gray D. Effect of microcrystallite preparation conditions on the formation of colloid crystals of cellulose. Cellulose 1998; 5(1):19-32.

132. Helbert W, Cavaille JY, Dufresne A. Thermoplastic nanocomposites filled with wheat straw cellulose whiskers .1. Processing and mechanical behavior. Polymer Composites 1996; 17(4):604-611.

133. Cao XD, Dong H, Li CM. New nanocomposite materials reinforced with flax cellulose nanocrystals in waterborne polyurethane. Biomacromolecules 2007; 8(3):899-904.

134. Cao XD, Habibi Y, Lucia LA. One-pot polymerization, surface grafting, and processing of waterborne polyurethane-cellulose nanocrystal nanocomposites. J. Mater. Chem. 2009; 19(38):7137-7145.

135. Auad ML, Mosiewicki MA, Richardson T, Aranguren MI, Marcovich NE. Nanocomposites made from cellulose nanocrystals and tailored segmented polyurethanes. J. Appl. Polym. Sci. 2010; 115(2):1215-25.

136. Liu DG, Zhong TH, Chang PR, Li KF, Wu QL. Starch composites reinforced by bamboo cellulosic crystals. Bioresource Technol. 2010; 101(7):2529-36.

137. Millet M, Moore W, Saeman J. Preparation and properties of hydrocelluloses. Ind. Eng. J. 1954; 46: 1493-1497.

138. Marchessault RH, Morehead FF, Walter NM. Liquid crystal systems from fibrillar polysaccharides. Nature 1959; 184(9): 632-633.

139. Marchessault RH, Morehead FF, Koch MJ. Hydrodynamic properties of neutral suspensions of cellulose crystallites as related to size and shape. J. Colloid Sci. 1961; 16:327-344.

140. Selim IZ, Zikry AAF, Gaber SH. Physicochemical properties of prepared cellulose sulfates: II. From linen pulp bleached by the H2O2 method. Polymer-Plastics Technol. Eng. 2004; 43(5):1387-1402.

141. Kamel, S. Nanotechnology and its applications in lignocellulosic composites, a mini review. Express Polym. Lett. 2007; 1(9): 546-575.

142. Pandey JK, Kim CS, Chu WS, Lee CS, Jang DY, Ahn SH. Evaluation of morphological architecture of cellulose chains in grass during conversion from macro to nano dimensions. E-Polym., 2009; 102:1-15.

143. Sjöström E. Wood chemistry: fundamentals and applications (second edition).Academic press, inc. San Diego, California 1993.

144. Natanya ML, David P. Sustainable Films and Coatings from Hemicelluloses: A review. Biomacromolecules, 2008; 9 (6):1493–1505.

145. Salmen L, Olsson AM. Interaction between hemicelluloses, lignin and cellulose: structure-property relationships. J. Pulp Pap. Sci. 1998; 24(3):99-103.

146. Ebringerova A, Hromadkova Z, Heinze T. Hemicellulose. Adv. Polym. Sci. 2005; 186:1-67.

147. Hettrich K, Schröder N, Engelhardt J, Drechsler U, Loth F. Derivatization and characterization of xylan from oat spelts. Macromolecular Symposia 2005; 232(1)1:37-48.

148. Saake B, Erasmy N, Kruse Th, Schmekal E, J. Puls, in Hemicellulose: Science and Technology. Ed. P. Gatenholm, M. Tenkanen, Washington: American Chemical Society, ACS Symposium Series 2003; 864, 52.

149. Matos Ruiz M, Cavaille JY, Dufresne A, Gerard JF, Graillat C. Processing and characterization of new thermoset nanocomposites based on cellulose whiskers. Compos. Interfaces 2000; 7(2):117-131.

150. Sturcova A, Davies GR, Eichhorn SJ. Elastic modulus and stress-transfer properties of tunicate cellulose whiskers. Biomacromolecules 2005; 6(2):1055-61.

151. Wang Y, Cao X, Zhan L. Effects of cellulose whiskers on properties of soy protein thermoplastics .Macromolecular Bioscience 2006; 6(7): 524–531.

152. Marcovich NE, Auad ML, Bellesi NE, Nutt SR, Aranguren MI. Cellulose micro/nanocrystals reinforced polyurethane. J. Mater. Res. 2006; 21(4):870-881

153. Auad ML, Contos VS, Nutt S, Aranguren MI, Marcovich NE.Characterization of nanocellulose-reinforced shape memory polyurethanes. Polymer International 2008; 57(4): 651-659.

154. Cao XD, Habibi Y, Lucia LA. One-pot polymerization, surface grafting, and processing of waterborne polyurethane-cellulose nanocrystal nanocomposites. J. Mater. Chem. 2009; 19(38):7137-7145

155. Wang YX., Tian H F, Zhang LN. Role of starch nanocrystals and cellulose whiskers in synergistic reinforcement of waterborne polyurethane. Carbohyd. Polym. 2010; 80(3):665-671.

156. Favier V, Canova GR, Cavaille JY, Chanzy H, Dufresne A, Gauthier C. Nanocomposite materials from latex and cellulose whiskers Polyrn. Adv. Technol. 1995; 6(5):351-355.

157. Favier V, Dendievel R, Canova GR, Cavaill JY, Gilormini P. Simulation and modeling of three-dimensional percolating structures: case of a latex matrix reinforced by a network of cellulose fibers Acta Metall. Mater. 1997; 45(4):1557-1565.

158. Favier V, Thtse de Docteur de 1'Institut National Polytechnique de Grenoble (1995).

159. Capadona JR, Shanmuganathan K, Trittschuh S, Seidel S, Rowan SJ, Weder C.Polymer nanocomposites with manowhiskers isolated from microcrystalline cellulose. Biomacromolecules 2009; 10(4):712-716.

160. Takayanagi M, Uemura S, Minami S. Application of equivalent model method to dynamic rheo-optical properties of a crystalline polymer. J. Polym. Sci.1964; 5(C):113-122.

161. Ouali N, Cavaille JY, Pe´rez J. Elastic, viscoelastic and plastic behavior of multiphase polymer blends Plast., Rubber Compos. 1991; 16(1): 55-60.

162. Paul B. Prediction of elastic constants of multiphase materials, transactions of the metallurgical society of AIME. 1960; 218: 36 -41.

163. Lee J, Sun QH, Deng YL, Nanocomposites from regenerated cellulose and nanoclay. Journal of Biobased Materials and Bioenergy, 2008; 2(2): 162-168.

164. Liu LQ et al. Mechanical properties of functionalized single-walled carbon-nanotube/poly (vinyl alcohol) nanocomposites. Adv. Functional Mater. 2005; 15(6):975-980.

165. Cadek M. et al. Morphological and mechanical properties of carbon-nanotube-reinforced semicrystalline and amorphous polymer composites. Appl. Phys. Lett. 2002; 81(27):5123-5125.

166. Gauthier R, Joly C, Coupas AC, Gauthier H, Escoubes M. Interfaces in polyolefin/cellulosic fiber composites: Chemical coupling, morphology, correlation with adhesion and aging in moisture. Polymer Composites 1998; 19(3):287-300.

167. Singh S, Ray SS. Polylactide based nanostructured biomaterials and their applications. J. Nanoscience and Nanotechnology 2007; 7(8):2596-2615.

168. Mallick PK. Fiber-reinforced composites: materials, manufacturing and design, 2nd ed: Marcel Dekker, 1993.

169. Favier V, Cavaille JY, Canova GR, Shrivastava SC. Mechanical percolation in cellulose whisker nanocomposites. Polym. Eng. Sci. 1997; 37(10):1732-1739

170. Hajji P. et al. Tensile behavior of nanocomposites from latex and cellulose whiskers. Polym. Composites 1996; 17(4): 612-619.

171. Dufresne A, Cavaille JY, Helbert W. Thermoplastic nanocomposites filled with wheat straw cellulose whiskers .2. Effect of processing and modeling. Polym. Composites 1997; 18(2): 198-210.

172. Embuscado M E. Edible films and coatings for food Applications (2009).

173. Gennadios A, Hanna MA, Kurth LB. Application of edible coatings on meats, poultry and seafoods: a review. Food Sci. Technol. 1997; 30(4):337-350.

174. Turhan KN, Sahbaz F. Water vapor permeability, tensile properties and solubility of methylcellulose-based edible films. J. Food Eng. 2004; 61:459-466.

175. Gontard N, Guilbert S, Cuq JL. Edible wheat gluten films: influence of the main process variables on film properties using response surface methodology. J. Food Sci. 1992; 57(1):190-195.

176. Banker GS. Film coating theory and practice. J. Pharm. Sci. 1966; 55(1):81-90.

177. Han JH. Innovations in Food Packaging 2008:418.

178. Coughlan MP, Hazlewood GP. Hemicellulose and Hemicellulases (Eds). Portland Press Ltd., NC, U.S.A (1993).

179. Ebringerová A, Heinze T. Xylan and xylan derivatives -- biopolymers with valuable properties. 1. Naturally occurring xylans structures, isolation procedures and properties Macromol. Rapid Commun. 2000; 21(9):542-556.

180. Gabrielli I, Gatenholm P. Preparation and properties of hydrogels based on hemicellulose J. Appl. Polym. Sci. 1998; 69(8): 1661-1667.

181. Saxena A, Elder T, Shaobo P, Ragauskas AJ. Novel nanocellulosic xylan composite film. Composite Part B 2009; 40B (8):727-730.

182. Peng X, Ren J, Zhong L, Sun R. Nanocomposite films based on xylan-rich hemicelluloses and cellulose nanofibers with enhanced mechanical properties. Biomacromolecules 2011; 12 (9): 3321–3329.

183. Hartman J, Albertsson AC, Lindblad MS, Sjöberg J. Oxygen barrier materials from renewable sources: material properties of softwood hemicellulose-based films J. Appl. Polym. Sci. 2006; 100(4):2985-2991.

184. Gröndahl M, Eriksson L, Gatenholm P. Material properties of plasticized hardwood xylans for potential application as oxygen barrier films. Biomacromolecules 2004; 5(4):1528-1535.

185. Dole P, Joly C, Espuche E, Alric I, Gontard N. Gas transport properties of starch based Films. Carbohyd.Polym. 2004; 58(3):335-343.

186. Butler BL, Vergano PJ, Testin RF, Bunn JM, Wiles JL. Mechanical and barrier properties of edible chitosan films as affected by composition and storage. J. Food Sci. 1996; 61(5): 953-955.

187. Arvanitoyannis I, Biliaderis CG. Physical properties of polyol-plasticized edible blends made of methyl cellulose and soluble starch Carbohyd. Polym. 1999; 38(1):47-58.

188. Gröndahl M, Eriksson L, Gatenholm P. Material properties of plasticized hardwood xylans for potential application as oxygen barrier films. Biomacromolecules 2004; 5(4):1528 -1535.

189. Linder A, Bergman R, Bodin A, Gatenholm P. Mechanism of assembly of xylan onto cellulose surfaces. Langmuir 2003; 19(12):5072-5077.

190. Hartman J, Albertsson AC, Lindblad MS, Sjöberg J. Oxygen barrier materials from renewable sources: material properties of softwood hemicellulose-based films J. Appl. Polym.Sci. 2006; 100(4):2985-2991.

191. Rindlav AW, Stading M, Hermansson AM, Gatenholm P. Structure, mechanical and barrier properties of amylose and amylopectin films Carbohyd. Polym. 1998; 36(2/3):217-224.

192. Mikkonen KS, Heikkinen S, Soovre A, Peura M, Serimaa R, Talja RA. Films from oat spelt arabinoxylan plasticized with glycerol and sorbitol. J. Appl. Polym. Sci. 2009; 114(1):457-466.

193. Edlund U, Ryberg YZ, Albertsson AC. Barrier films from renewable forestry waste Biomacromolecules 2010; 11(9):2532-2538.

194. Miranda SP, Garnica O, Lara-Sagahon V, Cárdenas G. Water vapor permeability and mechanical properties of chitosan composite films. J. Chilean Chem. Soc. 2004; 49(2): 173–178.

195. Aydinli M, Tutas M. Water sorption and water vapor permeability properties of polysaccharide (locust bean gum) based edible films. Food Sci. Technol. 2000; 33(1):63–67.

196. Mikkonen KS, Heikkilä MI, Helén H, Hyvönen L, Tenkanen, M.Spruce galactoglucomannan films show promising barrier properties. Carbohyd. Polym. 2010; 79(4):1107–1112.

197. Mikkonen KS, Heikkinen S, Soovre A, Peura M, Serimaa R, Talja RA.et al. Films from oat spelt arabinoxylan plasticized with glycerol and sorbitol. J. Appl. Polym. Sci. 2009; 114(1):457–466.

198. Péroval C, Debeaufort F, Despré D, Voilley. Edible arabinoxylan based films. 1. Effects of lipid type on water vapor permeability, film structure, and other physical characteristics. J. Agri. Food Chem. 2002; 50(14):3977–3983.

199. Samir MASA, Alloin F, Dufresne A. Review of recent research into cellulosic whiskers, their properties and their application in nanocomposite field. Biomacromolecules 2005; 6(2):612-626.

200. Kvien I, Sugiyama J, Votrubec M, Oksman K. Characterization of starch based nanocomposites. J. Mater. Sci. 2007; 42(19):8163-8171.

201. Petersson L, Kvien I, Oksman K. Structure and thermal properties of poly (lactic acid)/cellulose whiskers nanocomposite materials. Composites Sci. Technol. 2007; 67(11-12):2535-2544.

202. Cao XD, Dong H, Li CM. New nanocomposite materials reinforced with flax cellulose nanocrystals in waterborne polyurethane. Biomacromolecules 2007; 8(3):899-904.

203. Harbaugh S, Loughnane NK, Davidson M, Narayanan L, Trott S, Chushak YG,Stone MO.
Elastic modulus and stress-transfer properties of tunicate cellulose whiskers. Biomacromolecules 2005; 6(2):1055-1061.

204. Oriakhi CO. Nano sandwiches. Chem. Br. 1998; 34(11):59-62.

205. Imai Y, Nishimura S, Abe E, Tateyama H,Abiko A,Yamaguchi A, Aoyama T, Taguchi H, High-modulus poly(ethylene terephthalate)/expandable fluorine mica nanocomposites with a novel reactive compatibilizer Chem. Mater. 2002; 14(2): 477-479.

206. Saxena A, Ragauskas AJ. Water transmission barrier properties of biodegradable films based on cellulosic whiskers and xylan. Carbohyd. Polym. 2009; 78(2):357-360.

207. Saxena A, Elder T, Kenvin J, Ragauskas AJ. High oxygen nanocomposite barrier films based on xylan and nanocrystalline cellulose Nano-Micro Lett. 2010; 2(4):235-241.

208. Hager J. Steam dying of porous Media, Ph.D. Thesis, Department of Chemical Engineering, Lund University, Sweden (1998)

209. Carniglia SC. Construction of the tortuosity factor from porosimetry. J. Catal. 1986, 102: 401-418

210. Wong KKY, Kibblewhite RP, Signal FA. Effect of xylanase and dosage on the refining properties of unbleached softwood kraft pulp. J. Wood Chem. Techn. 1999; 19(3): 203 – 212.
211. Simkovic I, Gedeon O, Uhliarikova I, Mendichic R, Kirschnerova S. Positively and negatively charged xylan films. Carbohydr. Polym. 2011, 83, 769–775.

212. Zhang Y, Shao H, Hu X. Atomic force microscopy of cellulose membranes prepared from the N-methylmorpholine-N-oxide/water solvent system. J.Appl. Polym. Sci. 2002, 86, 3389–3395.

213. Stamatialis DF, Dias CR, de Pinho MN. Atomic force microscopy of dense and asymmetric cellulose-based membranes. J. Membr. Sci.1999, 160, 235–242.

214. Thire RMSM, Simao RA, Andrade CT. High resolution imaging of the microstructure of maize starch films. Carbohydr.Polym. 2003, 54, 149–158.

215. Gabrielii I, Gatenholm P. Preparation and properties of hydrogels based on hemicelluloses. J. Appl. Polym. Sci. 1998, 69, 1661–1667.

216. Kvien I, Tanem BS, Oksman, K. Characterization of cellulose whiskers and their nanocomposites by atomic force and electron microscopy. Biomacromolecules. 2005; 6(6): 3160–3165

217. Hu Y, Topolkaraev V, Hiltner A, Baer E. Measurement of water vapor transmission rate in highly permeable films. J. Appl. Polym. Sci 2000; 81 (7):1624–1633

218. Saxena A, Elder T, Kenvin J, Ragauskas AJ. Moisture barrier properties of xylan composite films. Carbohyd. Polym. 2011; 84(4):1371-1377.

219. Khan RA, Salmieri S, Dussault D, Uribe-Calderon J, Kamal MR., Safrany A, Lacroix M. Production and properties of nanocellulose-reinforce methylcellulose-based biodegradable films. J Agr. Food Chem. 2010; 483; 58:7878–7885

220. Cao X, Chen Y, Chang PR., Muir AD, Falk G. Starch-based nanocomposites reinforced with flax cellulose nanocrystals. Express Polym. Lett. 2008; 2(7): 502–510.

221. Akeholm M, Hinterstoisser B, Salmen L. Characterization of the crystalline structure of cellulose using static and dynamic FT-IR spectroscopy. Carbohyd. Res. 2004; 339(3): 569-578

222. Dammström S, Salmén L, Gatenholm P. On the interactions between cellulose and xylan, a biometric simulation of the hardwood cell wall. Bioresources 2009; 4(1): 3-14.

223. Ioelovich M. Cellulose as a nanostructured polymer: a short review. BioResources 2008; 3(4):1403-1418.

224.Hui YH, Ghazala S,Graham DM, Murrell KD, Nip WK. Handbook of Vegetable Preservation and Processing (Food Science and Technology), 2003.

225. Larsson P, Hult E, Wickholm K, Pettersson E, Iversen T. Iversen, T. CP/MAS 13C-NMR spectroscopy applied to structure and interaction studies on cellulose I. Solid Solid State Nucl. Magn. Reson. 1999; 15:31-40.

226. Liiti T, Maunu SL,Hortling B,Tamminen T, Pekkala O, Varhim A. Cellulose crystallinityand ordering of hemicelluloses in pine and birch pulps as revealed by solid-state NMR spectroscopic methods. Cellulose 2003; 10:307-316

227. Bhattacharya D, Germinario LT, Winter WT. Isolation, preparation and characterization of cellulose microfibers obtained from bagasse. Carbohydr. Polym. 2008; 73(3): 371-377.

228. Larsson P, Wickholm K, Iversen T. A CP/MAS C-13 NMR investigation of molecular ordering in celluloses. Carbohydr. Res.1997; 302:19-25.

229. Newman RH, Hemmingson JA, Carbon-13 NMR distinction between categories of molecular order and disorder in cellulose. Cellulose 1995; 2:95-110.

230. Lopez M, Bizot H, Chambat G, Marais M, Zykwinska A, Ralet M, Driguez H, Buleon A. Enthalpic studies of xyloglucan-cellulose interactions. Biomacromolecules 2010; 11(6):1417-1428.

231. Mothe CG, Tavares MB. Biodegradability of polysaccharide/EVA reject blends by high resolution NMR and mechanical property. Polym. Degrad. Stabil. 1998; 61(2):253-257.

232. Menon R, MacKay AL, Burgess AE, Swanson JS. J. An NMR determination of the physiological distribution in wood during drying. Appl. Polym. Sci. 1987; 33:1141-1155.

233. Araujo CD, MacKay AL, Whittall KP, Hailey JR. A diffusion model for spin-spin relaxation of compartmentalized water in wood. J. Magn. Reson. Ser. B 1993; 101:248-261.

234. Foston M, Ragauskas AJ. Changes in the structure of the cellulose fiber wall during dilute acid pretreatment in Populus studied by 1H and 2H NMR. Energy Fuels 2010; 24(10):5677-5685.

235. Saxena A., Foston M, Kassaee M, Elder T, Ragauskas A.J. Biopolymer nanocomposite films reinforced with nanocellulose whiskers. Journal of Nanoscience and Nanotechnology 2012; 12(1):218-226.

236. Mikkonen KS, Mathew AP,Pirkkalainen K, Serimaa R, Xu C, Willför S, Oksman K and Tenkanen M. Glucomannan composite films with cellulose nanowhiskers .Cellulose 2009; 17(1): 69-81

237. Park S, Baker JO, Himmel ME, Parilla PA, Johnson DK. Cellulose crystallinity index: measurement techniques and their impact on interpreting cellulase performance Biotechnol.Biofuels 2010; 3:10.

238. Ruland W. X-ray determination of crystallinity and diffuse disorder scattering. Acta Cryst. 1961; 14(11):1180-1185.

239. Sathitsuksanoh N, Zhu Z, Wi S, Zhang YH. Cellulose solvent-based biomass pretreatment breaks highly ordered hydrogen bonds in cellulose fibers of switchgrass. Biotechnol. Bioeng. 2011, 108(3), 521-529.

240. Gumuskaya E, Usta M. Crystalline structure properties of bleached and unbleached wheat straw (Triticum Aestivum L.) soda-oxygen pulp.Turk J. Agric. For. 2002, 26,247-252.

241.Jumaa M, El Saleh F, Hassan I, Muller BW, Kleinebudde P: Influence of cellulose type on the properties of extruded pellets. Part I. Physicochemical characterisation of the cellulose types after homogenisation. Colloid Polym. Sci. 2000, 278,597-607.